UNIVERSITY OF OKLAHOMA

GRADUATE COLLEGE

INVESTIGATION OF THE EFFECTS OF WEIGHT ON BIT AND ROTATIONAL SPEED ON DIRECTIONAL DRILLING PARAMETERS AND DRILLSTRING MECHANICS

A THESIS

SUBMITTED TO THE GRADUATE FACULTY

in partial fulfillment of the requirements for the

Degree of

MASTER OF SCIENCE

By

EMMANUEL AKITA
Norman, Oklahoma
2020

INVESTIGATION OF THE EFFECTS OF WEIGHT ON BIT AND ROTATIONAL SPEED ON DIRECTIONAL DRILLING PARAMETERS AND DRILLSTRING MECHANICS

A THESIS APPROVED FOR THE
SCHOOL OF AEROSPACE AND MECHANICAL ENGINEERING

BY THE COMMITTEE CONSISTING OF

Dr. Zahed Siddique, Chair

Dr. Catalin Teodoriu, Co-Chair

Dr. Wei Sun

© Copyright by EMMANUEL AKITA 2020
All Rights Reserved.

To my caring parents, Rebecca and Theophilus, and my siblings, Princess Daisy and Paul.

Thanks for all the love, encouragement, and support.

Acknowledgments

I would like to express my sincere gratitude to Dr. Ramadan Ahmed for his continuous academic guidance and unwavering support. His immense knowledge and insight have greatly helped in designing the mini rig for the Drillbotics competition and winning it for the second time in 2019. I felt humbled to have been given the opportunity to lead the 2019 team to victory. Dr. Ahmed was very understanding and always motivating, trusting the decisions I made as the team lead, and always helping me realize my true potential.

I would like to thank Dr. Catalin Teodoriu for his critical suggestions for improving the rig design. His phenomenal insight into mechanics helped us greatly in perfecting the design for Drillbotics. I am also grateful to him for taking an interest in my research and providing valuable recommendations as a co-chair.

I would like to thank Dr. Siddique for sustaining interest in my project and providing valuable feedback when needed. Also, very grateful to Dr. Sun for always being willing to listen and to help whenever approached.

I am thankful for the SPE DSATS team for organizing the Drillbotics competition. I am grateful to the Mewbourne Oil Company for providing the funding during the school year, and to Weatherford International for providing funding during the summer months of my experiments. I deeply appreciate all the help I received from my teammates; Forrest Dyer, Savanna Drummond, Monica Elkins, Payton Duggan. I am especially grateful to Forrest Dyer for his expert help during

the design phase, and during the building and testing phase of the project. Special thanks to Jeff McCaskill for his technical support whenever we were stuck with a technical issue. I am extremely grateful to Jack Borer and Aditya Sharma for all the technical help with the controls and to Aditya Sharma for all his help with the sensor systems. Without the help and support of my family and friends, this project would not have been a tremendous success and I am forever indebted to all who directly and indirectly helped me during this journey.

Nomenclature

BHA	Bottom hole assembly
DOF	Degree of Freedom
DAQ	Data Acquisition
DSATS	Drilling Systems Automation and Technical Section
FEM	Finite Element Model
ID	Inner diameter of pipe, inches
KOP	Kick off point
IMU	Inertial Measurement Unit
MWD	Measurement While Drilling
OD	Outer diameter of pipe, inches
PDM	Positive displacement motor
ROP	Rate of penetration, inches/minute
RPM	Rotations per minute
TD	Total Depth, inches
WOB	Weight on bit

Table of Contents

List of Tables

List of Figures

Chapter 1. Introduction

1.1 Overview

The issue of optimization has plagued the oil and gas industry for a while. With a growing human population and an increase in access to modern technologies, demand for energy has never been higher. Drilling efficiency must be dramatically increased to satisfy this demand, as more challenging geologies are explored.

Furthermore, peaks and troughs are characteristic of the nature of the oil and gas industry. With current prices hovering just above $60 per barrel (Bloomberg, 2019), it has never been a better time to increase the efficiency of the drilling process. This increased efficiency also benefits the industry in peak times as well, as there is a general trend towards leaner, more efficient drilling solutions in the industry. Added to this is the increase in complexity in drilling, as more difficult unconventional sources are being explored using innovative exploration and drilling techniques.

The general setup involved in drilling consists of a rotating drill bit attached to a Bottom Hole Assembly (BHA) which is attached to a long drillstring of several tubulars. These tubulars transfer torque and axial force (**Figure 1**) to the drill bit for drilling. The tubulars and the BHA form the main two sections of the drilling setup. The drill string is usually made of tubular connections of a stand of three 30 ft. drill pipes connected, with multiple stands being added as drilling continues. The BHA, on the other hand, consists of drill collars, heavyweight drill pipes, Measurement While Drilling (MWD) tools stabilizers, reamers, bent sub, and mud motor.

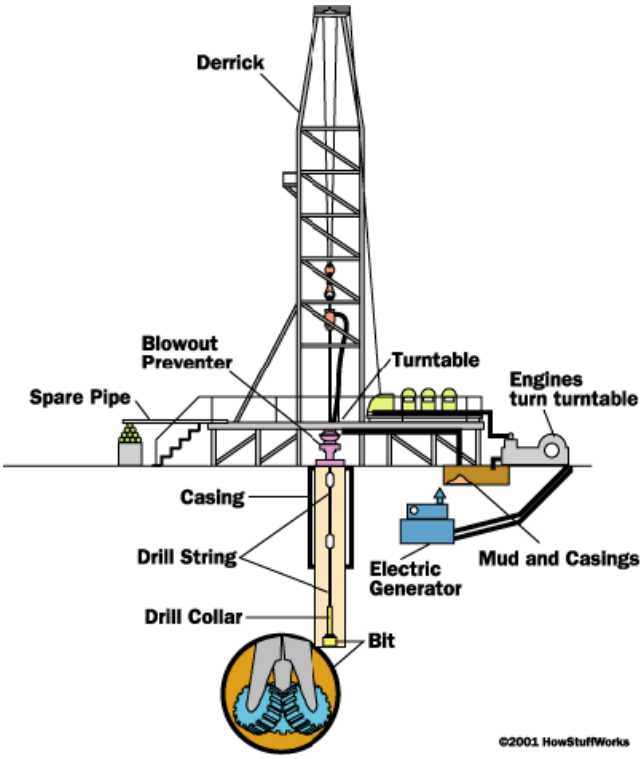

Figure 1. Schematic of drilling rig setup (Freudenrich and Strickland, 2001)

A huge part of drilling efficiency is the mitigation of drill string vibration in the drilling process. Elements such as bit-rock interaction, drillstring-borehole interaction, hydraulics, and varying rock geology are extremely problematic in drilling and contributing to inducing several vibrations. Some issues that arise from this are borehole instability, borehole deviation, and damage to BHA, all of which result in costly drilling downtime.

As earlier mentioned, more challenging environments are being explored for hydrocarbon extraction. Technology advancements in drilling such as horizontal and multilateral wells, extended reach wells, better completion mechanisms allow for the economical exploitation of hydrocarbons from complex terrains. Also, research into mitigation of vibration is at the heart of drilling advancements. Since the occurrence of vibration cannot be completely avoided in drilling, understanding of the different factors influencing vibrations will help in its reduction. Vibration

dampening tools and control of surface drilling parameters are some of the ways. This research focuses on the control of surface parameters to understand vibrations in directional wells.

1.2 Problem Statement

To increase efficiency by optimization, automation has become synonymous with increased drilling efficiency. The oil and gas industry has slowly been adopting automation and process control to improve safety, increase efficiency and reduce downtime on drilling rigs. One cannot properly automate a process without fully understanding and properly modeling the said process. Knowing the output of the process at a specific input helps engineers design the system constraints for automation.

In other words, how does one go about optimizing drilling of directional wells? Advances have indeed been made in hydraulics, bit design, tubular strength, downhole sensors, and mud motors. Optimization of efficiency has been studied extensively by several researchers. Finnie and Bailey, Dykstra et al., Jogi et al., Bailey et al., Patil and Teodoriu, among others have developed models and lab scaled experiments to this effect. Typical drillstrings in drilling are too long to allow for accurate surface tracking of downhole vibrations. It is thus imperative to gain a deeper understanding of how surface parameters affect downhole vibrations on a lab-scale at the different weight on bit (WOB) and rotational speeds, especially as applied to directional drilling. For downhole vibrations, there are three modes that come into play during drilling. These are torsional, lateral and axial (Sotomayor et al., 1997, Patil and Teodoriu 2013).

Axial vibrations cause what is known as “bit bouncing”, a phenomenon in which the bit continuously touches and separates itself from the bottom hole. This is usually seen in vertical

wells. It could show on the surface as shaking of the top drive or Kelly and fluctuations in WOB values. Mitigation of this is usually done through reducing the WOB and the increasing of revolutions per minute (RPM), changing the bit design as well as the option to include a shock sub in the BHA (Ashley et al., 2001).

Lateral vibrations cause what is known as "whirling", a phenomenon where the borehole and the drill pipe repeatedly collide in intermittent shock patterns. In this scenario, the drill bit and/or the BHA undergo an eccentric rotation around the wellbore instead of its rotating center. BHA whirling can be recognized at the surface because it usually induces other types of vibration problems such as bit bouncing. Whirling usually happens when there isn't a stabilizer on the BHA or there isn't enough lubrication in the borehole while drilling (Ashley et al., 2001).

Finally, torsional vibrations cause what is known as "stick-slip". In this vibration mode, the bit stops intermittently, causing the string to torque up. This occurs because the torque differs from the downhole toque. After torquing up, there is a release of force in a spring motion when the torque is sufficiently high, spinning free back and forward until it reaches an equilibrium point, or it continues its vibration. (Tucker and Wang, 1999, Omojuwa, et al., 2011). This drilling dysfunction is characterized by large oscillations of the bit rpm (Pavone and Desplans, 1994). Deviated wells with high angles usually induce this problem, "…when aggressive PDC bits are used and in environments where the BHA to wellbore friction is high" (Ashley, et al., 2001). This dysfunction usually presents itself in fluctuating surface torque and rpm readings. Left unchecked, this could lead to damage of BHA and removal of cutters from PDC bits and teeth from roller cone bits. Typical ways of mitigating this is to reduce WOB and RPM and using roller reamers or increasing mud lubricity to reduce well friction (Ashley, et al., 2001).

These vibration problems usually lead to BHA failure, bit failure, reduce the rate of penetration (ROP) significantly, cause damage to the downhole sensors, destroy bit cutters and BHA components, and induce borehole instability. Axial and lateral vibrations are usually recognized using specialized downhole tools such as MWD. They can be mitigated by stopping momentarily drilling operations or reducing WOB and increasing RPM (Ashley, et al., 2001).

All these drilling vibrations are always present in drilling operations, but they only become a problem when the oscillations in any axis, thus lateral, axial and torsional, come close to the natural frequencies of the system, thus reaching resonance. A summary of the frequencies at which these vibrations become an observable problem is presented by Esmaeili et al. (2012) from field measurements presented in Macpherson et al. (1993). The frequency ranges are shown in **Figure 2** below.

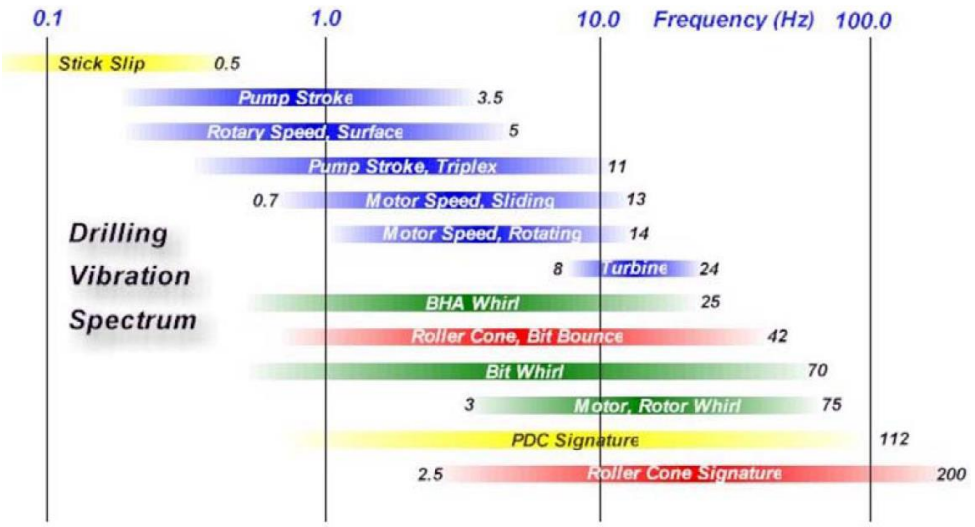

Figure 2. Frequency range for drilling vibrations (Esmaeili et al., 2012)

This study is conducted to thus add to the current understanding of optimization and efficiency, by specifically considering lab-scale directional drilling. An experimental and simulation setup is utilized to investigate the factors affecting drillstring vibrations, response torque, and ROP, and calculated mechanical specific energy.

1.3 Research Objectives

A deeper understanding of drilling factors will help to mitigate vibrations. Several models have been put forth to this end, however, understanding of said factors in directional drilling is lacking. This research project focusses on investigating controllable surface parameters and their effect on BHA vibrations.

The main objectives are as follows:

- To explore the automation system utilized for studying lab-scale directional drilling and the novel technique of directional BHA design.
- To use an experimental setup to understand how surface parameters such as WOB and rotational speed affect response torque ROP, and by extension, calculated mechanical specific energy for vertical wells.
- To compare drilling results for vertical wells drilled from a rotating drill bit, and a novel BHA tool.
- To use an experimental setup to understand how surface parameters such as WOB and rotational speed affect response torque ROP, inclination build and by extension, calculated mechanical specific energy for directional wells.
- To use an FEM simulation of the experimental test setup and modal analysis to understand the effect of drillstring vibrations on vertical drilling.
- To use an FEM simulation of the experimental test setup and modal analysis to understand the effect of drillstring vibrations on directional drilling.

1.4 Methodology

A literature review is conducted on some of the work done thus far on the subject of drillstring mechanics. This is done to obtain understand drilling parameters' effect on drilling vibrations, and what to expect from the experiments and simulation.

An automated drilling rig constructed for Drillbotics competition was used to investigate how rotational speed and WOB affect drill string vibration, torque, and ROP for vertical wells and directional wells. Novel BHA tools were developed for this competition and were used in the research study. The control algorithm for the drilling rig is written in LabVIEW and is used for drilling automation. In this algorithm, the control parameters are calibrated and set to constant values. Test runs were then conducted using a test matrix of varying WOB and rotational speed, and results collected and analyzed. Experiments were conducted by varying said parameters for two types of vertical drilling techniques, and for directional drilling. Data from vertical wells were drilled for reference information. Then this data is compared to directional wells at the same RPM and WOB values. The inclination data from directional wells are collected, and the vibrational data analyzed. Measurements are analyzed and compared with the results of previous studies.

An FEM model is also built to study the modal vibrational response and drillstring mechanics of the simulated experimental study. These simulations are run at the same operational constraints for the experiment to understand how the physics of rotation and applied weight affect the drill string independent of the rock.

1.5 Thesis Outline

This document is divided into 7 chapters. Chapter 2 discusses the literature review on vibrations in general and work done by other researchers in this field. Chapter 3 discusses the downscaling

of field equipment to the lab scale. Chapter 4 discusses the experimental setup and procedure, the detailed rig components, the automation of the drilling process and the novel BHA tools developed for the study. Chapter 5 explores the data analysis and results of the experiment, with preliminary conclusions. Chapter 6 discusses the FEM setup, the simulation methodology, and the modal analysis, with preliminary conclusions. Chapter 7 discusses the conclusions of the study and recommendations for future work. The Appendices contain all supplemental figures.

Chapter 2. Literature Review

2.1. Mechanical Vibrations

Mass and stiffness are the main components of any mechanical system. Also, the said the system will have some damping associated with it. According to Newton's 2nd Law, the mass component of the system relates to the system's forces and acceleration. Its motion consequently generates the potential energy of the system. Furthermore, according to Hook's Law the stiffness component relates to the system's forces and displacement. Finally, the damping component will be responsible for energy dissipation. Whatever the source of the damping of the system is, it will convert kinetic and potential energy into heat, which is lost. (Schmitz and Smith, 2011). This explains the reasoning behind mechanical vibrations, which can be defined as the periodic exchange of potential and kinetic energy.

Schmitz and Smith discuss three general categories for mechanical vibrations: free vibrations, forced vibrations, and self-excited vibrations.

Free Vibration occurs when a system is initially at rest and in a stable equilibrium condition, then it is disturbed with a force out of its equilibrium position. The system will vibrate until it reaches its initial equilibrium condition again. An example of free vibration's behavior is shown in **Figure 3** below, and this shows a generic example, where the vibration is an exponentially decaying, and periodic response to the initial disturbance (Schmitz and Smith, 2011).

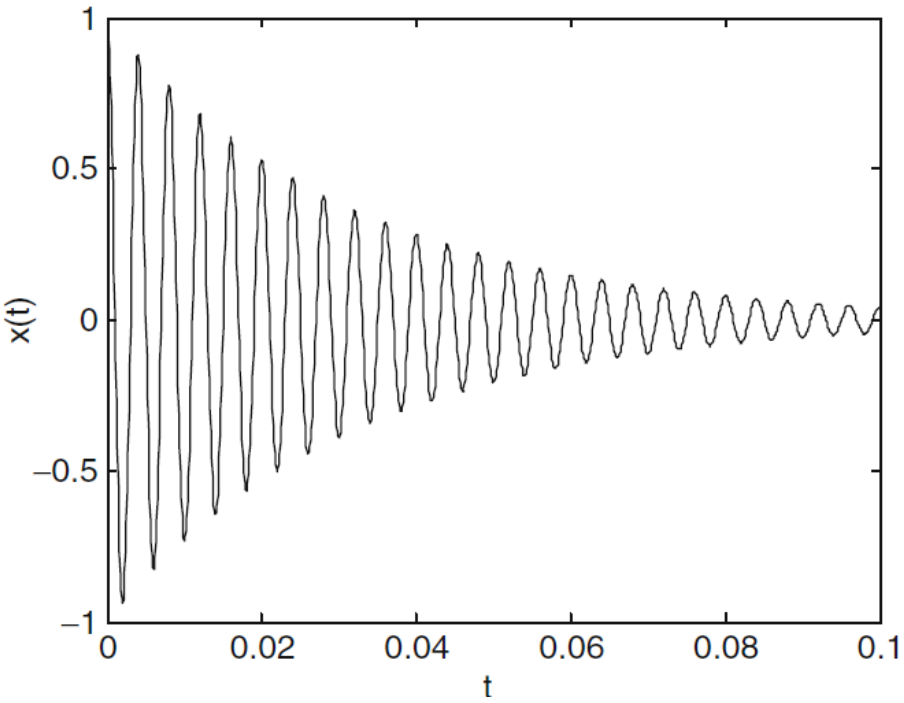

Figure 3. Free vibration example. (Schmitz and Smith, 2011)

Forced Vibration occurs when instead of a single disturbance to the system, a continuing periodic excitation is applied. The system will experience a transient state behavior to then reach a steady state in which the system response will be like the disturbance function and the system's vibrating frequency matches the forcing frequency. In this vibration type, the system will become a free vibration system and return to its original equilibrium position once the periodic excitation stops. **Figure 4** below shows this vibration in a magnitude vs. frequency domain. (Schmitz and Smith 2011). There are instances where the forcing frequency becomes equal to the natural frequency of the system. This is called resonance.

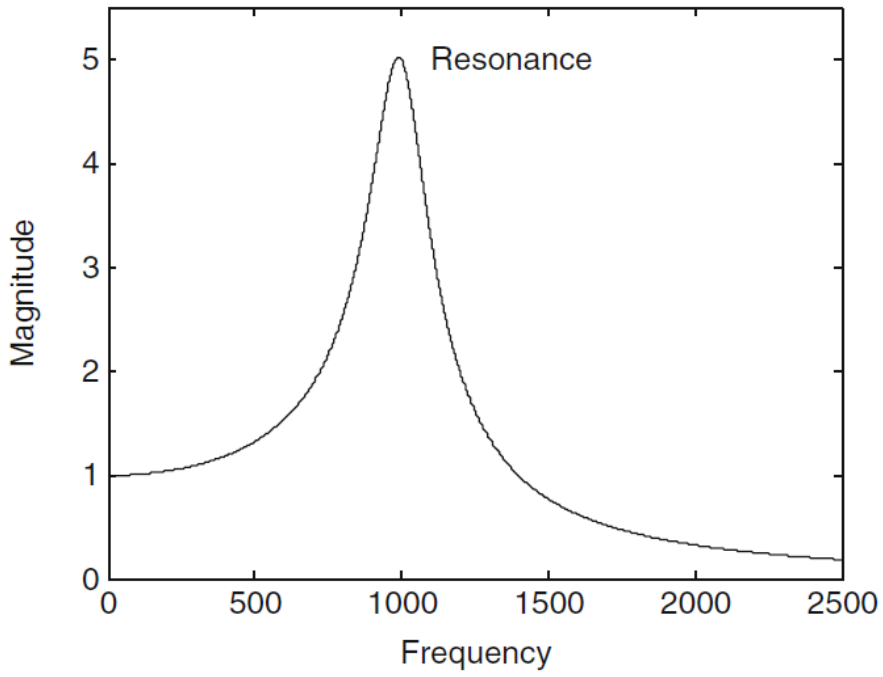

Figure 4. Example of Forced vibration in magnitude vs frequency domain. (Schmitz and Smith, 2011)

In Self-Excited Vibration, "a steady input force is modulated into vibrations near the system's natural system" (Schmitz and Smith 2011). This differs from free vibration in that it is long-lasting, and it differs from forced vibration in that it is steady and revolves around the system's natural frequency. Schmitz and Smith (2011) discuss the example of a bow and a string make in a violin, where different sounds are generated (vibrations due to the string and bow friction) depending on the speed with which the bow moves across the string. **Figure 5** below shows an example of this (Schmitz and Smith, 2011).

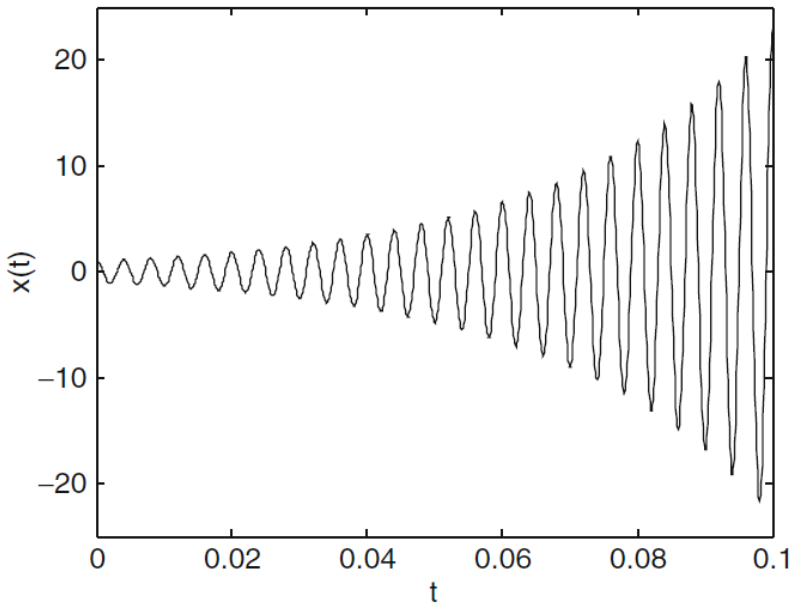

Figure 5. Self-excited vibration. (Schmitz and Smith, 2011)

2.2 Dampening of Harmonic Systems

There are three types of damping that are used for physical models: Viscous Damping, Coulomb damping, and Solid damping. Viscous Damping is one that relates the resistance to a body that is moving through a fluid at a certain velocity. It is one of the more preferred damping methods due to its mathematical simplicity. Coulomb Damping represents the energy dissipation due to the frictional interaction between two dry surfaces (Schmitz and Smith, 2011). For the purposes of this research, this type of dampening will not be considered as it escapes the scope and objective of this study.

Finally, Solid Damping arises due to the dissipation of internal energy in a vibrating solid (Schmitz and Smith, 2011). Every solid body will have the tendency to damp any vibration that it's affecting it.

2.3 Rayleigh Damping

Liu and Gorman discuss Rayleigh Damping as a functional tool that is used to deal with systems that involve multiple degrees of freedom and consider the system to have equivalent viscous damping even if there is no fluid in the system. The viscous damping assumption is that damping is directly proportional to the velocity. Ansys Workbench V 19.1 is used in this project for vibrational analysis. In the help section of ANSYS, it is discussed that constants used for calculating Rayleigh damping "…are not generally known directly but are calculated from modal damping ratios…"

2.4 Previous Studies

Researchers have used several analytical, FEM and experimental models to predict drill string behavior. FEM has been especially useful since it handles complicated geometries, different material loadings, and properties which are too complex to be considered in analytical models. It does so by breaking down the entire system model into discrete elements connected by nodes and solves said properties for each element. These models have become more complex since the 1960s, as research in computational power increased (Leine et al., 2002, Darein and Livesay 1968). Taking it even further are experimental setups, which validate results from analytical and FEM studies. Experimental setups help to circumvent the costly nature of running tests in the field. Even though they are limited in size (maxing out at about six feet in height), they have helped provide multiple insights into the drillstring vibrational analysis problem. The discussion below is not an exhaustive list but gives an idea of what has been done.

Firstly, analytical approaches are fundamental to any engineering study. Darein and Livesay discuss drillstring modeling with two approaches: a soft-string model, which assumes a continuous borehole-drillstring contact, and a stiff-string model, which calculates bending and potential contact points with the borehole (1968). **Figure 6** below shows a schematic of a simplified drill-sting in the form of a pendulum. This is the simplest method to study and recreate drill-sting mechanics behavior. The schematic includes axial and angular vibrations, and the authors made an assumption of the vibrations being independent of one another.

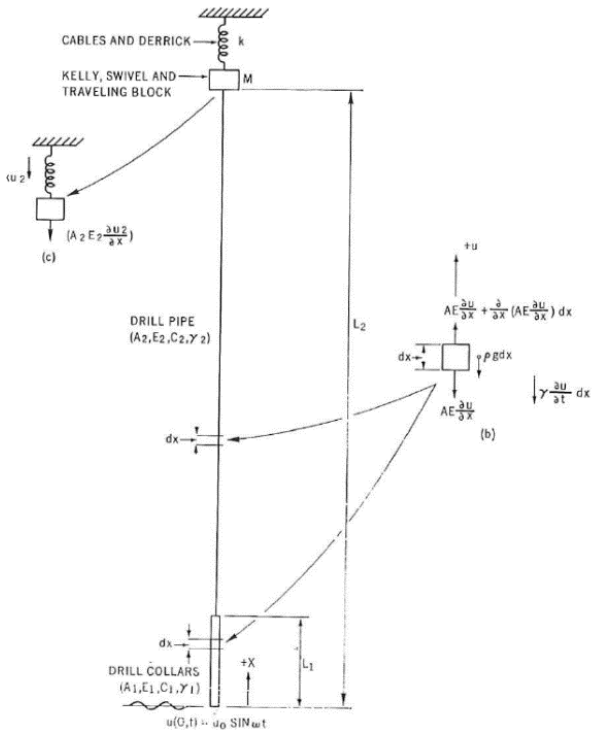

Figure 6. Analytical model pendulum schematic (Darein and Livesay, 1968)

Omojuwa et al. investigated vibrations in a horizontal well. In said wells, vibrations are minimum, even though they still exist, despite the high friction forces on the drill string. **Figure 7** below shows dynamic analysis done by Omojuwa et al. on the forces acting on a nearly straight section of an extended reach well sandwiched by two stabilizers (2012).

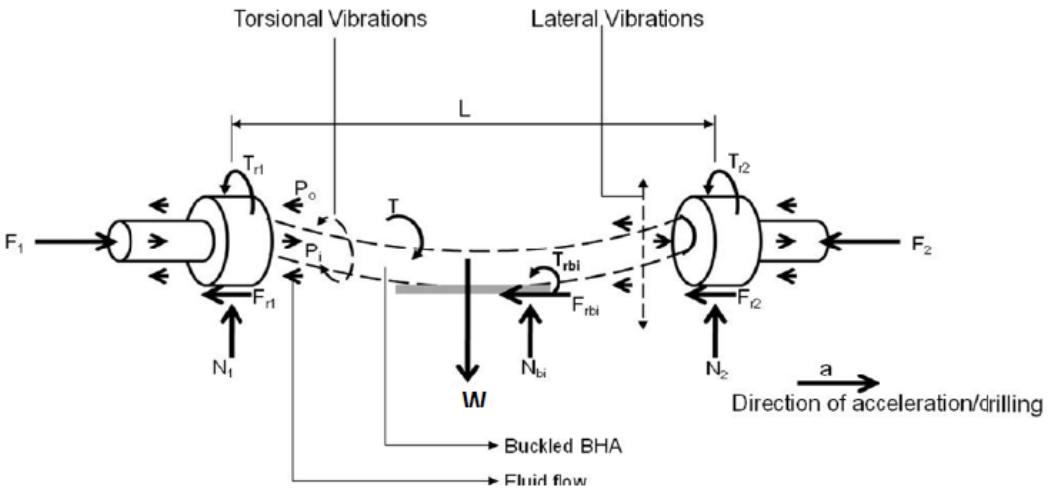

Figure 7. Analytical Model for Horizontal String (Omojuwa et al., 2012)

A mathematical model was developed by Patil (2013) to study stick-slip. Non-linear equations were developed, where the nonlinear friction forces represented bit-rock interaction. Simulink/MATLAB was used in simulating a 5 in diameter 18,700 ft. pipe, and a 6 ¾ in diameter 591 ft. BHA (Patil and Teodoriu, 2013). It was conducted that stick-slip converted to torsional vibrations when the RPM was increased, increasing the ROP as well. Also, reducing WOB decreases this phenomenon, but reduces ROP as well. The schematic is shown in **Figure 8** below.

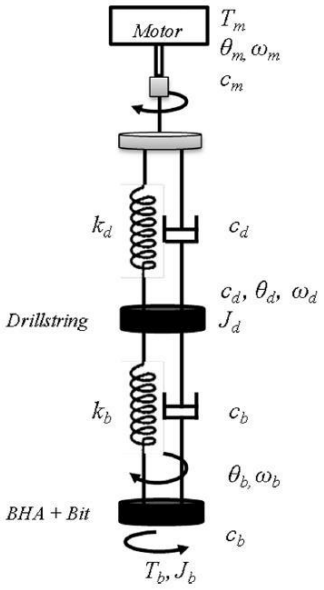

Figure 8. Stick-slip analytical schematic for the model (Patil and Teodoriu, 2013).

Secondly, FEM accounts for multiple variables too complex to solve analytically through discretization. Millheim et al. used FEM to investigate drillstring dynamics on the BHA using beam elements and simple beam support as shown in **Figure 9a**. By placing stabilizers shown in **Figure 9b**, they explored four different configurations (Millheim, et al., 1978).

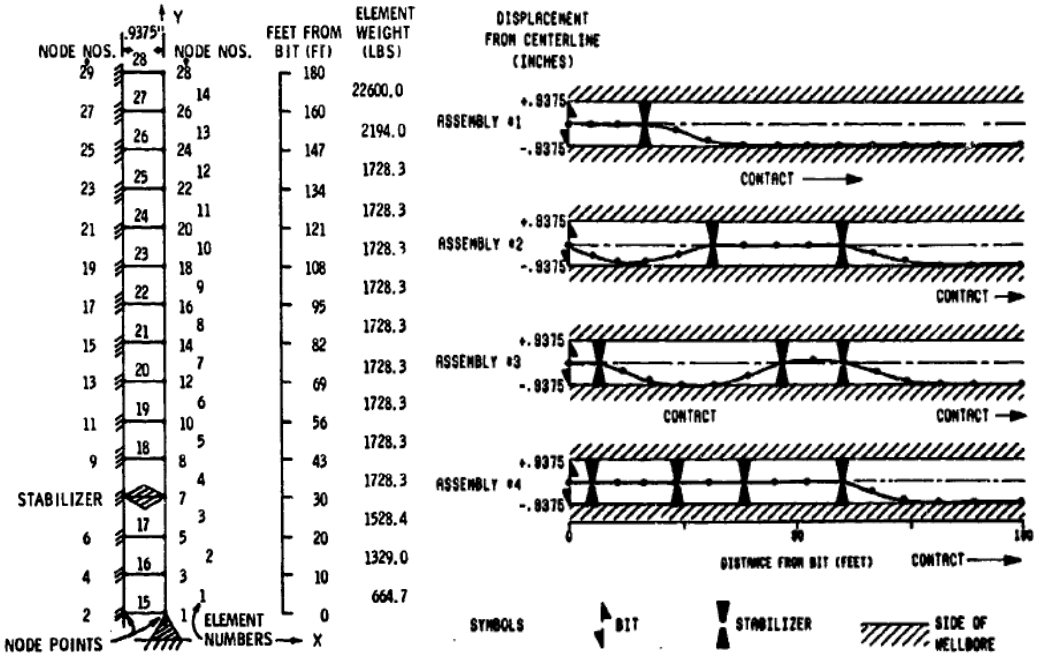

Figure 9. a) FEM Drill String Simplification b) Stabilizer Configurations (Millheim et al., 1978)

Similarly, Spanos et al. (**Figure 10**) utilized an FEM model to focus studies on more than one mode of vibration by considering the borehole-drillstring contact. Results indicated consistency in field data, drill string vibration uncertainty (2002).

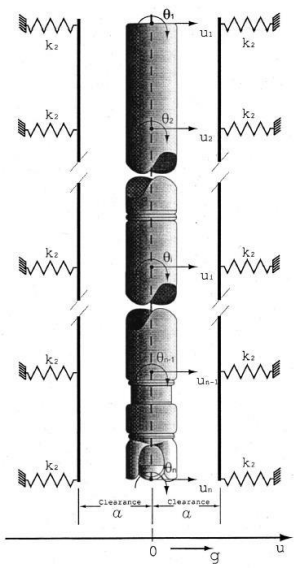

Figure 10. Schematics for the FEM model (Spanos et al., 2002).

Finally, experimental setups have helped to validate the aforementioned methods. Khulief and Al-Sulaiman researched the interaction of drillstring-wellbore mechanics using the setup in **Figure 11** below. Allowances were made on their experimental setup to track torsional and axial bending nonlinear coupling. This didn't quite provide a dynamic model to couple the various modes of vibration, thus more work needed to be done. A drillstring length of 6.56 ft. and diameter 0.08 – 0.28 in was used. This was enclosed in a 0.24 -0.40 in plexiglass shell, and tests were run from 50 – 1000 RPM (Khulief and Al-Sulaiman, 2009).

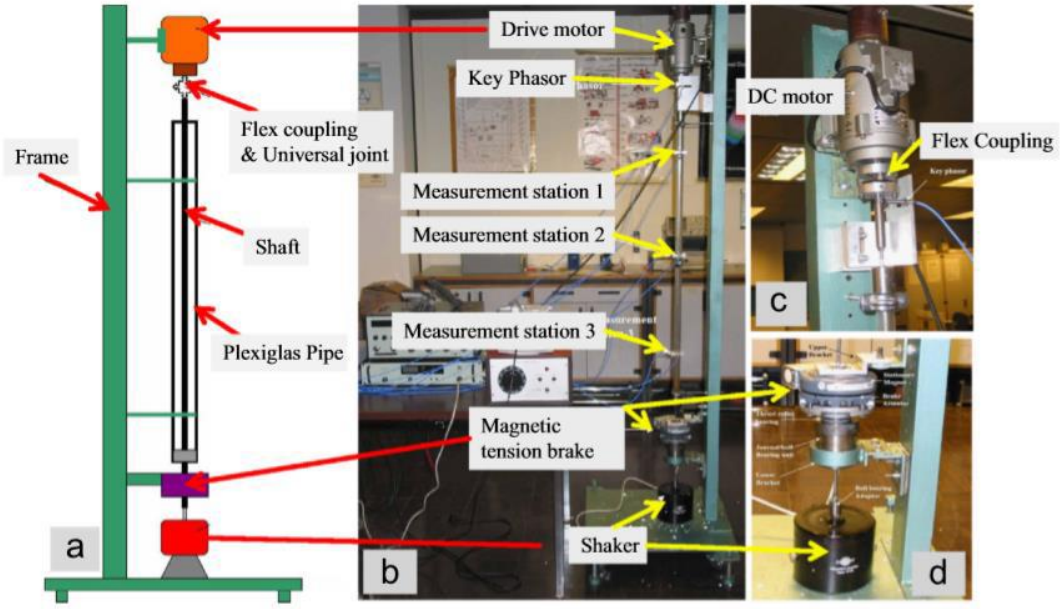

Figure 11. Laboratory investigation of drillstring vibration (Khulief and Al-Sulaiman, 2009)

Lu et al. investigated stick-slip vibration for the D-OSKILL mechanism using an experimental setup. This setup provided a small ROP since there was a loss of optimized WOB applied. It, however, was effective at reducing stick-slip vibrations. The stiffness of 0.5 ft.-lbf /rad, an RPM of 190 and a nominal WOB of 40.5 lbf were used in the experiment, as seen in **Figure 12** below.

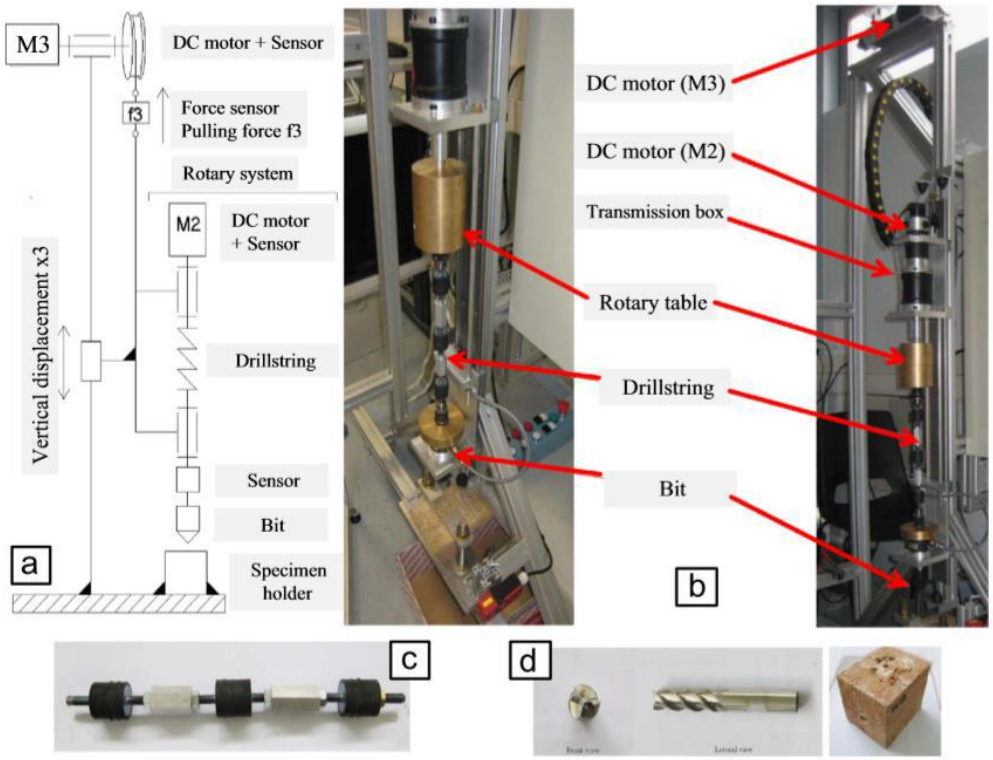

Figure 12. Schematic and experimental setup of the rotary system (Lu et al., 2009)

Kapitaniak et al. also investigated the dynamics of the drillstring. The Finite Element Model (FEM) used for setup calibration. Interestingly, pipe torque was computed from WOB and RPM, and not measured directly. As shown below in **Figure 13**, their setup attempted to replicate optimum parameters for WOB, torque on bit (TOB) and pipe stiffness. This was done to replicate stick-slip vibrational behavior in pipes and was done by the utilization of multilayered and multi-wired flexible shafts. Some of their findings were that increasing WOB increased TOB, and that increasing rotational speed decreased TOB up to a threshold point, after which TOB increased.

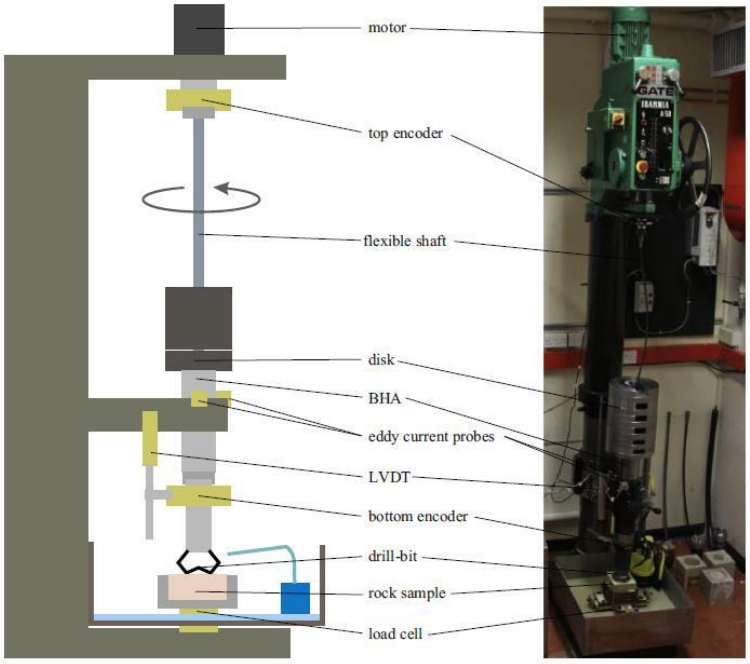

Figure 13. Experimental setup schematic used by Kapitaniak, et al. (2015).

Following a piqued interest in vibration dampening, Foster et al. (2010) investigated and quantified an asymmetric vibration dampening tool (AVDT). An inertial wheel was used as the top drive to simulate torsional disturbances. A 0.32 in diameter drill bit was connected to 0.04 in tensile steel wire as the drill pipe, as seen in **Figure 14** below. After testing in the field, it was concluded that AVDT improved torsional vibrations and that more research is needed into the BHA (Foster et al., 2010).

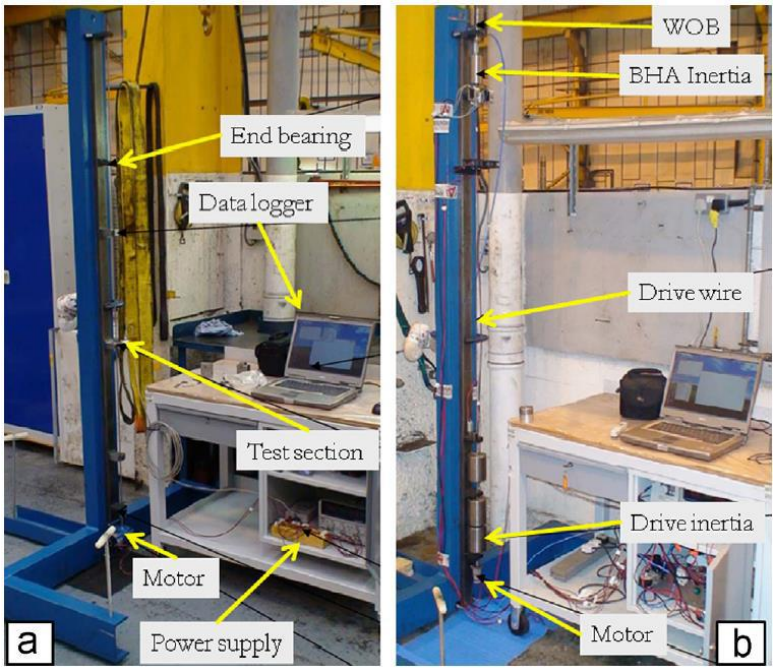

Figure 14. Foster et al., 2010 Experimental setup

Bavadiya investigated the effects of rotational speed and WOB on drill string vibrations, torque, and ROP. Using a lab-scale drilling rig outfitted with sensors for automation, a 0.3 inch by 36-inch drill pipe was used to drill several test holes and data gathered. Among the conclusions, Bavadiya stated that the increase in lateral vibrations in hard sandstone is higher than in soft sandstone indicating a formation dependency. It was concluded that there was a corresponding change in axial vibrations with a change in torque, indicating a coupled relationship. Also, that axial vibration had less dependency on rotational speeds than WOB (Bavadiya, 2017).

Several more experiments have been successfully used to investigate drill string dynamics such as the one downscaled rig set up by Patil and Teodoriu (2013b). This was used to study parameters such as rotational speed, WOB, pipe stiffness on the torsional disturbances. Finally, in field studies by Wolf et al. (1985), it was concluded that drilling at rpm values above the resonant speed of the system can help mitigate several vibrational issues since the drill pipe's natural frequency tends to be much higher.

Chapter 3: Downscaling for Research Study

An efficient, practical and inexpensive way to study drilling dysfunctions is to recreate the drilling system on a smaller scale. This section describes the geometrical and mechanical parameters used to this effect.

3.1 Application of Law of Similitude

The law of similitude is used in testing engineering models. This allows identifying various similarities between the two models. The criteria satisfied via this application are as follows: geometric similarity, which depends on model shape and size; kinematic similarity, which depends on dynamic parameters such as fluid flow which may be transient, and dynamic similarity depending on the ratio of forces acting on the boundary surfaces. This technique is widely used in the dimensional analysis where the relationship is identified between different physical quantities such as height, width, length and other.

This law is used in designing the experimental mini drilling rig used for this research study. The geometrical parameters of length, diameter, inertia, and stiffness are considered for drill string scaling. Critical to this is the replication of a model that behaves similarly to real scale drilling systems, as some could span thousands of feet in length.

To satisfy both the dynamic and geometric downscaling, three key parameters were identified (Chacin, 2017). These are essential in determining the dimensions of the downscaled model. They are as follows:

1. Critical buckling force
2. Angular deflection

3. Power and torque required

3.2 Downscaling Factor

The ratio of the measured depth of the drill string to the measured depth of the drill pipe in the lab results in a downscaling factor ‘n’.

$$n = \frac{MD_{lab}}{MD_{ac}}$$

Where

MD_{lab} = Laboratory measure length (ft.)

MD_{ac} = Measured depth in the actual drilling rig (ft.)

When a typical 5” drill-pipe is used to downscale to lab models, there is a resulting impractical value that is not readily available on the market. To circumvent this issue, the smallest readily available OD is used together with a typical drill-pipe OD to find the value of ‘n’. The expression to find the downscaling factor is as follows,

$$n = \frac{OD_{model}}{OD_{drillpipe}}$$

OD_{model}= smallest available outside diameter (in)

$OD_{drillpipe}$= actual value of outside diameter for a drill pipe (in)

With this downscaled factor, an ‘upscaling’ of the setup is made to determine the MD that the setup will be able to represent.

3.3 Shear Modulus and Maximum Torque

A critical part of this study is to recreate a model that can generate torsional vibrations. The torque formula expressed below aids in its formulation:

$$Torque = \frac{\tau J}{R}$$

Where,

τ: Shear stress (psi)

J: Polar moment of inertia of an area (in^4)

R: Distance from the center to stressed surface in the given position (in)

Furthermore, the polar moment of inertia is expressed as,

$$J = \frac{\pi}{4}\,(OD^4 - ID^4)$$

Where,

OD: Outer diameter of the cylinder or pipe (in)

ID: Inner diameter of the cylinder or pipe (in)

Solving for the shear rate and equating both the real and downscaled expressions, downscaled torque is expressed as,

$$T_{model} = \frac{T_{real}}{n}\frac{G_{model}}{G_{real}}\frac{(od^4 - id^4)}{(OD^4 - ID^4)}$$

Where,

$Tmodel$: Torque needed in the model (lbf ft.)

$Treal$: Torque applied in the real case scenario (lbf ft.)

$Gmodel$: Shear modulus of the model's material (psi)

$Greal$: Shear modulus of the real case material (steel) (psi)

3.4 Weight on Bit

To recreate similar vibrational responses in the downscaled model, WOB is crucial. Going back to the 2nd law of motion, a field value of 5 tons is selected. Assuming the same acceleration,

$$F_{real} = M_{real}a = F_{ds}$$

$$F_{ds} = 2000 * WOB * n \frac{(od^4 - id^4)}{(OD^4 - ID^4)} \frac{\rho_{ds}}{\rho_r}$$

Where,

WOB= Weight on bit (tons)

n= Downscaling factor

od= Downscaled outside diameter (in)

id= Downscaled inside diameter (in)

OD= Outside diameter (in)

ID= Inside diameter (in)

ρds= Density of the selected material (aluminum) (lb/in^3)

ρr= Density of steel (lb/in^3)

The maximum allowable WOB to avoid buckling is expressed as

$$F_{cr} = \frac{2(EIWsin\theta)}{r}$$

Where,

E= Young modulus (psi)

I= Axial moment of inertia ($in4$)

W= Weight per unit length (lb/in)

θ= Inclination

r= Radial clearance (in)

3.5 Lateral Forces

In the experimental tests, forces are induced during the drilling process. These are not quantified due to the lack of another laser displacement sensor for the experiments; typically, a laser sensor could be used to measure lateral disturbances. However, these are tracked in the simulation by means of using displacements instead of forces to recreate whirling and lateral vibrations. A displacement array is generated using the sine function and is applied to the bit at a certain frequency and fixed maximum deflection magnitude. The use and description of this will be presented in a future section.

Chapter 4. Experimental Setup

This work is an extension of work done for the Drillbotics 2019 competition. The current OU mini rig shown in **Figure 15** was outfitted with newly designed parts to allow for directional drilling. The tried and tested technique of using bent motors while sliding the pipe have often been used for directional drilling (Akita et al., 2020). A traditional bent motor was thus designed, built and used for this research work. Its appeal specifically was due to the nature of the research study. A bent motor at a fixed angle allowed for easy control of bent sub angle while adjusting WOB and RPM for investigation. A novel lab-scale cable drilling technique was implemented, whereby the drill pipe slides during the drilling process and an inner rotating cable sends torque downhole to the drill bit. The BHA doesn't rotate. This coupled with the sliding drill pipe allows for easy upward and downward trajectory steering of the drill bit by surface parameter changes.

4.1 The OU Mini Rig

Since its inception in 2015, the design of the OU Mini rig has been refined by several Drillbotics teams. The rig structure was designed to support the linear motion of the traveling block. Hinges used on the derrick allow folding and reclining on top of the derrick for transport. The rig also has wheels attached to each leg. The use of hinges on the derrick and wheels allow the rig to fit through small doorway spaces, and to be mobile. Separate compartments house all high voltage components of the rig for safety purposes. In its fully erect form, the rig dimensions are as follows: 109 inches in height, 82 inches in width and 28 inches in breadth. A 32-inch gap below the rig table allows rock samples to be placed for drilling. Extensive details on the rig components and design are provided elsewhere (Akita et al., 2018).

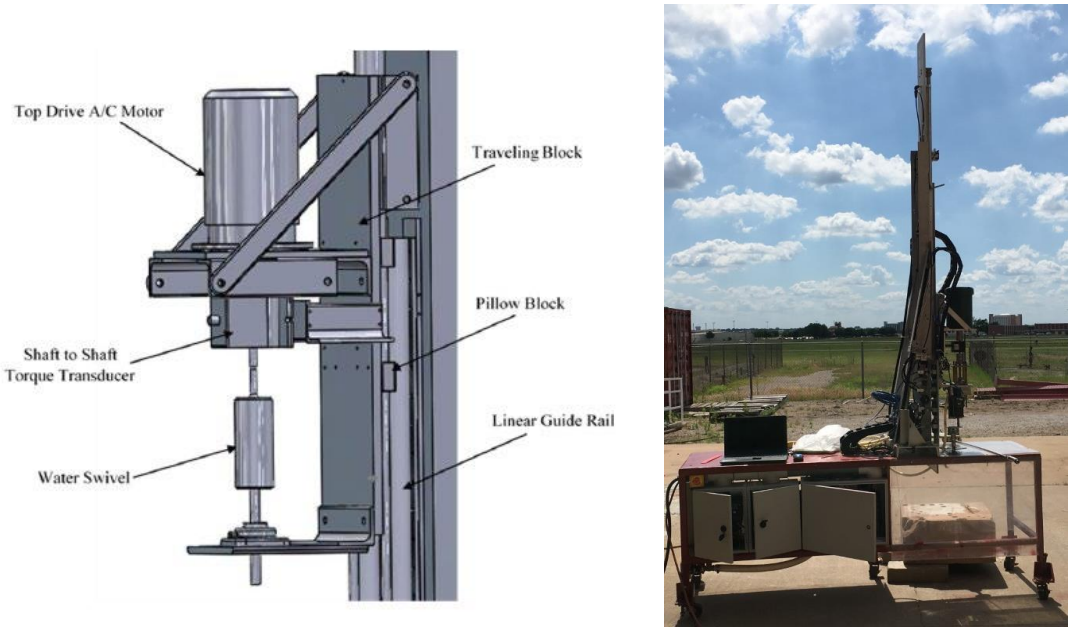

a) b)

Figure 15. a) CAD drawing of a mini drilling rig (Akita et al, 2018). B) Actual mini rig

The concept of cable drilling relies heavily on efficient torque transmission downhole. Torque transmission was thus obtained by means of a square 3/16th inch stainless steel rod. Stainless steel was used since it doesn't easily corrode and could withstand maximum torsional stresses applied during drilling. More details on material choice and cable geometry optimization are presented elsewhere (Akita et al., 2018, Akita et al., 2020). The rig modifications made are discussed below.

4.1.1 The Top Assembly

Figure 16 (CAD model) and **17** (actually built parts) show the entire top assembly, which is made up of a top spider, Camlock system, drill string and a 3/16th inch cable. The cable rod is placed within the drill pipe. It is inserted into a groove on the top spider seen in **Figure 18**. A bolted 2-inch-thick aluminum block allows for ease of future rig modifications to be made. The Camlock was integrated into the design to allow for a quick disconnect of drill pipe connections while maintaining fixed azimuth during the drilling process. A rotary union is used to isolate the attached

gear/chain system and drill pipe while allowing fluid flow from the water hose, and transmission of torque from the cable on its interior. The gear/chain component is connected to a stepper motor. The top spider in Figure 16 threads onto a top drive shaft. Its purpose is to transmit rotation downhole by means of the square cable and allow fluid through the top assembly to the drill pipe.

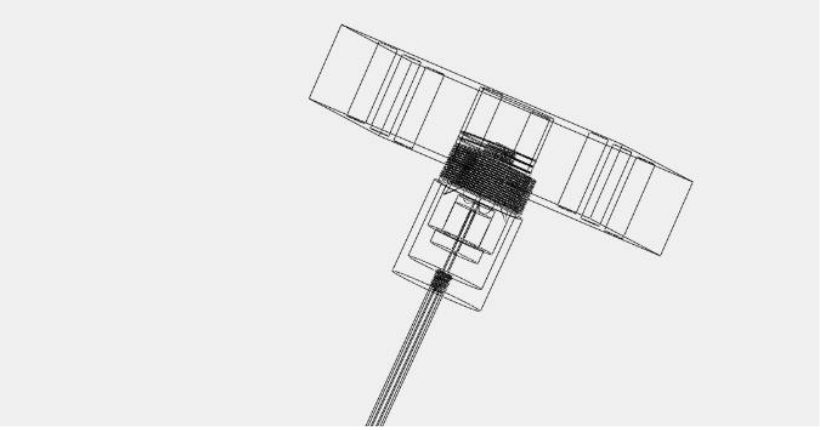

Figure 16. Top assembly CAD model showing internal features (Akita et al., 2018)

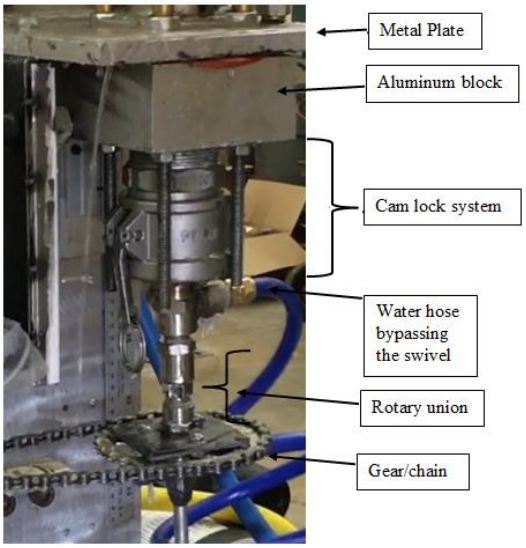

Figure 17. Built parts on the mini rig

Figure 18. Top spider: a) Initial version b) Final version

4.1.2 Bottom Assembly; Bent Sub

As the focus was to drill directional wells, a lot of focus was put into the design of a bent sub capable of deviating the path of the drill bit from a straight central axis to a deviated angle. A stabilizing housing made of steel rod holds the internal components of the bent sub while sliding during drilling. Its dimensions are 1-inch OD and 0.75-inch ID. The concept was kept simple, which resulted in welding two metal pieces at a 12° angle as seen in **Figure 19.** Details are provided elsewhere **(**Akita et al., 2018, Akita et al., 2020). The internal components on the left (a) comprises of metal rods, threaded holes for set screws, a metal bearing, and a race, and the 1.25-inch Baker Hughes micro-bit (Akita et al., 2020). The length of the micro-bit is 1.25 inches with 25° cone cutters (1-2) and 20° shoulder cutters (PDC Micro-Bit, 2019). The BHA roughly approximates to about 5 inches total in measured length. The drilled holes along the interior rod allow for water flow to the bit, as seen in **Figure 20**.

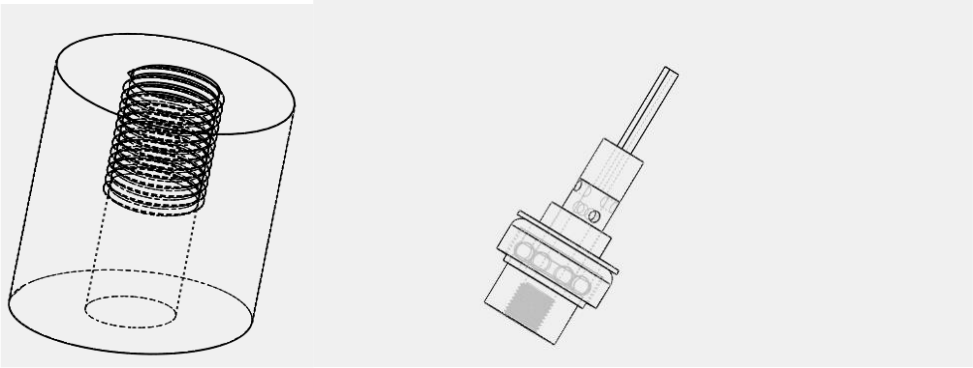

Figure 19. CAD model inner components; a) Top portion of BHA b) Bottom portion of BHA

Figure 20. Bent sub and bit assembly: a) interior; and b) exterior

4.1.3 Bottom Assembly; Straight Sub

Straight wells are drilled to serve as a basis of comparison to directional wells. A straight BHA similar to the bent sub is thus designed and built for this purpose. This straight BHA also works on the same principle of Cable drilling, where a cable within the drill pipe sends the rotation downhole, thus preventing the actual rotation of the drill pipe during drilling. For further

comparison purposes, experiments were run to compare the conventional rotating drill pipe for a straight well to the cable drilling pipe for the straight well. In the conventional system, the whole entire top assembly described above is removed, allowing the drill pipe to thread unto a shaft directly as in **Figure 21**.

Figure 21. Straight Sub design

4.1.4 Rotating Drill pipe Setup

Tests were run to compare results from conventional drilling setup, where the entire drill pipe rotates. This was done to see if any notifiable changes would emerge in terms of minimizing overall energy input and maximizing ROP. **Figure 22** below describes the process. The left image (a) depicts how the cable drilling setup reverts to the conventional setup where the drill pipe threads directly into a shaft at the bottom of the metal plate. The right image (b) shows the bottom portion of the drill pipe with the micro-bit attached.

a) b)

Figure 22. Rotating drill pipe setup a) Top portion b) Bottom portion

4.1.5 Azimuth Control

The azimuth is fixed during the experiments and thus is not a variable investigated. This is set by means of a stepper motor and a 1:3 gear ratio system, as shown in **Figure 23** below. The stepper is an ISM 7413 E motor attached to the gear/chain component. The torque generated downhole during the drilling process tends to drift the drill pipe towards the right. The stepper motor was thus set to utilize its maximum holding torque of 21 lbf-in, to overcome this drift. This was done by increasing the idle stepper current to 90% of its total value using the proprietary NI Stepper Configuration Utility software. At the rotational speeds used for this research study, the holding torque was more than adequate to prevent pipe drift during the drilling experiments.

Figure 23. Stepper Motor with Azimuth Control Mechanism (Akita et al., 2020)

4.1.6 Drill pipe

The drill pipe used was a round aluminum 6061 T6 tube with dimensions 0.375-inch OD × 0.277-inch ID × 36-inch length. This pipe is outfitted with steel compression fittings to allow for pipe connections. For the directional drilling tests, the drill pipe threads onto the bottom piece of the Camlock, as seen in Figure 17 and the top part of the bent sub, as seen in Figure 19. It doesn't rotate during the drilling process but slides the whole way. This drill pipe houses a 316-grade stainless steel 3/16th inch square cable of about 48 inches which rotates at variable RPM values to send torque downhole. For the conventional rotating straight well tests, it threads directly unto the shaft, as seen in Figure 22 a.

4.1.7 Stress Analysis for Drill Pipe

The original design was intended for a 16.7° bend. An analysis was run to determine how favorable the drill pipe was going to perform, for this angle of deviation. Thus, to determine the maximum

limits of the design, the theoretical stresses on the drill pipe had to be determined independent of the rock sample and didn't consider bit-rock interactions, angle of BHA, and rock material strength. It is known that the stress analyses with all these other components will influence the stress distributions on the pipe, however, the focus was to determine the maximum values on the pipe, and not necessarily the coupled drill pipe-rock system. A Finite Element Model (FEM) analysis was performed using ANSYS^{TM} (**Figure 24).** The KOP used in this analysis was set at 4 inches depth. The model ignores the changes in stresses from surface weight on bit (i.e. WOB measured at the surface), as it considers the resultant horizontal stress in isolation when the drill pipe hits a target in a 24-inch vertical length rock sample. Since the drilling rock samples used for this research was 12 inches, this was seen to be more than enough.

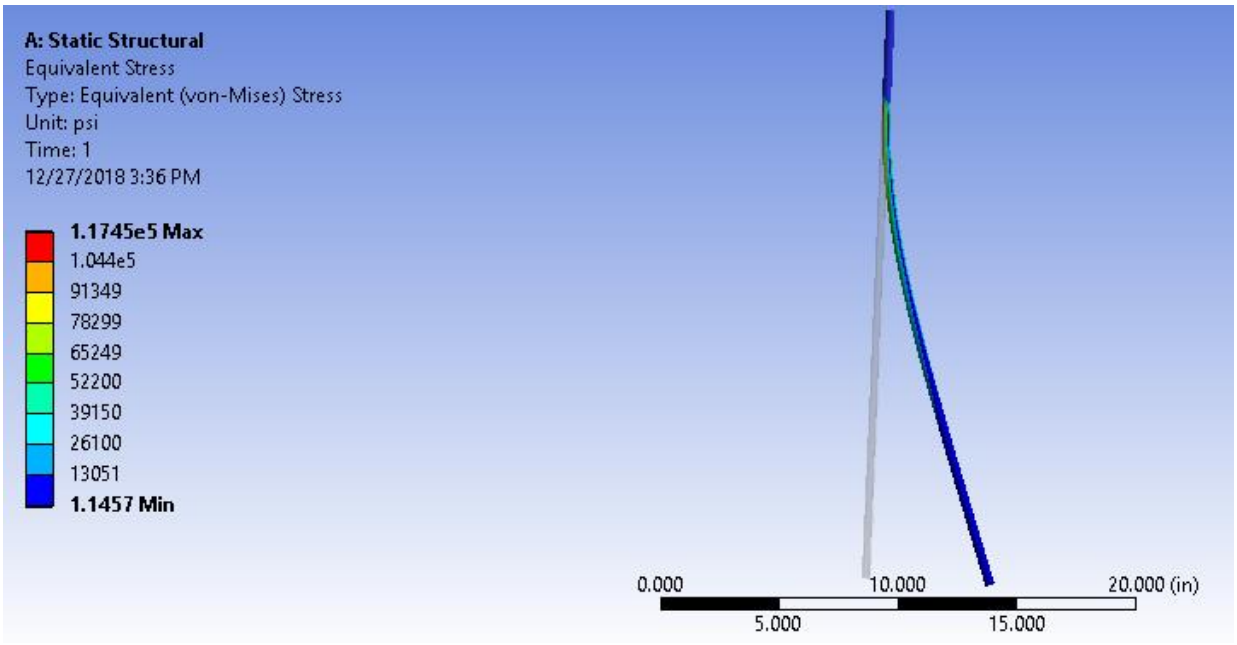

Figure 24. von Mises stress analysis on drill pipe (Akita et al., 2018)

For the approximate 16.7° bend, the model solves for a von Mises stress value of 117 ksi. Aluminum undergoes plastic deformation since it exceeds its yield strength of 35 ksi. It, however, doesn't fail, since the maximum stress value of 117 ksi is not reached. The pipe behaved exceptionally well in the multiple tests run during Drillbotics trials. Together with the Ansys maximum stresses, this drill pipe was more than adequate for the proposed research study.

4.2 Rock Sample

One rock sample with unconfined compressive strength ranging from 2200 to 6200 psi (15.17 to 42.74 MPa) was used for the test. **Figure 25**

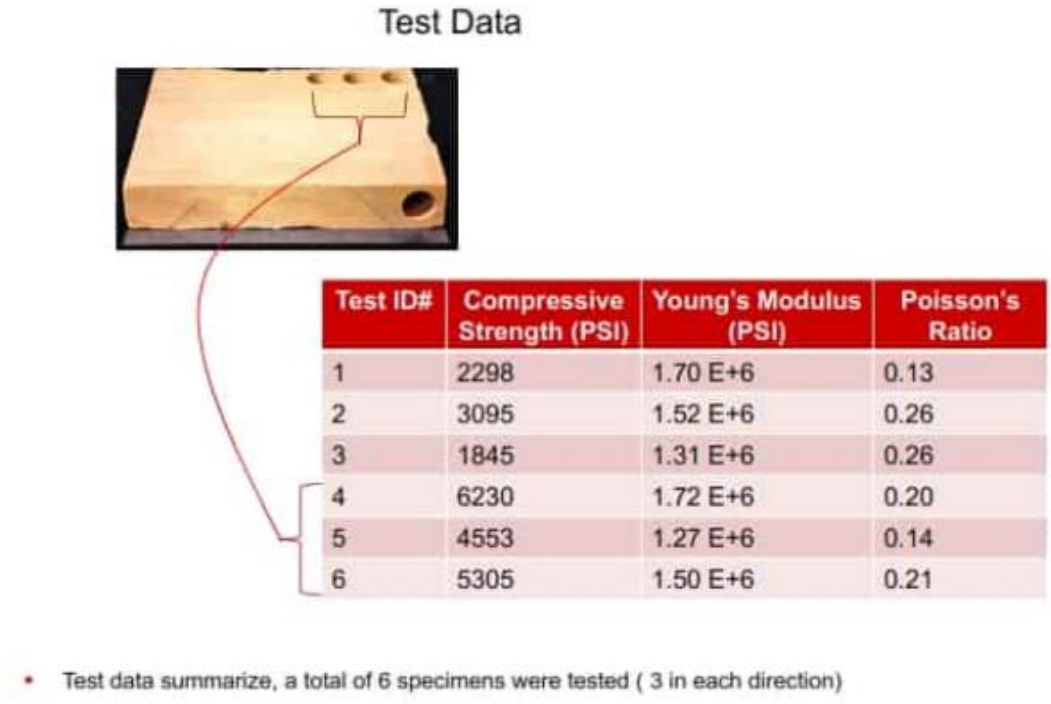

Figure 25. Rock sample mechanical properties (Drillbotics.com, 2019)

Figure 26 below shows the actual rock sample used for the tests and sample wells drilled.

a. Rock sample before drilling

b. Series of vertical wells drilled

c. Series of directional wells drilled

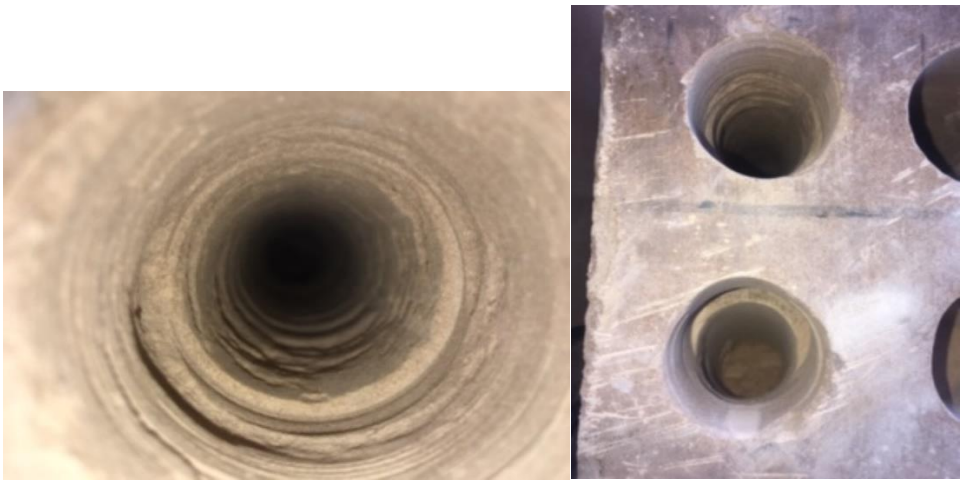

d. Vertical well profile e. Directional well profile

Figure 26. Rock sample with test wells

4.3 Experimental Test Matrix

WOB and RPM are two surface parameters that can be controlled. Thus, tests were conducted by changing WOB and rotational speed (**Table 1**). The minimum WOB was 20 lbf and the maximum applied was 50 lbf.

Table 1. Matrix of test parameters

	Rotational Speed (RPM)		
WOB (lbf)	**350**	**600**	**850**
	20	20	20
	35	35	35
	50	50	50

4.4 Controls Algorithm

The rig control is based on voltage. Voltage is generated from electromechanical sensors and is calibrated to specific field parameters. The sensors used are as follows: laser distance sensor, optical tachometer, torque transducer, WOB load cell, pneumatic air cylinder, and downhole

inclination sensor. The control architecture, as shown below in **Figure 27**, explains the data flow from the initiation of drilling to the end.

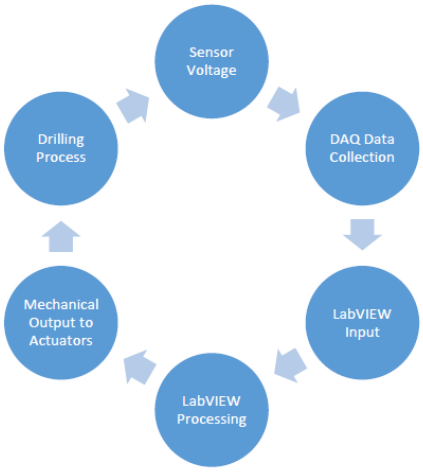

Figure 27. Control Architecture Process (Akita et al., 2018)

The output values from the rig sensors are continuously monitored during the drilling process. The recorded signals go through a central data hub or DAQ system (**Figure 28 a**) which connects to the rig software by means of a USB. The downhole inclination is read using an IMU 9DOF sensor (**Figure 28b**). The software is written in LabVIEW, as this is optimized for the DAQ system.

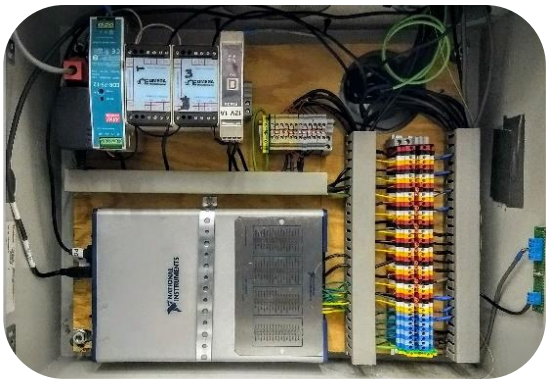

Figure 28. a) DAQ system (Akita et al., 2020) b) Downhole inclination sensor

4.5 Sensors and Sensor Calibration

For reliable data to be recorded and used for analysis, the sensors must be calibrated properly and periodically. This calibration is a way of eliminating any structural errors that may exist in the sensor output. Said structural errors are differences between a sensor expected output and its measured output, which show up consistently every time a new measurement is taken (Agarwal, 2019). The calibration is typically a linear relationship with the sensor signal output and its expected output.

Multiple sensors systems and control devices were used for measuring and collecting data. These are a displacement sensor, an rpm sensor, a torque sensor, a load cell, variable frequency drives, electro-pneumatic transducers, signal conditioners, and data acquisition module). These are used on the rig to monitor the performance of the drilling process.

a. Load cell

A load cell (Omega LC-203-100) is used to measure WOB during experiments. It has a range of measurements from 0-100 lbf with 2 mV/V output. The signal is amplified using a signal conditioner. It is installed between the piston rod and the traveling block at the back of the traveling block sensor. Since the rig control is based on voltage, a known weight is applied to the pneumatic cylinders. The weight corresponding to the load cell sensor is calibrated against the tension at the hook based on the hook load. The equations below show the calibration for the load cell where y is the weight value in lbf and x is the voltage in V. The first is corresponds to the directional BHA, and the second corresponds to the straight BHA.

$$y = -16.153x + 148.07$$

$$y = -14.193x + 131.25$$

b. Torque Sensor

A rotating shaft to shaft torque sensor (Omega TQ513-62) has been mounted above the swivel with a torque rating of 62 inch-pounds. It provides a 2 mV/V output which is amplified using a signal conditioner. It has a maximum measuring capacity of 5000 rpm with a shaft diameter of 3/8 inch. The assumption is that torque measured by the torque sensor is the torque due to bit-rock interaction as the friction due to wall-bit sub interaction is considered negligible due to roller bearing cage. The calibration equation is shown below, where y is the torque value in lbf-in and x is the voltage.

$$y = 3.876x + 0.226$$

c. Displacement Laser Sensor

A laser sensor (Banner LE55OUQ) is mounted about 0.5 inches above the traveling block on the mast. It is capable of measuring displacement up to 39.37 inches with a resolution of less than 0.04 in. By means of an aluminum reflective strip attached to the top of the traveling block, the laser is reflected to give distance readings. The calibration equation is shown below, where y is the depth value in inches and x is the voltage.

$$y = 3.664x * -5.415$$

d. Optical Rotational Tachometer

An LED-based, reflective type optical rotational speed sensor (Monarch ROS-P), which can measure up to 250,000 rpm, is mounted on the cage of the swivel. Reflective tape is attached to the spring coupling above the torque sensor, which allows the rpm readings to be made. It

has a range of detection up to 3 ft. The calibration equation is shown below, where y is the speed value in rpm and x is the voltage.

$y = 997.92x * -1.490$

e. Frequency Drive

Control of the three-phase motors is achieved using variable frequency drives. The top drive Leeson 1 HP motor is controlled by a 1-HP rated Hitachi NES1-007LB. A pump motor for fluid circulation is controlled by a 2- HP rated Hitachi NES1-0015LB.

f. Electropneumatic Transducers

Airflow inside a piston in the hoisting system was controlled by piston Electropneumatic transducers (Omega IP211X120-10V). These transducers vent air slowly as well in case of a power failure, acting as a safety feature. A pressure output of 3-120 psi in a voltage supply range of 0-10 V was the working range.

g. Signal Conditioners

With an output range of 0 - 10 Vdc, signal conditioners are used to amplify the signal from the Load cell and another from the torque sensor. Another signal conditioner (Monarch F2A3X) is used to convert the TTL signal from the optical sensor to analog form.

h. Data Acquisition Module

An Omega DAQ card (Omega OMB-DAQ-3001) is used for data collection. It provides a 16-bit resolution at 1 MHz frequency with an analog input range of 0 to 10 Vdc. It has 16 single-ended or 8 differential ended analog input channels and 24 digital input/output channels. 4 analog output channels are also provided along with 4 counter and 2 timers.

4.6 General Drilling Workflow

After the rig is set up, the rock is placed beneath the rig floor, as seen in Figure 15 b. A coring bit is used to initiate a tiny hole and later to core out 1.5 inches of rock. The appropriate BHA is then put on the drill string and sensors calibrated. The parameters for the test are set on the controls in LabVIEW, the test is initiated, and a stopwatch started. During the drilling process, the parameters on the controls front end are carefully monitored. The test is then stopped after 20 minutes, or after the BHA exits the well, whichever one comes first. The data is saved, the bit is inspected, and the process is repeated.

4.7 Mechanical Specific Energy (MSE)

Mechanical specific energy (MSE) is defined as work done to excavate a unit volume of rock (Chen et al., 2017). This is used to track the drilling efficiency process and has been used to maximize ROP as well. Several models have been developed over the years which have their uses in specific situations. Pessier and Fear, Dupriest and Koeteritz, Cherif among others have used parameters improved on the accuracy of MSE models for drilling optimization, bit selection among others. MSE is one of the parameters investigated in this study. A series of equations are used in determining the MSE values, and conclusions are made on which combination of parameters drilling should be performed at for maximum efficiency. Furthermore, since all drill bits drill in the same manner, and since bit mechanics is not considered in this study, the study was limited to results obtained from the micro-bit from Baker Hughes.

According to Chen, at perfect drilling efficiency, the MSE should equal the compressive strength of the rock (Chen et al, 2017). However, since drill bits are only about 30% efficient even at peak performance, this factor is applied to the MSE calculation.

Teale proposed the following equation in 1965.

$$MSE = 0.3 * \frac{WOB}{Area} + \frac{2\pi * RPM * Torque}{Area * ROP}$$

Where

MSE = Mechanical Specific Energy, psi

WOB =Weight on bit, lbf

Area = Drill bit area, in^2

RPM = rotations per minute

ROP = rate of penetration, in/min

However, Pessier improved on it with a way to determine downhole torque efficiently in the equation below.

$$MSE = 0.3 * WOB * \left(\frac{1}{A_b} + \frac{13.33 * \mu_b * RPM}{D_b * ROP}\right)$$

$$\mu_b = 36 * \frac{T}{D_b * WOB}$$

Where

D_b = drill bit diameter, in

T= surface torque, lbf-in

A_b = area of drillbit, in^2

μ_b = friction factor, which accounts for accurate downhole torque determination

MSE calculation in Teale's model typically uses surface data. Thus, it could lead to wrong assessments, especially when drilling directional wells since surface torque and WOB don't consider the friction losses between the borehole and the drillstring. A comparison of the MSE

values generated from Teale and those generated from Pessier can be seen in **Tables 2** and **3** below, and it was determined that they are close. However, since Pessier accounts for downhole torque, his model was used in this project for MSE calculation. Thus, the analysis was continued using Pessier's model, since it was an improvement on Teale's model, and it gave accurate downhole torque estimations.

The vertical well data displayed in Table 2 was drilled in the initial stages, where the experiment's constraints were still being determined. Thus, it was run for 1 hour to get as much data as possible. The total depth drilled was 1.35 inches. The trend of the ROP changes significantly from 0.3 to 0.083 after the system's WOB values stabilize. This can be seen in the ROP column in that table. Thus, it has extremely high MSE values, indicative of the fact that it's a highly inefficient combination of drilling parameters. The vertical well data displayed in Table 3 is the final well drilled for the cable wells. The MSE data for both Teale and Pessier match as well. Total drilling time = 5 minutes. Total depth drilled = 10.23 in.

Table 2. Results for Cable Drilling; 20 lbf WOB and 115 RPM

	WOB, lbf	ROP, in/min	Torque, lbf-in	MSE_Teale, psi	MSE_Pessier, psi
Max	23.64	0.34	8.18	43,357,220.68	43,172,833.03
min	19.05	0.00	3.53	12,253.46	12,201.42
average	21.32	0.05	5.04	300,515.34	299,237.39

Table 3. Results for Cable drilling; 50 lbf WOB and 850 RPM

	WOB, lbf	ROP, in/min	Torque, lbf-in	MSE_Teale, psi	MSE_Parsely, psi
Max	51.67	2.54	21.78	31,597.37	31,463.04
min	46.90	0.90	10.64	5804.97	5,780.34
average	49.15	1.61	14.02	11839.21	11,788.91

From Figure 29 below, ROP values are relatively high at the start of the drilling process, with correspondingly low MSE values.

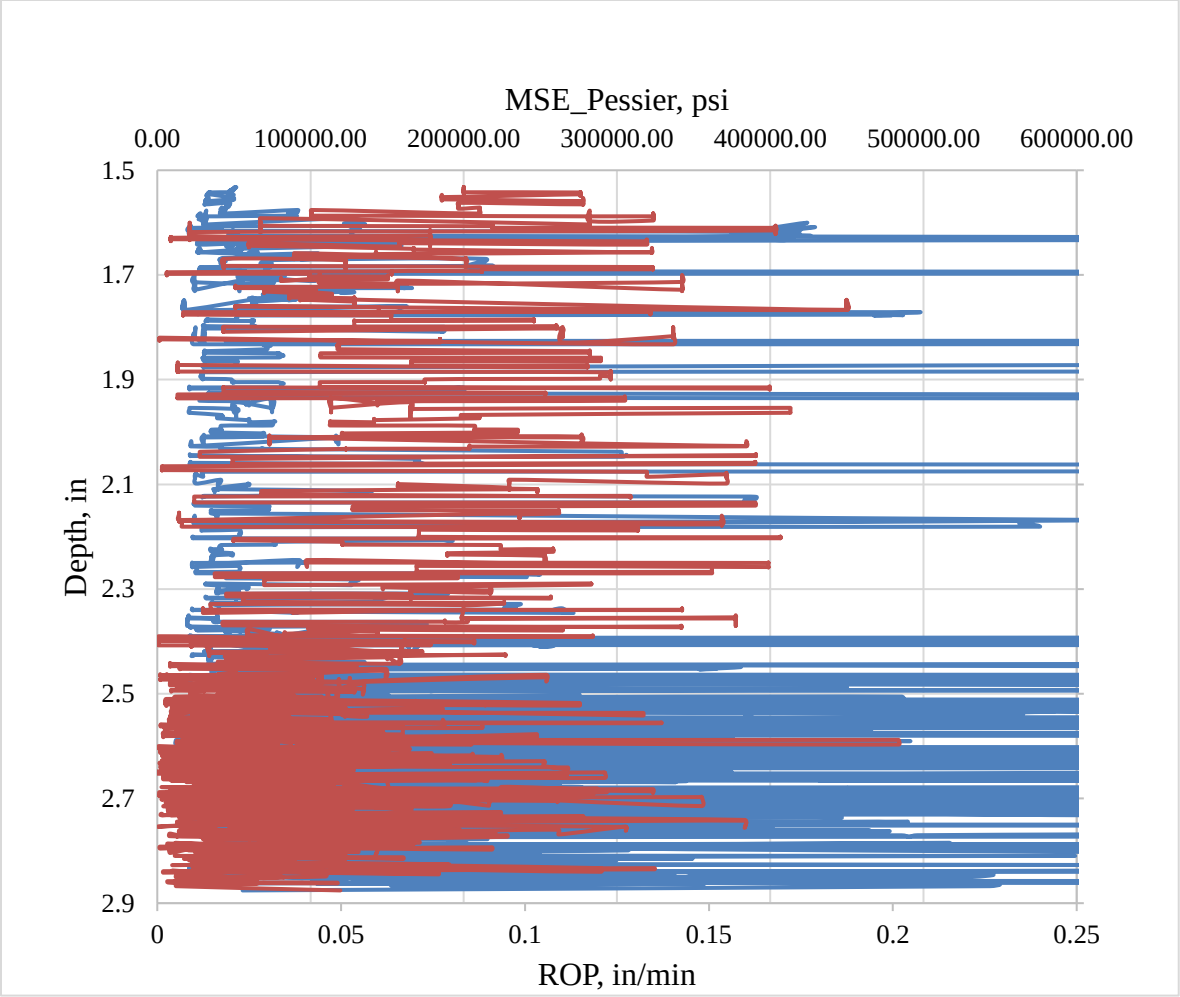

Figure 29. Depth vs ROP for calculated MSE values.

However, as the depth increases, ROP values become lower. There's obviously an inverse relationship between MSE and ROP. For illustration purposes, the MSE axis was cut off at twice the average value. If this hadn't been done, the values at the high end of the MSE curve would have eclipsed the entire scale and made it difficult to see the phenomenon being described here. Interestingly, however, the plot above tells us that there are regions in the "homogenous" rock where ROP decreases significantly. At such low WOB and RPM values, the bit just performs a scraping action, which is highly inefficient in drilling.

For directional wells, since the coefficient of friction plays a big role in determining, downhole torque and WOB, the data collected from the experiment are run through the following equations below to determine these parameters

$$MSE = 0.3 * WOB_b * \left(\frac{1}{A_b} + \frac{13.33 * \mu_b * RPM}{D_b * ROP}\right)$$

$$WOB_b = WOB * e^{-\mu\gamma_b}$$

$$T_b = \frac{\mu_b * WOB_b * D_b}{3}$$

Where

T_b = bottom hole torque, lbf-in

$\mu = \mu_b$ = 0.85

WOB_b= bottom hole weight on bit, lbf

D_b = drill bit diameter, in

WOB = surface Weight on bit, lbf

γ_b = hole inclination, radians

4.8 Optimizing Drilling Time

Generally, when the test is started, the top drive is run for a few minutes, to generate some data such as torque when there's no contact with the rock, and then the program is initiated. Thus, for the data analysis, each well data set had to be treated differently. One had to look for the actual start of drilling, which is characterized by changes in WOB, response torque and ROP. As initial tests proceeded, the drilling time was halved, and sufficient data was still recorded, as seen in **Table 4** below. As compared to 115 rpm, the test for 350 rpm was run for 27 minutes and drilled 3.3 in.

Table 4. Results for Cable Drilling; 20 lbf WOB and 350 RPM

	WOB, lbf	ROP, in/min	Torque, lbf-in	MSE_Pessier, psi
Max	23.35	0.29	7.49	2,271,163.96
min	17.84	0.00	4.86	38,765.31
average	20.15	0.13	6.12	132,144.44

Chapter 5. Results and Analysis

The effects on depth, ROP, MSE, and inclination are discussed in this section. For the vertical wells, the rotating drill pipe and the cable drilling techniques are used. The bent sub is used for the directional well. All graphs seen in this chapter have legends on the right hand side stated in RPM speed values.

5.1 WOB vs Depth

As earlier stated, the WOB values are kept constant 20 lbf, 35 lbf and 50 lbf, a 15 lbf incremental value. RPM values are kept at constant 350, 600 and 850, at 250 incremental values. The section below discusses the results and analysis for the directional wells drilled.

5.1.1 Rotating Drill pipe

As can be seen from **Figure 30**, total depth (TD) increases significantly as WOB increases with increasing RPM. The linear trend lines seem to fit the data quite well for 600 and 850 RPM and could be a basis for interpolation or extrapolation of actual data based on the linear relationships. However, extrapolation using data for 350 RPM should be done with caution, as further data is needed to establish a better relationship. All the data should, however, be looked at with some associated uncertainty, as the true data WOB values recorded were averages.

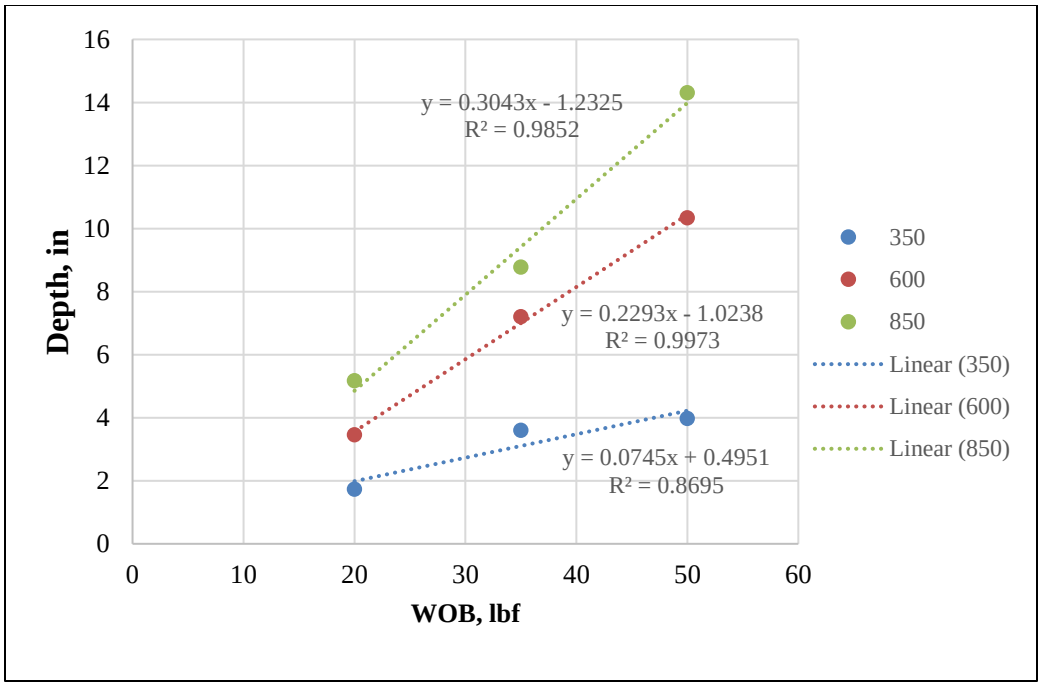

Figure 30. Depth vs WOB for rotating drill pipe

Further analysis shows that increasing RPM by 145.9% (from 350 to 850 RPM) leads to a corresponding increase in TD of about 198.3% at 20lbf, 143.4% at 35 lbf and 260.2 % at 50 lbf. Moreover, at 350 RPM, TD for wells drilled at 20 lbf increases by 107.6% when drilled at 35 lbf and increases at only 10.2% when drilled at 50 lbf. This reduction in percentage TD gain could be linked to WOB being a limiting factor in the increase of TD in this drilling system. Thus, increasing RPM is more beneficial than increasing WOB. Also, at 800 RPM, TD for wells drilled at 20 lbf increases by 69.4% when drilled at 35 lbf and increases at only 63.1% when drilled at 50 lbf. At 800 RPM, the increase in TD from 10.2% to 63.1% could be attributed to the 145.9% increase in RPM and is more pronounced in the rotating drill pipe than in the directional sliding system.

The TD gained in any drilling process is tightly governed by the friction between the drill pipe and rock during the drilling process. Since this drill pipe rotates, the pipe-hole friction plays a role in

ROP gain. The drill pipe-hole friction interaction was not investigated in this study since it was being compared to systems that were sliding during the entire drilling process.

Some interesting observations were made for the rotating drill pipe during the experimental test. As earlier stated, the tests were all run for 20 minutes. This allowed for enough data to be collected for the 10-minute mark analysis in this work. For the rotating drill pipe system however, it exhibited a peculiar behavior at the 8-inch mark. At 20 lbf, 850 RPM the system stopped drilling around the 8-inch mark. This was repeated in the 35 lbf, 600 RPM, 35 lbf, 850 trial, the 50 lbf, 600 and the 50 lbf 850 tests. The test was completed before this could be seen in 20 lbf, 350 RPM 20 lbf 600 RPM and 50 lbf, 350 RPM. An explanation could be the increase in lateral and axial vibrations took away from the drilling process and lent itself to extensive side-to-side inefficient motion. Thus, modal analysis was done to study this and is discussed in the FEM portion. A stabilizing unit could have helped to solve this problem.

To allow the study of drilling data at the 10-minute mark, however, the average ROP values for each of the tests which exhibited these interesting behaviors were multiplied to the remaining time to determine what the TD would have been.

TD is more heavily correlated to RPM than to WOB. Thus, it's better to increase the speed of drilling within reasonable limits (MSE values), than to increase WOB values. This is evidenced in the increase in slope values as one moves from 350 RPM to 800 RPM in the various graphs for directional well and straight well.

5.1.2 Cable Drilling

As can be seen from **Figure 31** below, the depth increases significantly as WOB increases with increasing RPM. The linear trend lines seem to fit the data quite well and could be a basis for interpolation or extrapolation of actual data based on the linear relationships. However, data at 600

RPM should be used with some caution, as further investigation is needed to establish a stronger relationship for prediction. All the data should, however, be looked at with some associated uncertainty, as the true data WOB values recorded were averages.

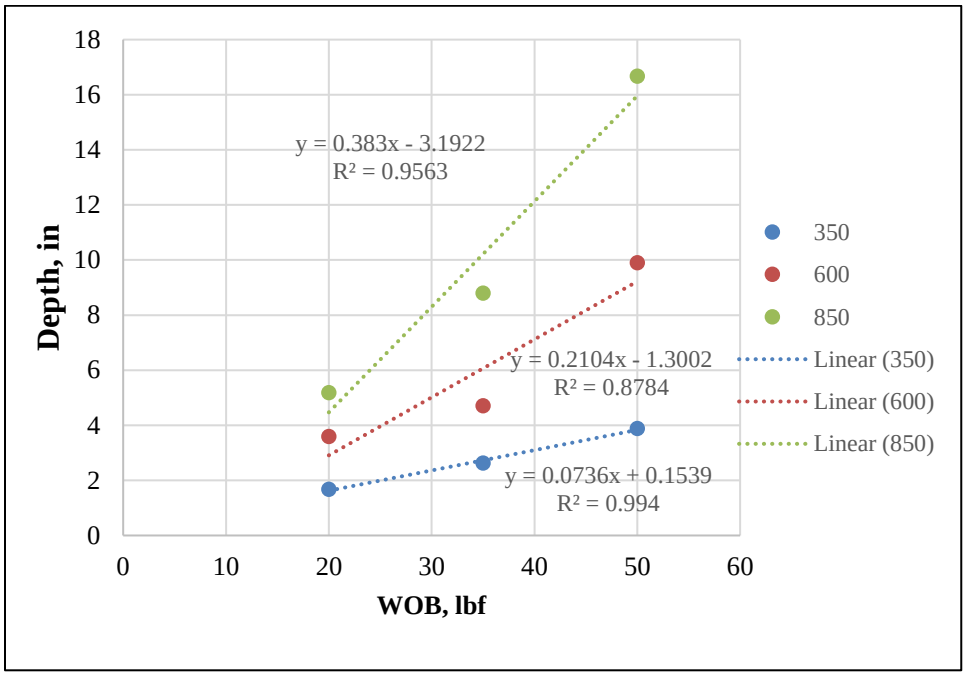

Figure 31. Depth vs WOB for cable drilling

Further analysis shows that increasing RPM by 145.9% (from 350 to 850 RPM) leads to a corresponding increase in TD of about 209.2% at 20lbf, 234.5% at 35 lbf and 329.5 % at 50 lbf. Moreover, at 350 RPM, TD for wells drilled at 20 lbf increases by 57.0% when drilled at 35 lbf and increases at only 47.6% when drilled at 50 lbf. Also, at 800 RPM, TD for wells drilled at 20 lbf increases by 69.9% when drilled at 35 lbf and increases at 89.5% when drilled at 50 lbf. The 89.5% increase is higher than the 63.1% increase in the rotating drill pipe and could be evidence of more efficiency at higher speeds for the vertical cable drilling system. Since the system is sliding during the vertical drilling process, friction plays a role, but this friction is not investigated in this study.

At 50 lbf, 850 RPM, the drill bit broke through the sample in 6 minutes. Thus, to get a normalized sample for comparison at 10 minutes, the average ROP was used to extrapolate the data. Also, the data at 20 lbf, 600 was initially recorded at 725 RPM. Thus, the proportional relationship was established, and the drilled depth at 600 RPM was determined.

5.1.3 Directional Well

From **Figure 32**, the depth increases significantly as WOB increases with increasing RPM. The linear trend lines seem to fit the data quite well and could be a basis for interpolation or extrapolation of actual data based on the linear relationships. The data should, however, be looked at with some associated uncertainty, as the true data WOB values recorded were averages.

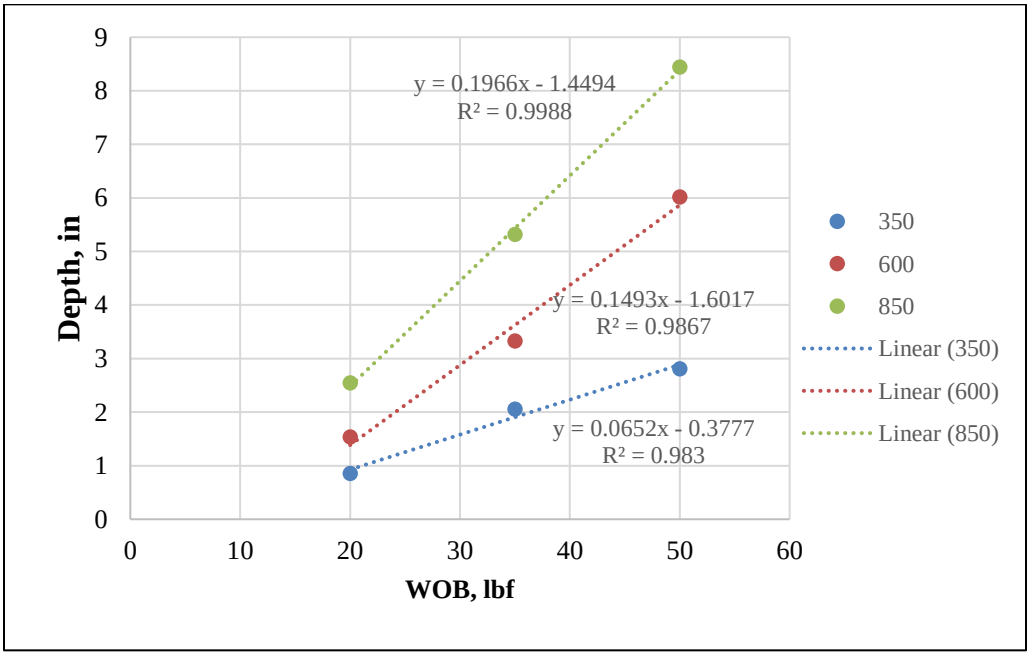

Figure 32. Depth vs WOB for directional well

Further analysis shows that increasing RPM by 145.9% (from 350 to 850 RPM) leads to a corresponding increase in TD of about 198.1% at 20lbf, 158.8% at 35 lbf and 200.4 % at 50 lbf. Moreover, at 350 RPM, TD for wells drilled at 20 lbf increases by 140.9% when drilled at 35 lbf and increases at only 36.8% when drilled at 50 lbf. This reduction in percentage TD gain could be

linked to the markedly sharp decrease in net inclination gain at 50 lbf. Also, at 800 RPM, TD for wells drilled at 20 lbf increases by 109.1% when drilled at 35 lbf and increases at only 58.8% when drilled at 50 lbf. Furthermore, at 800 RPM, the slight increase in TD from 36.8% to 58.8% could be attributed to the 145.9% increase in RPM.

The TD gained in any drilling process is tightly governed by the friction between the drill pipe and rock during the drilling process. Since these are directional wells, the inclination gained (γ) thus governs friction values, and thus affects TD as well.

5.1.4 Comparison of Rotating Drill pipe and Vertical Cable Drilling

From **Figure 33**, the linear equations on the left represent the cable drilling relationships and those on the right represent the rotating drill pipe relationships. It can be seen that generally, the TD values are very close, except at a high RPM value of 850, where the cable drilling method has a much higher calculated TD than the rotating method. Thus, cable drilling might be a better system over the rotating pipe at higher RPM values. Further investigation of other drilling parameters is necessary to clarify these two systems

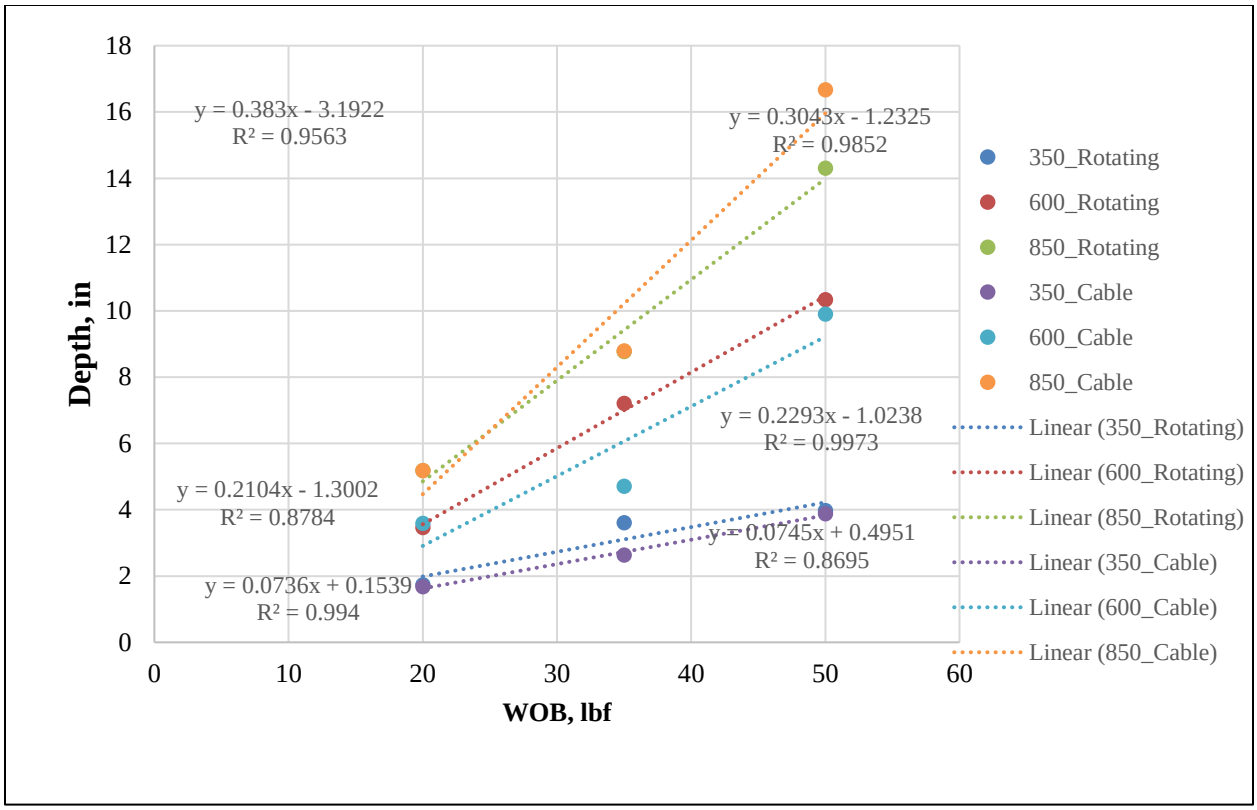

Figure 33. Depth vs WOB for rotary drilling and cable drilling for comparison

5.2 ROP

5.2.1 Rotating Drill pipe

As can be seen from the plot below, ROP follows the same trend seen in the previous graphs for other parameters. As with the other data the data should, however, be looked at with some associated uncertainty, as the true data WOB values recorded were averages.

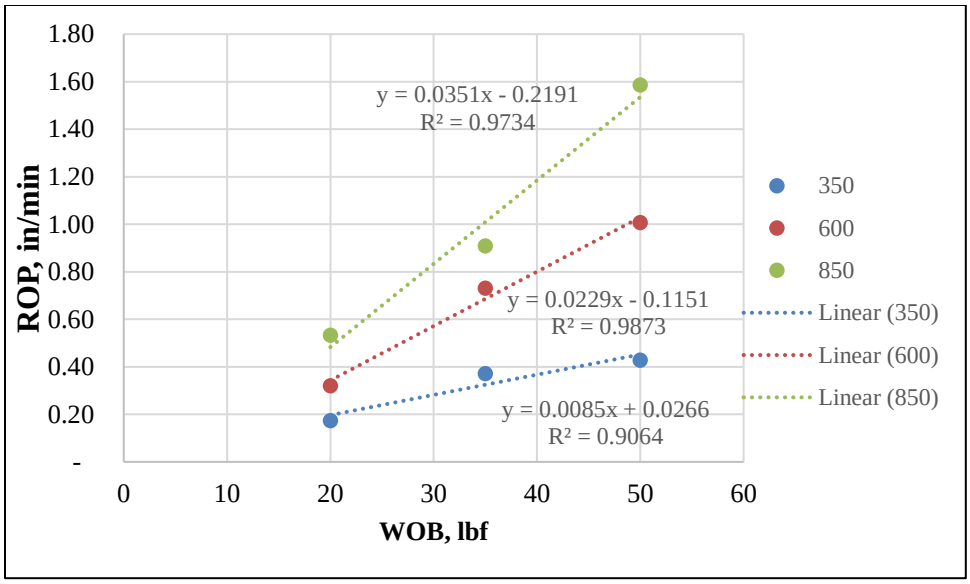

Figure 34. A plot of ROP vs WOB

Further analysis shows that increasing RPM by 145.9% (from 350 to 850 RPM) leads to a corresponding increase in ROP of about 207.7% at 20lbf, 144.3% at 35 lbf and 270.0 % at 50 lbf. Moreover, at 350 RPM, ROP for wells drilled at 20 lbf increases by 114.8 % when drilled at 35 lbf and increases at only 15.2% when drilled at 50 lbf. This reduction in percentage ROP gain could be linked to WOB being a limiting factor in the increase of ROP in this drilling system. Thus, increasing RPM is more beneficial than increasing WOB. Also, at 800 RPM, TD for wells drilled at 20 lbf increases by 70.4% when drilled at 35 lbf and increases at 74.5% when drilled at 50 lbf.

Interestingly, at 20 lbf, 850 RPM, a high ROP of 0.84 in/min is reached. Also, at 35 lbf, a high ROP of 1.5 in/min is reached, and similarly, a high ROP of 2.4 in/min is reached for 50 lbf at 850. Furthermore, a similar explanation for the ROP gained in any drilling process is similar to the discussion section for the above parameters; friction.

5.2.2 Cable Drilling

As can be seen from the plot below, ROP follows the same trend seen in the rotating drill pipe graph. As with the other data the data should, however, be looked at with some associated uncertainty, as the true data WOB values recorded were averages.

Further analysis shows that increasing RPM by 145.9% (from 350 to 850 RPM) leads to a corresponding increase in ROP of about 251.7 % at 20lbf, 239.1% at 35 lbf and 294.8 % at 50 lbf. Moreover, at 350 RPM, ROP for wells drilled at 20 lbf increases by 63 % when drilled at 35 lbf and increases to 65% when drilled at 50 lbf. This reduction in percentage ROP gain could be linked to WOB being a limiting factor in the increase of ROP in this drilling system. Thus, increasing RPM is more beneficial than increasing WOB. Also, at 800 RPM, TD for wells drilled at 20 lbf increases by 57.1% when drilled at 35 lbf and increases at 92.1% when drilled at 50 lbf.

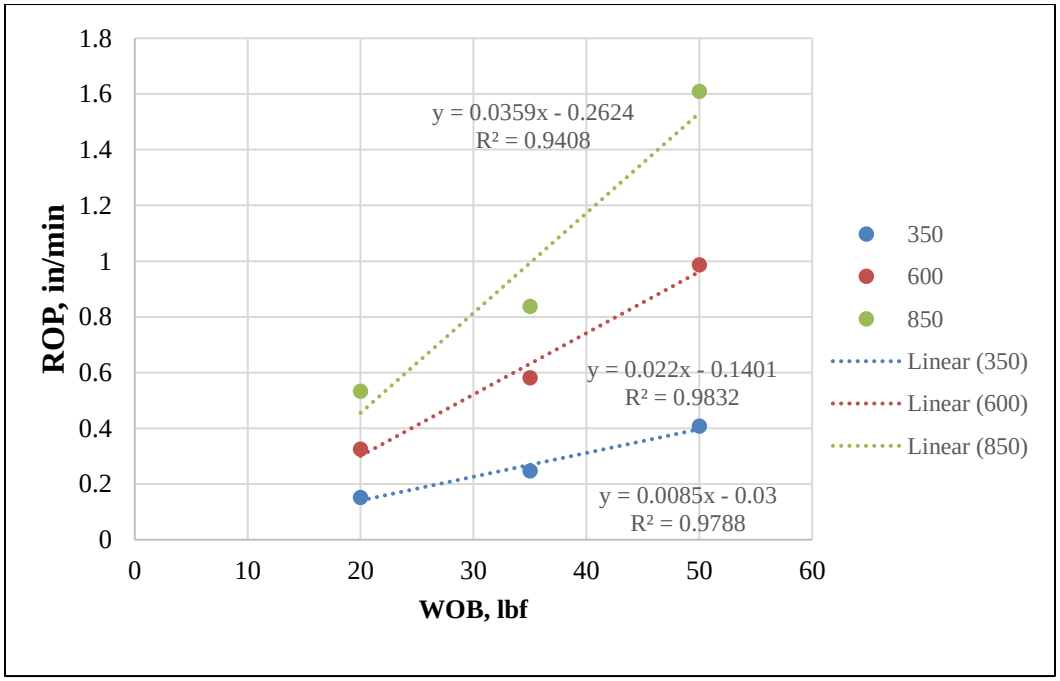

Figure 35. ROP vs. WOB for Vertical Cable drilling

5.2.3 Directional Wells

From **Figure 36**, ROP increases significantly as WOB increases with increasing RPM. The linear trend lines seem to fit the data quite well and could be a basis for interpolation or extrapolation of actual data based on the linear relationships. The data should, however, be looked at with some associated uncertainty, as the true data WOB values recorded were averages.

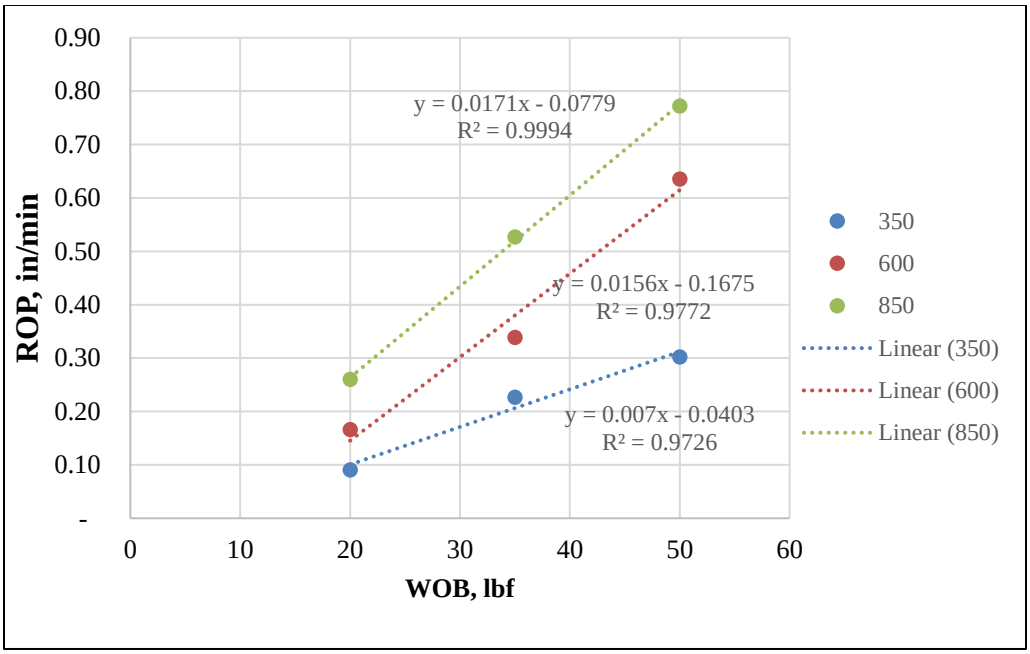

Figure 36. ROP vs WOB for directional well

Further analysis shows that increasing RPM by 145.9% (from 350 to 850 RPM) leads to a corresponding increase in ROP of about 187.5% at 20lbf, 132.2% at 35 lbf and 155.8% at 50 lbf. Moreover, at 350 RPM, ROP for wells drilled at 20 lbf increases by 150.9% when drilled at 35 lbf and increases at only 33.1% when drilled at 50 lbf. This reduction in percentage ROP gain could be linked to the markedly sharp decrease in net inclination gain at 50 lbf, as was the case in the TD discussion. Also, at 800 RPM, TD for wells drilled at 20 lbf increases by 102.7% when drilled at 35 lbf and increases at only 46.5% when drilled at 50 lbf. At 800 RPM, the slight increase in TD from 46/5% to 102.7% could be attributed to the 145.9% increase in RPM.

Interestingly, at 20 lbf, 850 RPM, a high ROP of 0.73 in/min is reached. Also, at 35 lbf, a high ROP of 1.17 in/min is reached, and similarly, a high ROP of 1.2 in/min is reached for 50 lbf at 600. There is a region in the 600 RPM data that instantaneous sharp increase in ROP, where 50 lbf 800 has a high ROP of 1.1 in/min. Such high ROP for 50 lbf significantly increases the TD as seen in the earlier discussion, but also takes away from the inclination build, as will be discussed down below. Furthermore, a similar explanation for the ROP gained in any drilling process is similar to the discussion section for the above parameters; inclination and thus friction.

5.3 MSE Values

5.3.1 Rotating Drill pipe

In this series of tests, the lowest MSE corresponds to 50 lbf at 600 RPM, with the highest corresponding to 20 lbf 350 RPM. At 20 lbf and 50 lbf WOB, high RPM values seem to be slightly more efficient than low RPM values. As seen in **Figure 37**, this trend, however, reverses at 35 lbf WOB, where low RPM becomes more efficient.

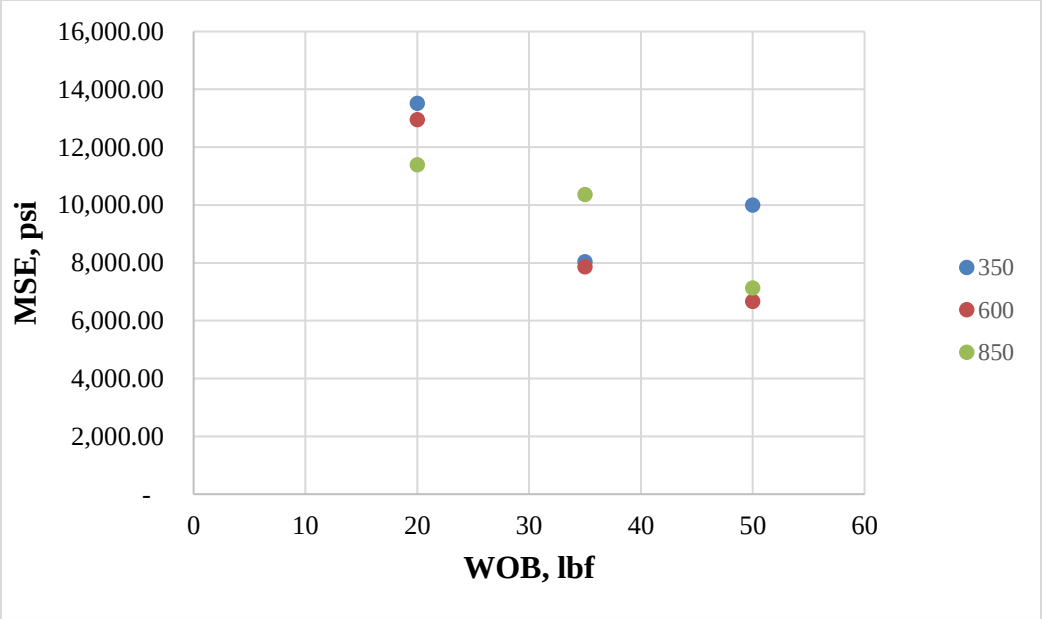

Figure 37. MSE vs WOB for Rotating Drill pipe

5.3.2 Cable Drilling

For the vertical cable drilling, the system is seen to be highly inefficient compared to the rotating drill pipe. This is shown by the high MSE values at each test point, as seen in **Figure 38**. This, however, gives some perspective on the efficiency of the directional system, which relies on the cable drilling technique. For 20 lbf WOB, low RPM values seem to be more efficient. This trend starts to reverse as the WOB increases to 50 lbf.

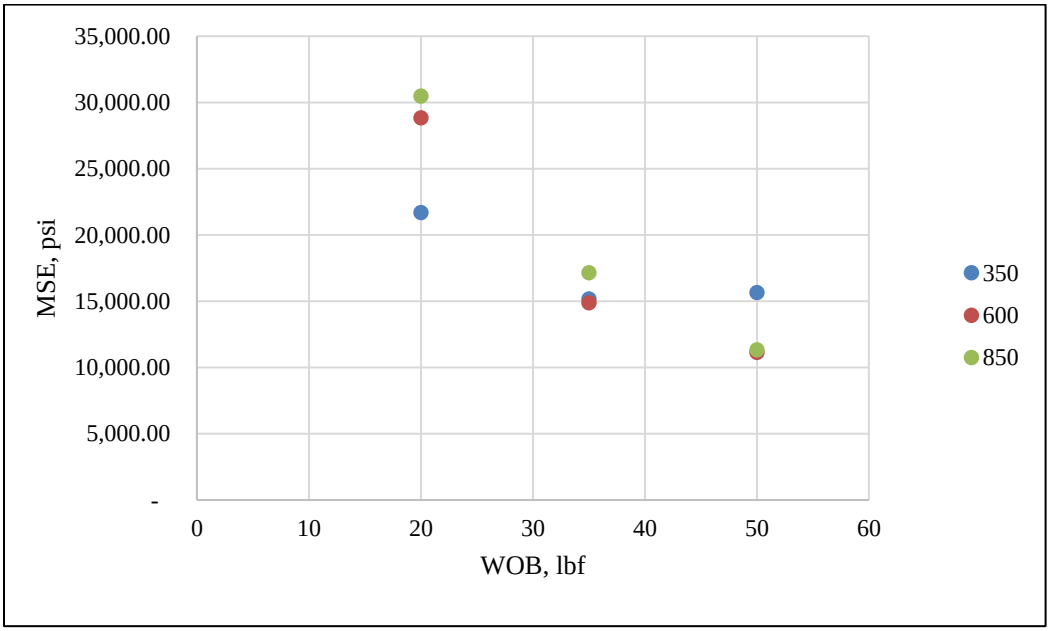

Figure 38. MSE vs WOB for vertical cable drilling

5.3.3 Directional Wells

From **Figure 39** below, it seems 35 lbf at 350 RPM is the most efficient drilling state, followed closely by 50 lbf at 600 RPM. The most inefficient is drilling at 20 lbf, 350 RPM. Thus, one should consider the total angle to be achieved, and break down the drilling plan based on the most efficient way to achieve overall well inclination. The MSE values were calculated using the average ROP, average RPM, and average WOB values. This showed to be a better technique, since calculating

the MSE for each data point and finding the corresponding average created data which skewed the results.

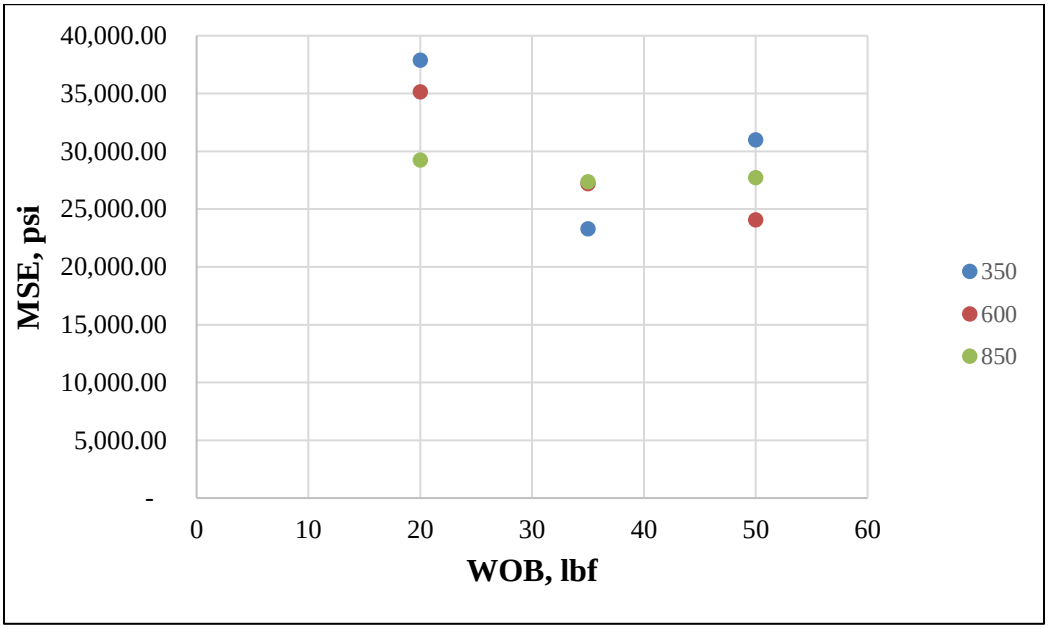

Figure 39. MSE vs WOB for directional well

That notwithstanding, it's not too clear why extremely low ROP values were recorded for the 20 lbf, 350 RPM and 35 lbf, 350 RPM test data, as seen in **Figure 40**. It could be that at these rotational speeds, and at the steep inclination being built, there were zones that were difficult to penetrate, and could be indicative of inflection points in the build of the curve. However, further research is required to fully investigate this behavior.

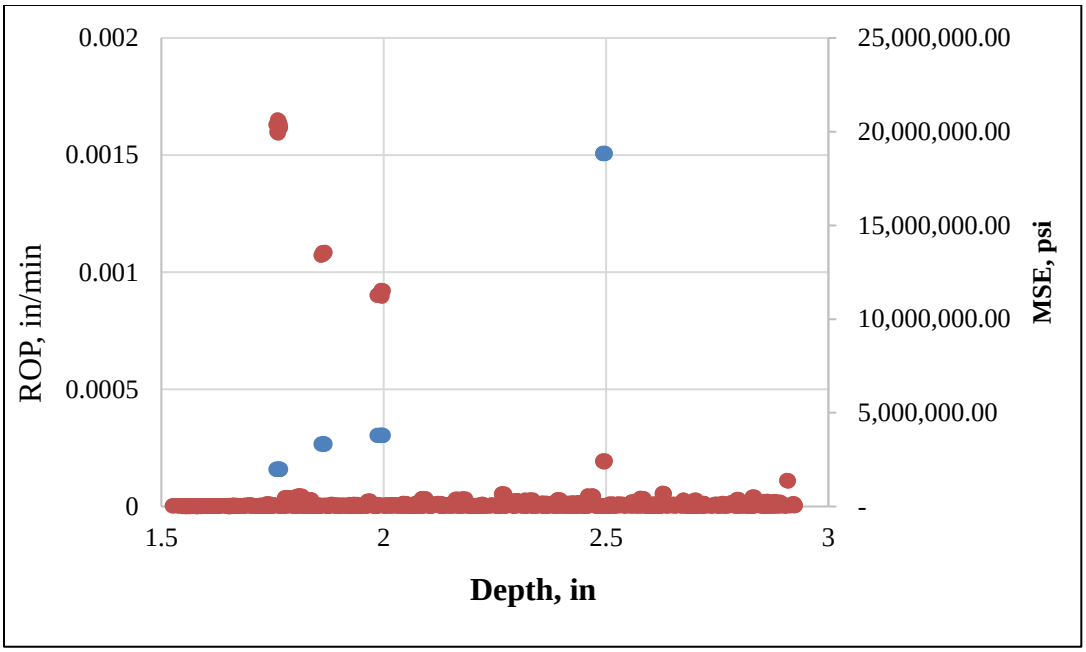

Figure 40. ROP, MSE vs. Depth for DW 20 lbf, 350 RPM

The ROP scale on the left is capped at 0.002 in/min to show how the incredibly low ROP values inversely agree with the high MSE values. It can be seen from the above plot that at 20 lbf, 350 RPM, there are markedly low ROP values and correspondingly high MSE values. It could be inferred that these are the regions during which the system reaches critical momentum to initiate an increase in inclination. By cross-referencing the data with the inclination data, it can be seen that this test had a high resulting inclination value.

Since MSE values are inversely correlated with ROP, the higher the ROP, the lower the MSE. In the 50 lbf 600 RPM data set, there was a recorded high ROP of 1.2 in/min, with a correspondingly low MSE of 25,422 psi. However, this momentary ROP was not used in the analysis of the average, as this skewed the data.

5.4 Inclination Response

The initial idea going into this project was that the higher the WOB, the higher the inclination. Thus, the goal was to quantify by how much increases in WOB affected inclination. Also, to investigate the effect of RPM on directional data. As can be seen from **Figure 41** inclination values increase as one moves from 20 lbf to 35 lbf, with the highest inclination values of 25.7° being recorded at 35 lbf 600 RPM. There is a reversal in the trend however, at high WOB of 50 lbf, where the maximum inclination value drops to about 13°, about half the reduction from 25.7°.

It is postulated that at high enough WOB values, the vertical component of the force in directional drilling overtakes the lateral component. Thus, this tends to move the BHA downward more that sideways to build angle. Also, the extremely low ROP regions seen in Figure 40 is indicative of the system putting in more energy to deviate, and not necessarily to increase TD. At 50 lbf, the lowest recorded ROP is 0.05 at 350 RPM and 0.26 at 600 RPM and 0.47 at 800 RPM. Thus, all the system's energy goes into pushing the bit downwards, and not sideways. The legend on the right hand side is stated in the format WOB_RPM.

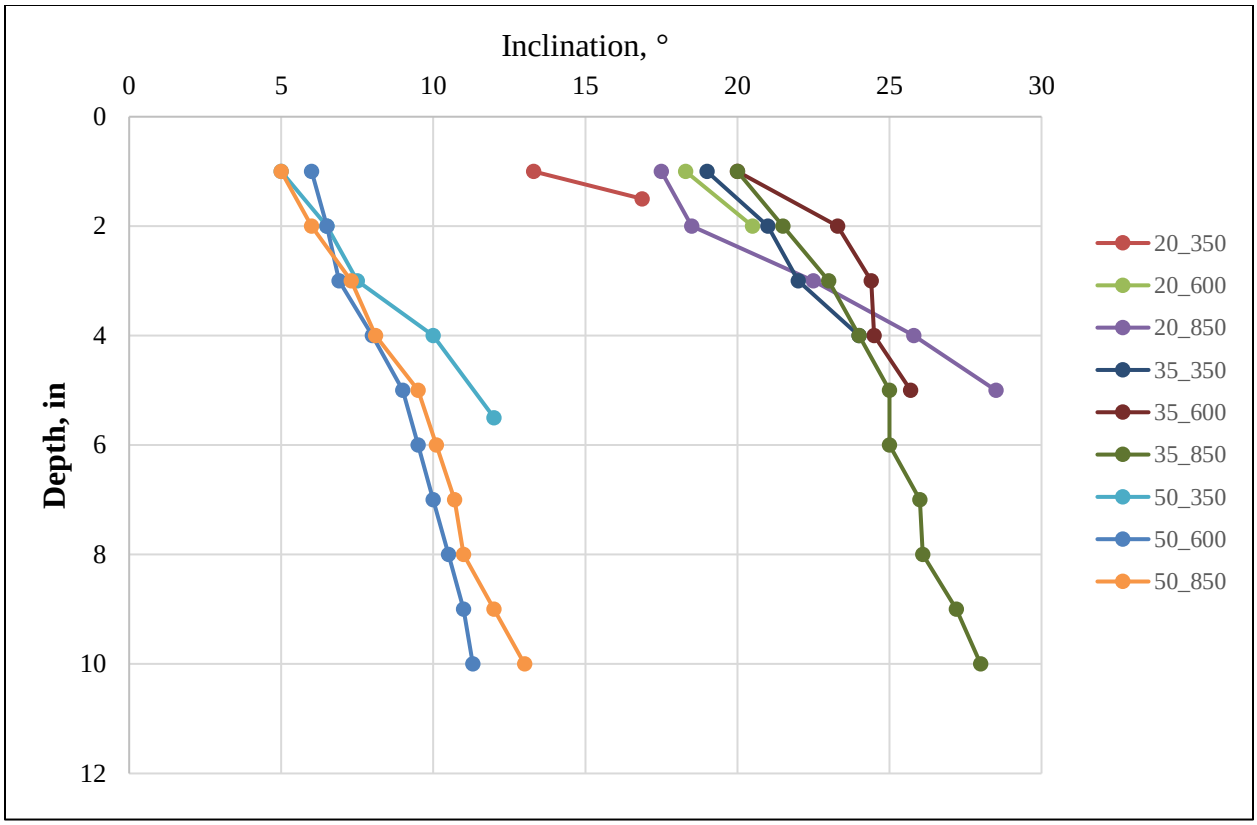

Figure 41. Depth vs. Inclination for Directional wells

5.5 Preliminary Conclusions

- TD is more heavily correlated to RPM than to WOB for this range of values tested. Thus, it's better to increase the speed of drilling within reasonable limits (MSE values) than to increase WOB values. This is seen in all drilling systems.
- For the rotating drill pipe, there is an increase of only 10.2% when WOB is increased from 35 lbf to 50 lbf. This reduction in percentage TD gain could be linked to WOB being a limiting factor in the increase of TD in this drilling system. Thus, increasing RPM is more beneficial than increasing WOB, for the range of values tested.
- For the rotating drill pipe, a stabilizing unit could have helped to solve the problem where drilling stops at 8 inches.

- At high RPM values, the cable drilling technique proves to drill more efficiently than the rotating drill pipe. This shows in the low MSE values calculated from the resulting drilling data. At low rpm values, however, the cable drilling technique is less efficient than the rotating drill pipe, as seen in the correspondingly high MSE values. Also, for the same drilling time, the cable drilling method generally has higher ROP and TD values, compared to the rotating drill pipe for high RPM. Furthermore, the response torque for the cable drilling technique is much higher than that of the rotating drill pipe, with about twice the torque values for higher RPM values.
- At 350 RPM, ROP for wells drilled at 20 lbf increases by a large percentage when drilled at 35 lbf but increases at a much smaller percentage when drilled at 50 lbf. This reduction in percentage TD and ROP gain across the drilling reduction could be linked to WOB being a limiting factor in the increase of TD, and consequently ROP in the drilling systems. Thus, increasing RPM is more beneficial than increasing WOB.
- As expected, total depth (TD) and ROP increase with increasing WOB and RPM. Similarly, response torque also increases, but only slightly.
- MSE values for directional wells increase due to significant friction in the borehole.
- Generally, higher RPM produces more torque in the drill pipe.
- Increasing WOB increases wellbore inclination up to a certain point, after which there is a net decrease in inclination gain.

Chapter 6. Vibration Simulation

As previously discussed in chapter 2, the Finite Element Method has significant usefulness in engineering applications, as it allows for the modeling and analysis of complex engineering problems. Premium software that allows for this analysis is ANSYS Workbench V19.1, and this is used in this simulation. This tool allowed for multiple cases to be run for the vertical and directional well configurations in order to qualitatively analyze the different vibration modes induced under specific loadings. The BHA response according to its deformation is compared.

6.1 FEM Simulation Setup

The objective of this study is to run an FEM analysis of the experimental setup used for vertical and directional wells and compare the three modes of vibrations to gain more insight into vibration mitigation. A transient analysis was selected for the modeling, and the simulation was run over a specific period.

The model was built in Solidworks 2019, which is a computer-aided design (CAD) software. As seen in the figures below, a drill pipe is connected to a drill bit with a stabilizer directly on top of the drill bit for the purpose of stabilizing the pipe. This is done for the vertical well configuration (**Figure 42**) and the directional well configuration (**Figure 43**). The dimensions of the model components are shown in **Table 5.**

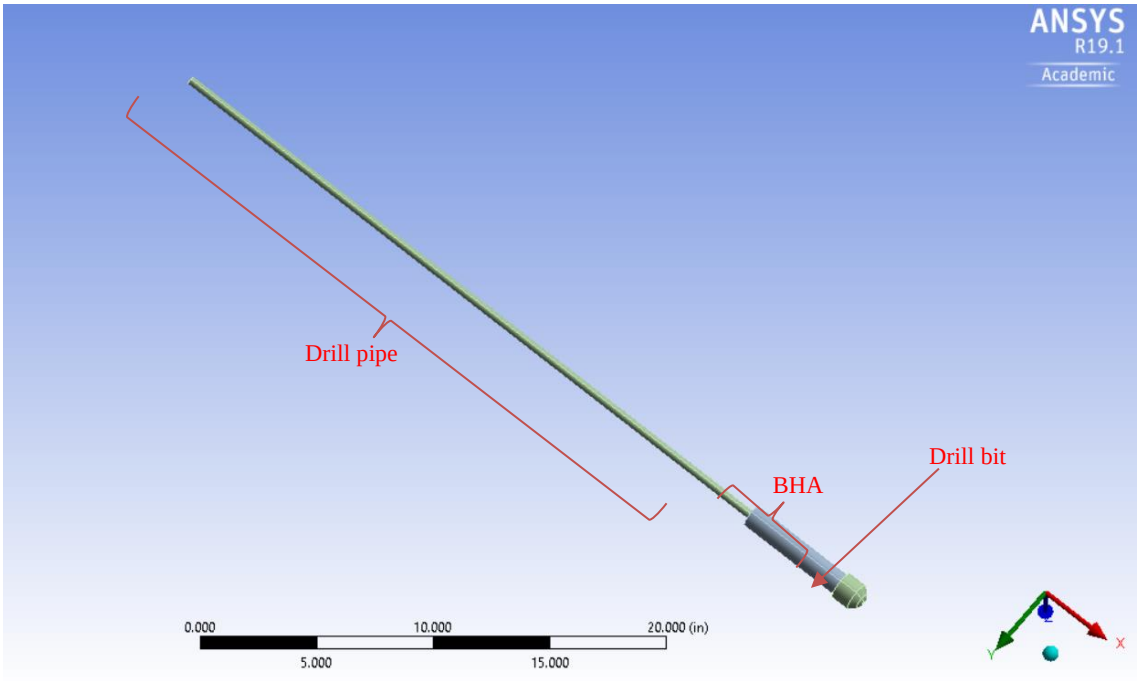

Figure 42. Vertical well configuration model setup used for simulation

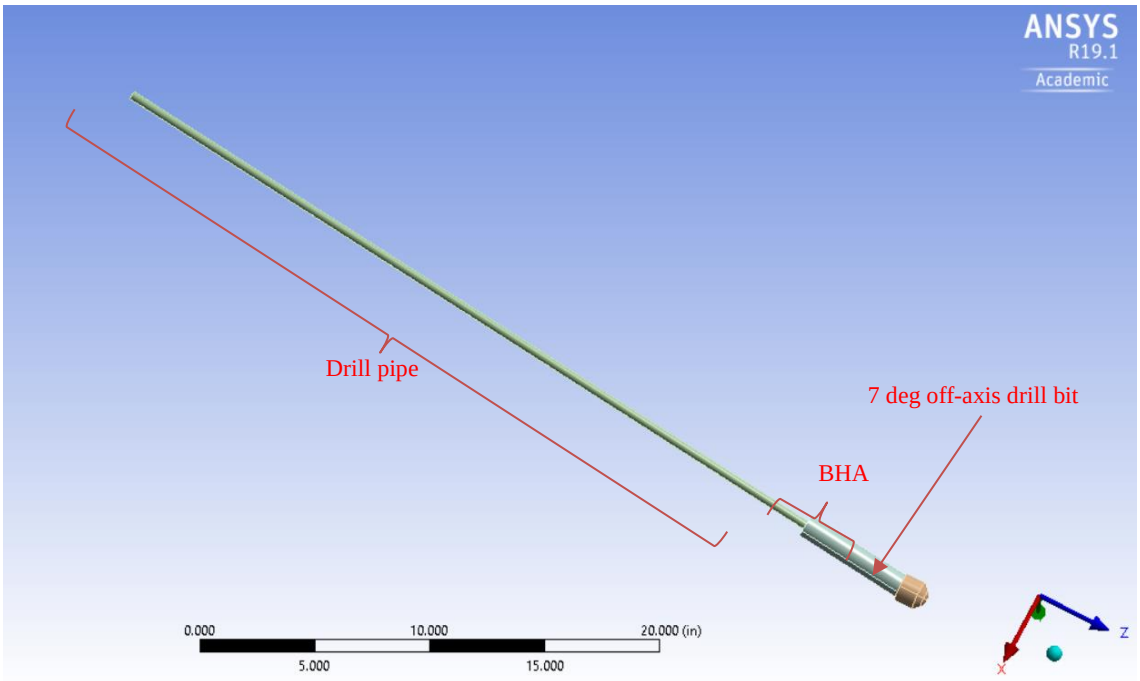

Figure 43. Directional well configuration model setup used for simulation

Table 5. Dimensions for the CAD model

Component	Length, in	OD, in	ID, in
Drill pipe	36	0.375	0.277
Stabilizer	5	1	0.375
Drill bit	1.5	1.5	-

It is overly obvious that wellbore friction has a critical effect on vibrations. However, due to computationally expensive analysis of including a wellbore, with no previous knowledge of studies to compare results to, it was decided to not include the wellbore geometry. Adding a wellbore will create a collision and non-linear dynamics, which requires more computing resources. Also, the purpose of the study is to examine the unaltered behavior of the drill string when the three vibration modes are induced and coupled in a single analysis. Including a wellbore will be detrimental, since it will influence the behavior of the pipe.

A curvature type size function with a tetrahedron shaped elements were used for the meshing. Aluminum was used as the material for the string and the drill bit for simplicity; this was available through the material's library preloaded into Ansys's Engineering Library. Structural steel was used for the BHA, and it was also available in the Library.

Careful attention was paid to the boundary conditions applied to this model. Chacin, 2017 runs a similar study on real-scale drill pipe, however, no other finite element model has coupled the three modes of vibration in a single analysis on a lab-scale (to the best of the author's knowledge). Thus, there wasn't much to compare to the initial conditions. Considering this, very careful attention was paid to the boundary conditions for this study.

The summary of the studied cases is shown in **Tables 6** and **7.** This details the torque applied, WOB (axial loading), and displacements. The average torque values from the experiments were used in order to recreate torsional vibrations, a torque, and this was applied in a sinusoidal function at an angular velocity of the set RPM used for that experiment as well. The WOB value also

corresponded to the average WOB values the experiments were run at. Finally, a sinusoidal function was used in generating the lateral disturbances. A displacement value of 1 inch was used in this study as this corresponded to the average elongation of the drilled wellbores from the experimental test. For the lateral displacements, Chacin et al. found the best configuration for application; this happens to be at 90 degrees between the time of application. Hence this was used (2017). Later, the rest of the cases run were done at the same drilling parameters investigated in the experimental setup to study the magnitudes of how the loads affected the overall vibrational response.

6.2 Boundary Conditions

For the first case, constant loads of WOB and torque were applied at the bit. Thus, only displacements were set using a sinusoidal function to recreate one mode of vibration. For this second case, a sinusoidal function was used to create the value of WOB and torque at different time intervals. This was to replicate a more realistic scenario, and also see the difference in response between constant torque application and torque being applied as some function, as all modes of vibration were thus being induced. This was done for both the vertical well configuration and the directional well configuration. Tables 6 and 7 below show the torque magnitude values in lbf-in for the cases run at different angular velocity and different WOB for the vertical well and directional well respectively.

Table 6. Values for Boundary Conditions for Vertical Well

RPM		350	600	850
WOB, lbf	20	4.37	4.52	4.67
	35	5.58	6.25	7.25
	50	7.15	7.33	8.69

*Lateral disturbance in X-axis = $Displacement * Sin(wt)$
*Lateral disturbance in Z-axis = $Displacement * Sin(wt + 90)$
*'w' corresponds to the different RPM values, in rad/s used to run each case.

The same was also done for the case of directional wells, as **Table 7** below shows the values used.

Table 7. Values for Boundary Conditions for Directional Well

RPM		350	600	850
WOB, lbf	20	6.34	6.33	5.82
	35	9.97	10.04	11.03
	50	17.28	16.70	16.38

*Lateral disturbance in X-axis = $Displacement * Sin(wt)$
*Lateral disturbance in Z-axis = $Displacement * Sin(wt + 90)$
*'w' corresponds to the different RPM values, in rad/s used to run each case.

Several time step values were considered, and it was decided to use a time step of 0.02 seconds was used in the simulation. This helped to cover the full spectrum of the load application without any observing any peak truncation. This also allowed for a reduction in computation time, without compromising on solution accuracy. Thus, total analysis time of 6 seconds was performed. This seemed to be adequate to obtain the desired response.

In order to properly replicate vibration in the simulation, a fixed support restriction was used on the top of the drill pipe. A frictionless support was placed around the stabilizers to assume ideal contact between the wellbore and stabilizers which is not of course, what is observed in the field. This, however, provided multiple errors and was thus removed.

6.3 Material Properties

The material used is aluminum and structural steel. **Table 8** below shows the properties acquired from the non-linear library in ANSYS.

Table 8. Material properties for metals used in the simulation

	Aluminum				Structural Steel			
	SI units		Standard units		SI units		Standard units	
Density	2770	Kg/m^3	172.93	lbf/ft^3	7850	Kg/m^3	490.06	lbf/ft^3
Young's Modulus	7.10E+10	Pa	1.03E+07	psi	2.00E+11	Pa	2.90E+07	psi
Poisson's Ratio	0.33	-	0.33	-	0.3	-	0.3	-
Bulk Modulus	6.96E+10	Pa	1.01E+07	psi	1.67E+11	Pa	2.42E+07	psi
Shear Modulus	2.67E+10	Pa	3.87E+06	psi	7.69E+11	Pa	1.12E+08	psi

6.4 Special Considerations

The first consideration was not to include the borehole, as this tremendously increases the complexity and computational resources used for the analysis. The second consideration was not to include fluid in this analysis. This will also aid in proving the unaltered behavior of the drill string when coupled modes of vibration are applied. The author knows there is fluid flow in the real case, as fluid aids in carrying the cuttings to surface, lubricating the drill bit, among other things. Fluid viscosity will affect vibration dampening in the drill string, and thus affect the response. Also, for the transient analysis settings, the 'large deformations' options were activated. This is because the drill pipe is quite thin at 0.049 inches in comparison to its 36-inch length. This activation allows ANSYS to consider material stiffness changes in this analysis due to large deflections.

Furthermore, for the damping controls in the analysis settings, a numerical damping value of 0.1 was used, as well as a value of 0 for both the stiffness and mass coefficients. Chacin analyzed the damping "Rayleigh model" and figured out this was a common initial value used by ANSYS for nonlinear analysis. For further work, "Damping vs. Frequency" data can be obtained and used as input for the software's analysis, as these values have a significant impact on non-linear models, especially ones with large deflections, where stiffness changes.

Finally, a 'Direct' type of solver was used instead of the 'Iterative' option in the analysis solver section. The 'Iterative' solver is usually used for large setups. Also, the benefits accrued from using the Iterative solver at such a small time step isn't significant.

6.5 Vibrational Response Results

The rotational speed seems to be the governing parameter since the force and torque values applied seemed to be very small. Thus, there isn't much different in the torsional response.

As can be seen from Appendix A, there isn't much difference in the amplitude of vibrations for different cases of loads applied. Thus, the analysis was restricted to rotating speeds, as this seemed to be the governing parameter in vibrations. All the graphs seen below have legends on the right hand side, stated in RPM speed values.

6.5.1 Axial Deflection Response

The higher the RPM, the higher the frequency. For the axial vibrations, 800 RPM seems to have the highest negative displacement, thus compression, and the higher amplitude at the beginning of the simulation. Other speeds have high amplitudes at the start of vibration, but then reduce as the disturbance goes on. This is the case for a constant application of load and torque. From **Figures 44** and **45**, the slower speeds have lower frequencies and less deformation in the negative direction. The maximum deformations are positive (not shown here), however, because the minimum deformations are so low, the average deformation tends to be negative. 850 RPM has the highest amplitude, as it's the higher frequency considered.

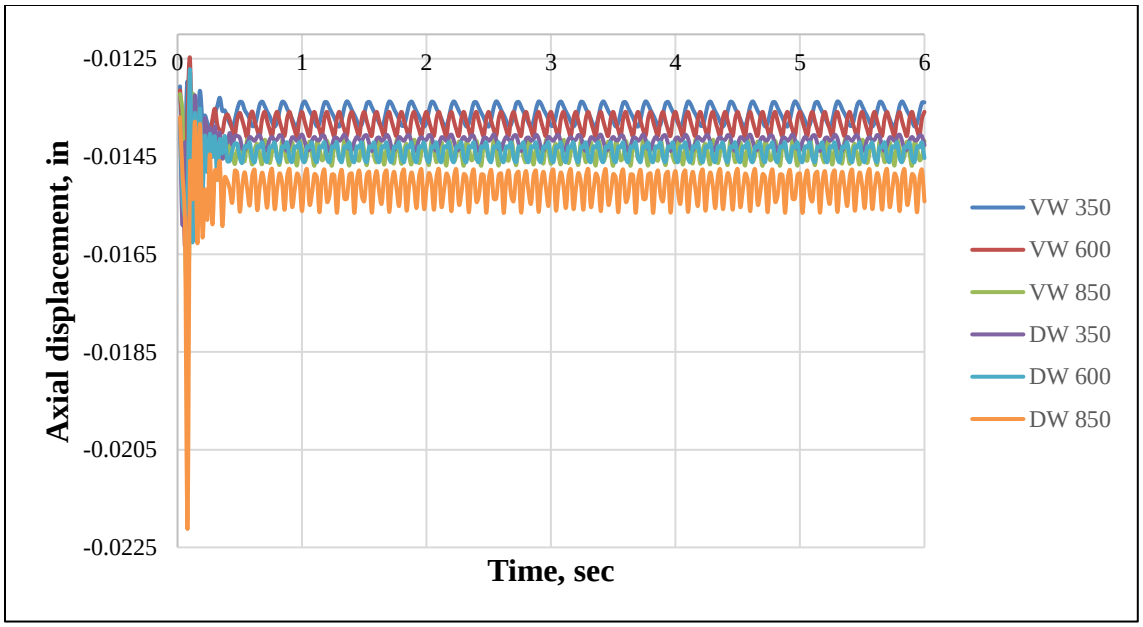

Figure 44. Average Axial Deflection plot; Constant Load Application, WOB = 35 lbf

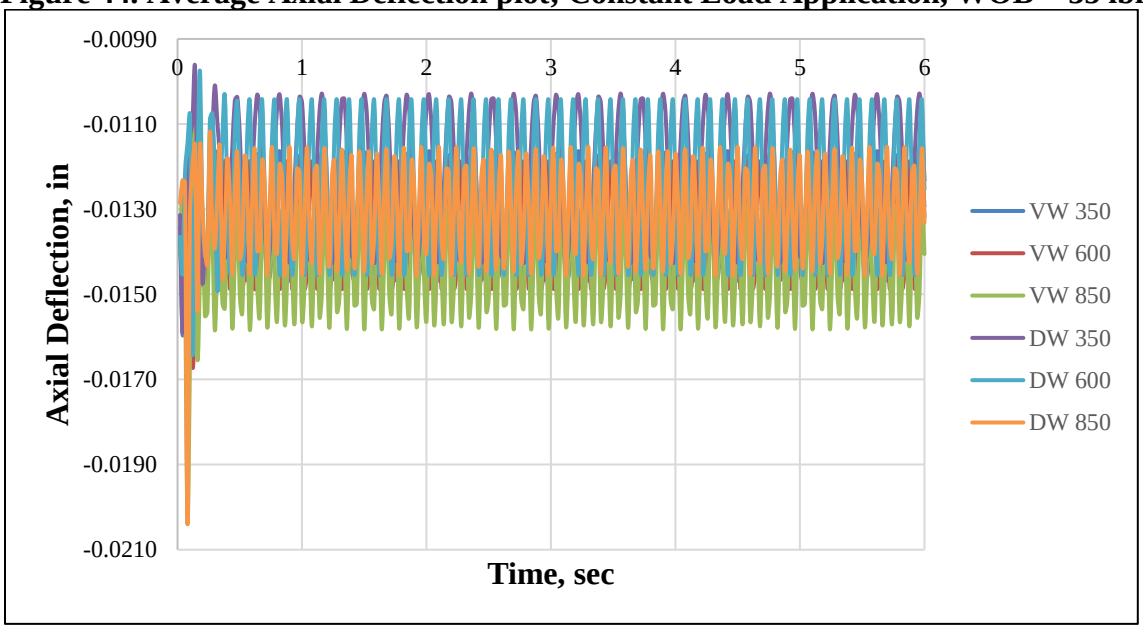

Figure 45. Average Axial Deflection plot; Sinusoidal Load Application, WOB = 35 lbf

Table 9. Maximum Average Axial Deflection

Vertical Well			Directional Well		
Constant Load			Constant Load		
350	600	850	350	600	850
-0.0130	-0.0125	-0.0132	-0.0133	-0.0127	-0.0137
Sinusoidal Load			Sinusoidal Load		
350	600	850	350	600	850
-0.0113	-0.0116	-0.0111	-0.0096	-0.0098	-0.0112

A careful examination of WOB values for the constant loading at 850 RPM shows that increasing loading in the principal axis increases more axial deflection, which is logical. It demonstrates, however, that directional wells have more compression in the axial axis than vertical wells, as seen in **Figure 46**.

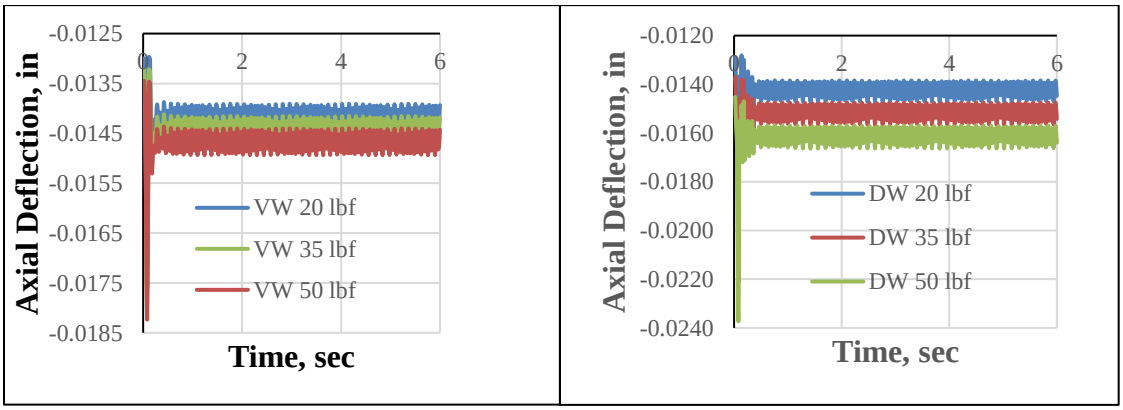

a) b)

Figure 46. Average Axial deflection graphs a) response in vertical well configuration b) response in a directional well configuration.

6.5.2 Lateral Deflection Response

Figure 47 below is a typical graph for maximum, minimum and average lateral deflection values for a vertical well configuration at 850 RPM and 35 lbf.

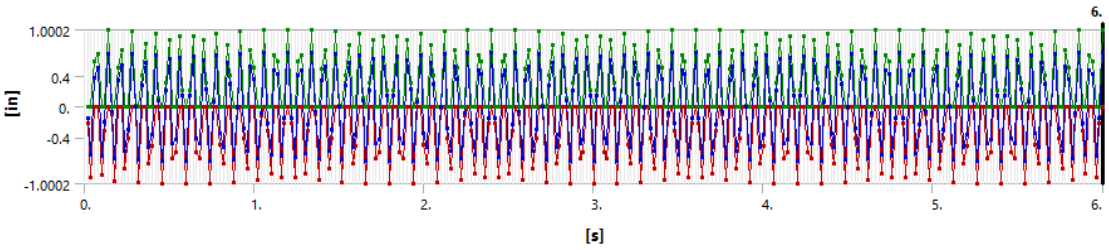

Figure 47. Vertical well; 850 RPM at 35 lbf

Figures 48 and **49** below focus on lateral deflections for 35 lbf WOB. As can be seen, the results are similar and are within a set range, and this shows at different WOB values and different rotational speeds. Please refer to graphs in the Appendix with the pictures at different magnitudes when loads are applied with a sinusoidal function.

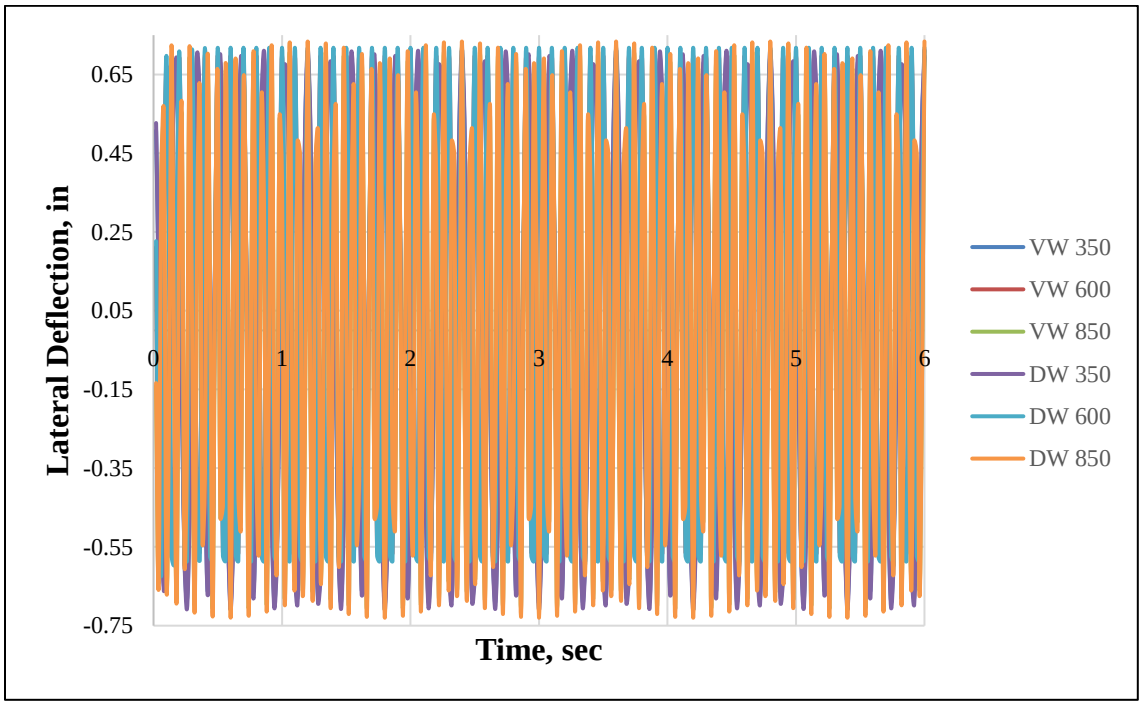

Figure 48. Lateral deflection plot; constant load application, WOB = 35 lbf

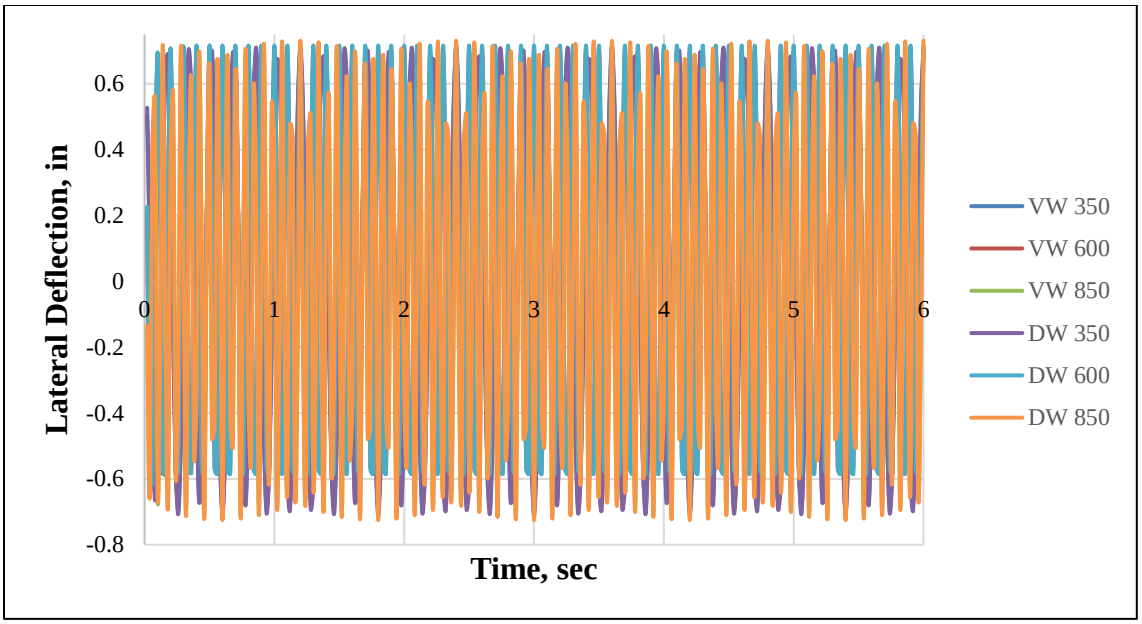

Figure 49. Lateral Deflection plot; Sinusoidal Load Application, WOB = 35 lbf

As stated earlier, the deflections are incredibly close for both the vertical configuration and the directional well configuration as seen in **Table 10** below.

Table 10 Maximum Average Lateral Deflection

Vertical Well			Directional Well		
Constant Load			Constant Load		
350	600	850	350	600	850
0.69338	0.69953	0.71008	0.71241	0.71817	0.73388
Sinusoidal Load			Sinusoidal Load		
350	600	850	350	600	850
0.6944	0.7014	0.71652	0.71183	0.71658	0.73076

6.5.3 Torsional Deflection Response

Figures 50 and **51**below all show similar behavior in the case of the lateral deflection as they are all within a specific range. **Table 11** shows the closeness of these results.

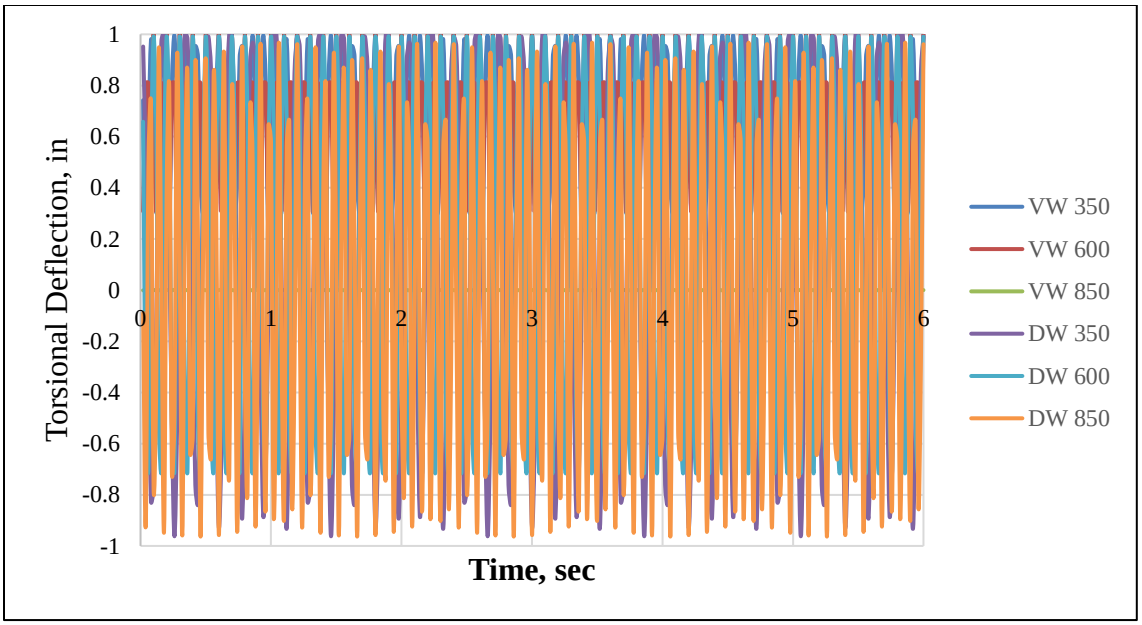

Figure 50. Torsional deflection plot; constant load application, WOB = 35 lbf

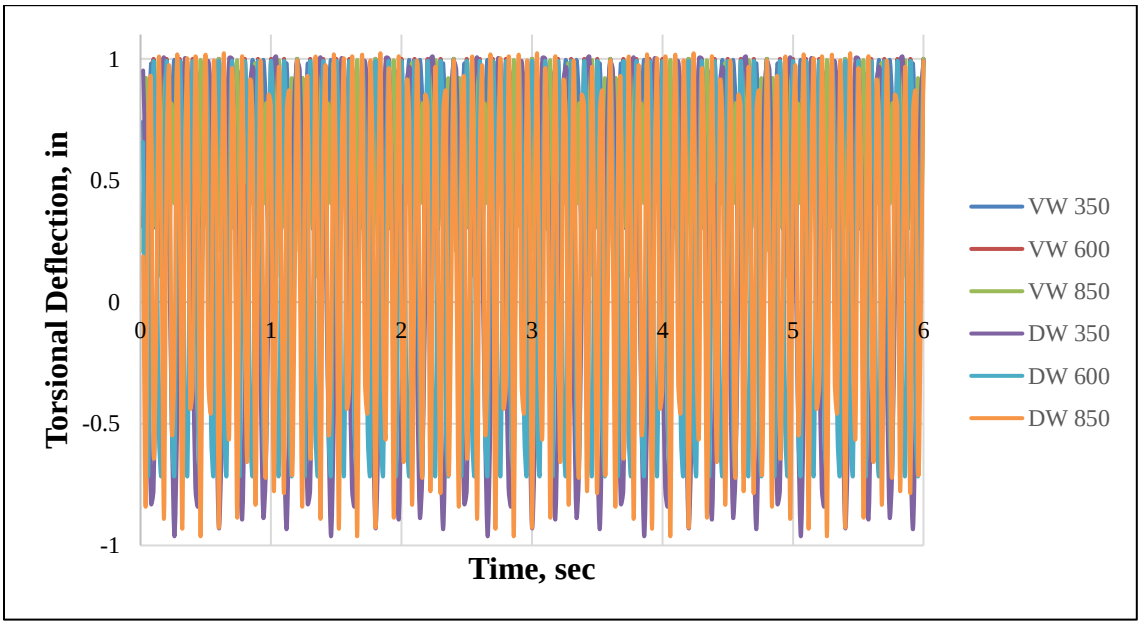

Figure 51. Torsional deflection plot; sinusoidal load application, WOB = 35 lbf

Table 11 below shows how incredibly close the deflections are.

Table 11. Maximum Average Torsional Deflection

Vertical Well			Directional Well		
Constant Load			Constant Load		
350	600	850	350	600	850
1	1.0001	0.000944	1.0089	0.9909	0.96758
Sinusoidal Load			Sinusoidal Load		
350	600	850	350	600	850
1	1.0001	0.99998	1.0087	0.99067	1.0088

6.5.4 Total Deflection Response

In the case of the total deflection, the directional well seems to have a slightly higher total deflection than the vertical well, as seen in **Figure 52** and **53** and **Table 12** Also, the application of load in a sinusoidal fashion seems to slightly increase the response in total deflection, than when a constant mode is applied. Again, this could be due to the scale of the experiments, and further work should be done to investigate this phenomenon.

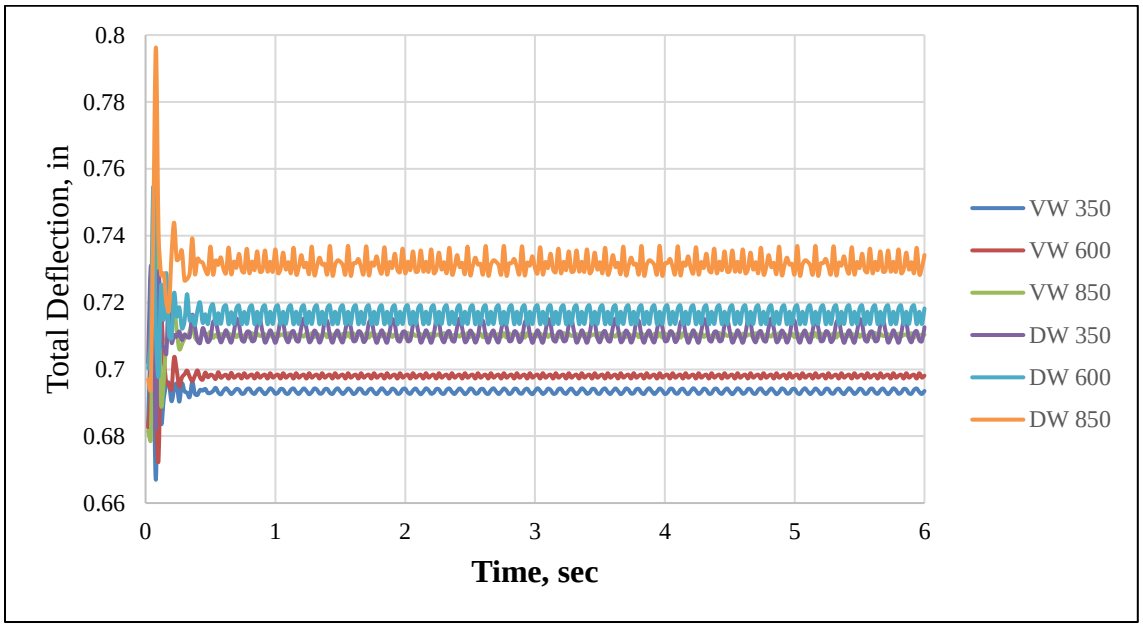

Figure 52. Total deflection plot; constant load application, WOB = 35 lbf

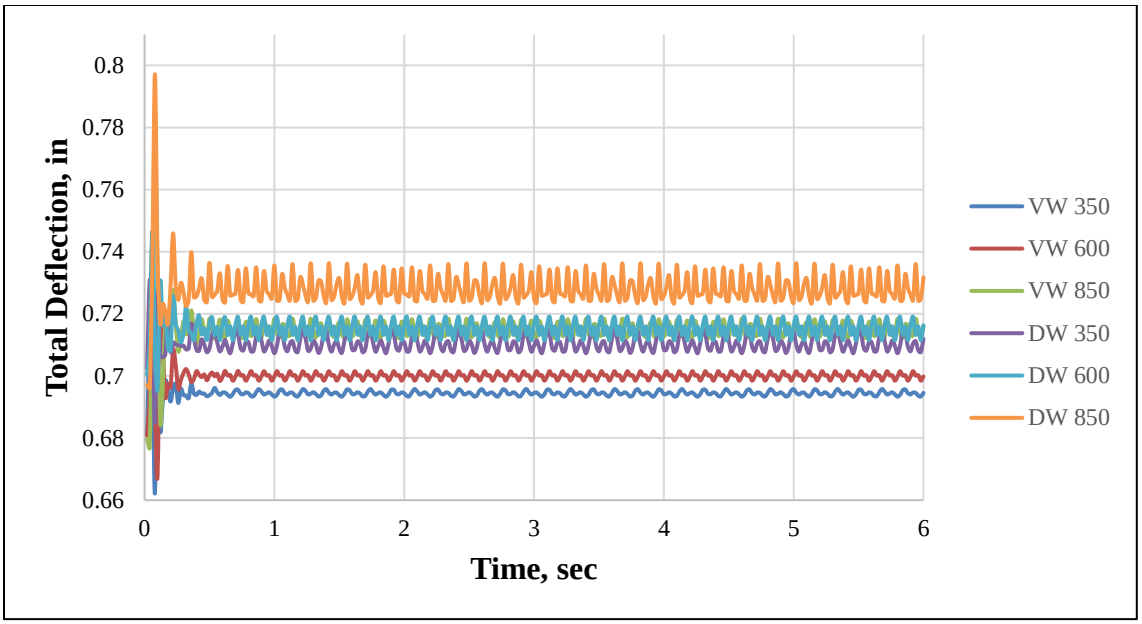

Figure 53. Total deflection plot; sinusoidal load application, WOB = 35 lbf

Table 12. Maximum Average Total Deflection

Vertical Well			Directional Well		
Constant Load			Constant Load		
350	600	850	350	600	850
0.71913	0.73657	0.75981	0.73073	0.75468	0.7963
Sinusoidal Load			Sinusoidal Load		
350	600	850	350	600	850
0.72452	0.74428	0.77992	0.73079	0.74669	0.79713

6.6 Modal Analysis

Modal analysis is typically used to study the response of a structure for dynamic loading.

It is used to determine the natural frequency and mode shapes of the vibration of a structure**.**

The simple model used to run the vibration simulation was used to run a modal analysis to identify the natural frequencies of the system to identify how they connect with the rotating speeds. However, none of the frequencies obtained were within the drilling speeds used. Thus, a more accurate model of the experimental tests was built as seen in **Figure 54** and the first five modes

were determined, as shown in **Table 13.** The first mode is 15.184 Hz which is closest to 14.16 Hz (850 rpm/60 sec). This explains why there is maximum vibration at the highest rotational speed run. These vibrations could be detrimental to the BHA and cause parts to be damaged more frequently.

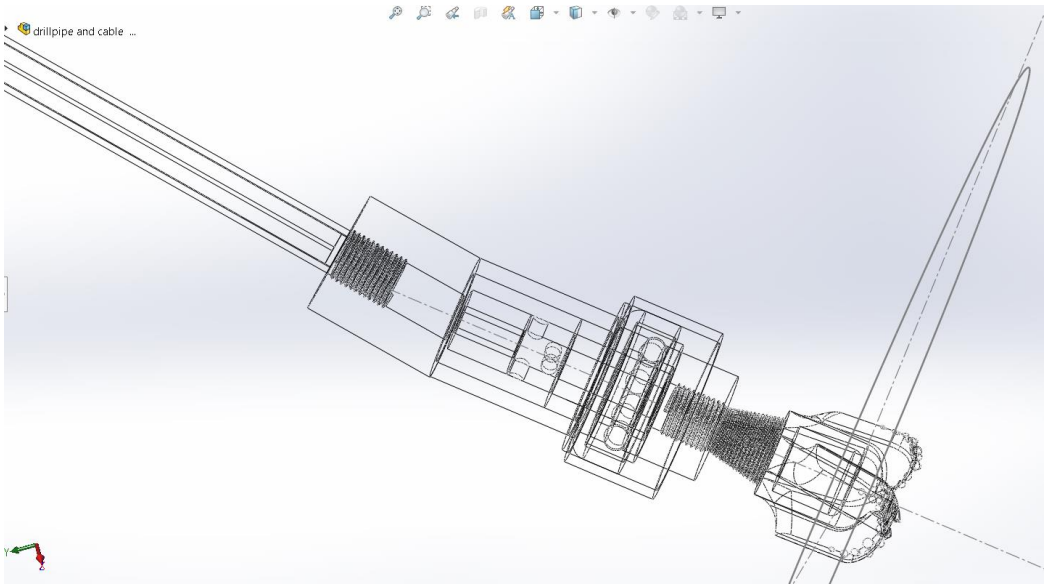

Figure 54. Model of BHA used for modal analysis

Table 13. First 5 modes for BHA System

Mode	Frequency, Hz
1	15.184
2	17.775
3	51.093
4	89.133
5	97.701

6.6 Preliminary Conclusion

- It can be seen that FEM allows one to study drill string dynamic vibration response.
- This qualitative analysis shows that on this scale, whether inducing one mode of vibration or all three modes of vibration doesn't significantly alter the deflection response.
- Also, directional wells seem to have a slightly higher deflection response than vertical wells. This could be explained by the transmission of mechanical energy from the main axis to the off-axis angle in order to build the deviation. In the experimental case, as the directional well depth increases, there is simultaneously an increase in damping in one area of the pipe, changing the effective vibration length, and thus changing the vibration response. This response is not seen here. Further work is needed to better understand how the different modes of vibrations are induced on this small scale.
- According to the experimental results, increasing RPM is more beneficial than increasing WOB, from a pure gain in TD perspective. However, as shown here, increasing WOB could also help reduce axial vibrations, and thus should be done with a consideration on MSE values for best optimization.
- From the simulations, torsional vibrations are within a set range, however, the experimental results show that higher torque is induced by an increase in RPM. More work should be done to explore the torsional vibrational response on this scale.

Chapter 7. Conclusion

In this study, parameters such as WOB and RPM were varied and their effects on depth drilled, response torque, ROP, MSE were studied for vertical well configuration and directional well configurations. The inclination build from these varying parameters was studied as well, and the drill string vibrational responses were explored, using experimental torque response data, and FEM simulation models.

7.1 Experimental Setup

- For the data range considered in this study, TD is more heavily correlated to RPM than to WOB. Thus, increasing RPM is more beneficial than increasing WOB for this range.
- Since the torsional vibration response is similar for vertical and directional wells, based on this study, 600 RPM is the most efficient for a directional well. Ideally, 350 RPM is the most efficient at 35 lbf WOB. However, since there is loss in ROP at 350 RPM, 600 RPM is a good compromise. This is also supported by the inclination build where even though 35 lbf and 800 RPM provides the highest inclination, one is best served at 35lbf at 600 RPM, which gives high enough inclination values for the setup considered. This helps to maximize the increase of inclination while simultaneously minimizing vibration and optimizing ROP.
- Total depth (TD) and ROP increase with increasing WOB and RPM. Similarly, response torque also increases, but only slightly.
- MSE values for directional wells increase due to significant friction in the borehole.
- Generally, higher RPM produces more torque in the drill pipe.

- Increasing WOB increases wellbore inclination up to a certain point, after which there is a net decrease in inclination gain.

7.2 FEM Setup

- Successful vibration simulations were ran on the experimental setup for two main configurations; one mode of vibration and all three modes of vibration.
- The response for axial, lateral, torsional and total deflection was compared and analyzed.
- For the range of data analyzed, it was observed that both configurations didn't have any significant effect on the response vibration for both vertical and directional well simulation setups.
- It was observed that rotational speed was the governing factor in vibration response behavior.
- This study looked at inducing vibrations at different frequencies, and no noticeable changes were determined for the speeds considered. However, it was observed that higher rotational speeds (higher frequencies) generally induced slightly more vibrations for all responses.
- For directional wells vibrations, all modes are almost always slightly higher than for vertical wells. A possible explanation could be due to the off-centered axis to achieve deviation.
- Even though directional well vibrations are slightly higher, they are only higher by a very small margin. A possible explanation could be because the simulation was run at a relatively smaller length scale. A different response might be seen when larger lengths are used, as is in the case of Chacin, 2017. An interesting observation with directional well

vibrations is the various amounts of pipe dampening that occurs when the well begins to deviate. This is not accounted for in the simulation, as this is beyond the scope of the thesis.

- According to Chacin, 2017 the constant load gave the worst-case case scenario, however, this was not the case in this simulation. An explanation in the discrepancy could be the different scales of work, and the load magnitudes.
- The 850 RPM is closest to the natural frequency of the system used, and thus has the most damage to the BHA if run at that speed.

It must be stressed that at such a small scale, the pipe stiffness plays a key role in the vibrational behavior, and should be considered when considering the results. Also, the results are only valid for the rotational speed range of 350 to 850 RPM and the weight on bit range of 20 to 50 lbf.

The overall conclusion of this work is to add to the existing body of knowledge in drilling mechanics, particularly the area of directional drilling. This shows the importance of incorporating all drill string mechanics in drilling programs to mitigate vibrations and to help drill wells efficiently.

7.2 Limitations and Recommendations for Future Work:

7.2.1 Limitations

The scale of the setup and the values at which the tests were run brings up a few limitations in this work.

1. Traditionally, the relationship between WOB and ROP is exponential, for varying RPM values (Chen, 2017). However, since low WOB values of 20 to 50 lbf and relatively low RPM values of 350 to 850 RPM are considered, there is a linear relationship exhibited in some of the graphs.

2. The stiffness of the short pipe plays a huge role in the vibrational analysis. The vibrational response outcome in the simulation is different from what may be typically seen in a full scale drillpipe in the field. Furthermore, the short length also means a short vibration wave propagation through the pipe. This doesn't show the wave energy distribution which might indicate differences in constant and sinusoidal load application. Thus, these vibration results outcome are only to be used qualitatively, with the study scale in mind. Chacin, 2017 does a similar full scale study with interesting results.
3. The results of the directional well inclination angles cannot be scaled up directly to field scale. This is specific to the lab-scale, and more work should be done to find upscaling factors to convert these values to field scale. However, these inclination results shed light on the relationship between WOB and inclination build as a function of BHA angle at the lab scale.

7.2.2 Recommendations for Future Work

1. The wellbore component could be added to improve on the modeling.
2. "Damping vs. Frequency" data can be obtained and used as input for the software's analysis.
3. Fluid could be added to the model to simulate a more real drilling situation.
4. Explore more parameters for simulations for vertical and directional wells to better understand the vibrational modes on this scale.
5. Increase the scale of the experiment to account for scale differences and continuously monitor vibrations.

6. Linear materials and behavior were used for this analysis. It will be beneficial to explore non-linear materials and behavior, as this will be more representative.

References

Akita, E., Dyer, F., Drummond, S., Elkins, M. and Duggan, P. 2018. 2019 Phase 1 Final Design Report, Drillbotics™ International University Competition, the Drilling Systems Automation Technical Section (DSATS) of SPE.

Akita E., Dyer F., Drummond S., Elkins M., Duggan P., Ahmed R., Florence F. Directional Drilling Automation Using a Lab-Scale Drilling Rig: SPE University Competition. IADC/SPE International Drilling Conference held in Galveston, Texas, USA, 3-5 March 2020.

Ashley, D.K., X.M. McNary, and J.C. Tomlinson. 2001. "Extending BHA Life with Multi Axis Vibration Measurements." *SPE/IADC Drilling Conference.* Amsterdam, The Netherlands: SPE/IADC.

Agarwal, S. 2019. Thesis on Automation and Investigation of Intelligent Drilling and its implementation in Experimental Setup. University of Oklahoma, Norman, USA.

Bailey, J. J. and Finnie, I. 1960. An Analytical Study of Drill-String Vibration. *ASME Journal of Engineering for Industry* 82 (2): 122-127.

Bailey, J. R., Biediger, E., Sundararaman, S. et al. 2008. Development and Application of a BHA Vibrations Model. International Petroleum Technology Conference, Kuala Lumpur, Malaysia, 3-5 December. IPTC-12737-MS.

Bavadiya A. V., 2017. Thesis on Experimental Investigation of the Effects of Rotational speed and Weight on Bit on Drillstring Vibrations, Torque and Rate of Penetration. University of Oklahoma, Norman, USA.

Bloomberg L.P. "CL1 Comodity Quote" (2019). Bloomberg database. Accessed on December 8, 2019. https://www.bloomberg.com/quote/CL1:COM

Chacin, A. R. Marquez, 2017. Thesis on Investigation of drill-string vibrations using finite element method simulations and design and implementation of experimental setup. University of Oklahoma, Norman, USA.

Chen, X., Yang, J., and Gao, D. (2017). Drilling Performance Optimization Based on Mechanical Specific Energy Technologies, Drilling, Ariffin Samsuri, IntechOpen. DOI: 10.5772/intechopen.75827.

Cherif H. FEA modelled MSE/UCS values to optimize PDC design for the entire hole section. In: Presented at the North Africa Technical Conference and Exhibition held in Cairo, Egypt; 20–22 February 2012. SPE 149372. DOI: 10.2118/149372 MS.

Darein, D. W., and B. J. Livesay. 1968. "Longitudinal and Angular Drillstring Vibrations with Damping." *Journal of Engineering for Industry* 671-679.

Dupriest FE, Koederitz WL. Maximizing drill rates with real-time surveillance of mechanical specific energy. In: SPE/IADC Drilling Conference; 23–25 February 2005, Amsterdam, Netherlands. DOI: 10.2118/92194-MS.

Dykstra, M. W., Chen, D. K., and Warren, T. M. 1994. Experimental evaluations of drill bit and drill string dynamics. SPE Annual Technical Conference and Exhibition, New Orleans, Louisiana, 25-28 September. SPE-28323-MS.

Esmaeili, A., B. Elahifar, R. K. Fruhwirth, and G. Thonhauser. 2012. "Laboratory Scale Control of Drilling Parameters to Enhance Rate of Penetration and Reduce Drill String Vibration." *SPE Saudi Arabia Section Technical Symposium and Exhibition.* Al Khobar, Saudi Arabia: Society of Petroleum Engineers.

Finnie, I. and Bailey, J. J. 1960. An Experimental Study of Drill-String Vibrations. *Journal of Engineering for Industry* **82** (2): 129-135.

Foster, I., Macfarlane, A.H.W., and Dinnie, R. 2010. Asymmetric Vibration Damping Tool Small Scale Rig Testing and Full Scale Field Testing. IADC/SPE Drilling Conference and Exhibition, New Orleans, Louisiana, 2-4 February. SPE-128458 MS.

Franca, F. P. 2010. Drilling Action of Roller-Cone Bits: Modeling and Experimental Validation. *Journal of Energy Resources Technology* **132** (4): 043101.

Jogi, P. N., Macpherson, J. D., and Neubert, M. 2002. Field verification of model-derived natural frequencies of a drill string. *ASME Journal of Energy Resources Technology*, **124** (3): 154-162.

Kapitaniak, M.; Hamaneh, V. V.; Chávez, J. P.; Nandakumar, K.; Wiercigroch, M. (2015): Unveiling complexity of drill–string vibrations: Experiments and modeling. International Journal of Mechanical Sciences, 101, 324-337.

Khulief, Y.A., Al-Sulaiman, F.A., 2009. Laboratory investigation of drillstring vibrations. J. Mech. Eng. Sci. 233 (Part C), 2249–2262.

Leine, R. I., D. H. Van Campen, and W. J. G. Keultjes. April 2002. "Stick-Slip Whirl Interaction in Drillstring Dynamics." *Journal of Vibration and Acoustics* 209-220.

Lu, H., Dumon, J., Canudas-de-Wit, C., 2009. Experimental study of the D-OSKILL mechanism for controlling the stick-slip oscillations in a drilling laboratory testbed. In: Proceedings of the IEEE Multi-Conference on Systems and Control. IEEE. Saint Petersburg, Russia, pp. 1551–1556.

Macpherson, J. D., and J. S. Mason. 1993. "Surface Measurement and Analysis of Drillstring Vibrations." *SPE/IADC Drilling Conference.* Amsterdam, Netherlands: SPE/IADC.

Millheim, K., S. Jordan, and C. J. Ritter. 1978. "Bottom-Hole Assembly Analysis Using the Finite-Element Method." *SPE-AIME 51st Annual Fall Technical Conference and Exhibition.* New Orleans, LA: Society of Petroleum Engineers.

Omojuwa, E., S. Osisanya, and R. Ahmed. 2011. "Measuring and Controlling Torsional Vibrations and Stick-Slip in a viscous-Damped Drillstring Model." *International Petroleum Technology Conference.* Bangkok, Thailand: International Petroleum Technology Conference.

Patil, P. A., and Teodoriu, C., 2013a. Model Development of Torsional Drillstring and Investigating Parametrically the Stick-Slips Influencing Factors. *Journal of Energy Resources Technology* **135** (1): 013103. JERT-12-1158.

Patil, Parimal Arjun, and Catalin Teodoriu. 2013. "A comparative review of modeling and controlling torsional vibrations and experimentation using laboratory setups." *Journal of Petroleum Science and Engineering* 227-238.

Pavone, D.R, and J.P. Desplans. 1994. "Application of High Sampling Rate Downhole Measurements for Analysis and Cure of Stick-Slip in Drilling." *SPE Annual Technical Conference and Exhibition.* New Orleans, Louisiana: SPE.

Pessier RC, Fear MJ. Quantifying common drilling problems with mechanical specific energy and a bit-specific coefficient of sliding friction. In: SPE Annual Technical Conference and Exhibition; 4–7 October 1992, Washington, D.C. DOI: 10.2118/24584-MS.

Schmitz, Tony L., and Scott K. Smith. 2011. *Mechanical Vibrations Modelling and Measurement.* Springer.

Sotomayor, Gabriel P.G, Joao Carlos Placido, and J.C Cunha. 1997. "Drillstring Vibration: How to Identify and Suppress." *Fifth Latin American and Caribbean Petroleum*

Engineering Conference and Exhibition. Rio de Janeiro, Brazil: Society of Petroleum Engineers, Inc.

Teale R. The concept of specific energy in rock drilling. International Journal of Rock Mechanics and Mining Sciences. 1965; 2(1):57-73

Tucker, R. W, and C. Wang. 1999. "An Integrated Model for Drill-String Dynamics." *Journal of Sound and Vibration* 123-165.

Wolf, S.F., Zacksenhouse, M. and Arian, A. 1985. Field Measurements of Downhole Drillstring Vibrations. SPE Annual Technical Conference and Exhibition in Las Vegas, Nevada, 22-26 September. SPE-14330-MS.

Appendix A

Sinusoidal function vibration deflection response for vertical well for different RPM and WOB values. Legend: RPM_WOB

350_20

Total Deflection

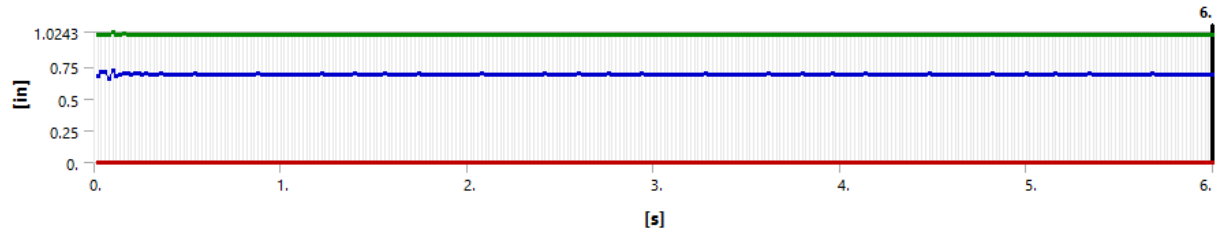

Axial Deflection

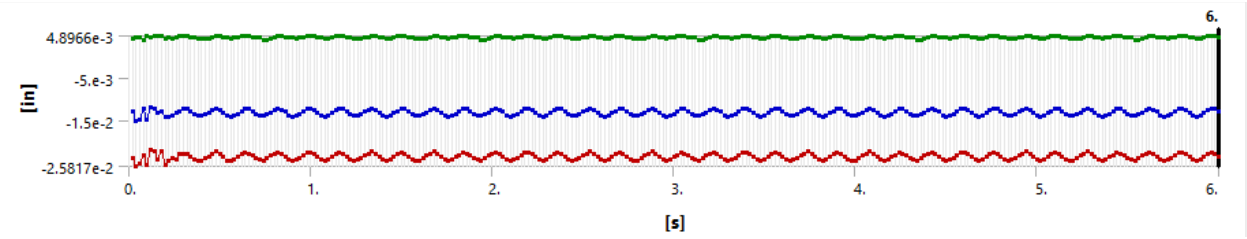

Lateral Deflection

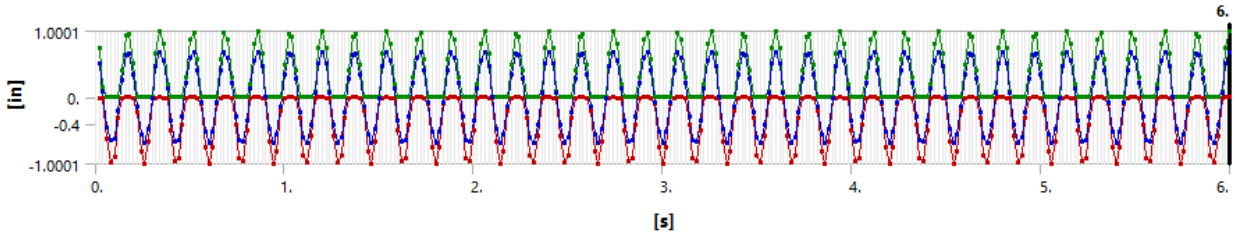

Torsional Deflection

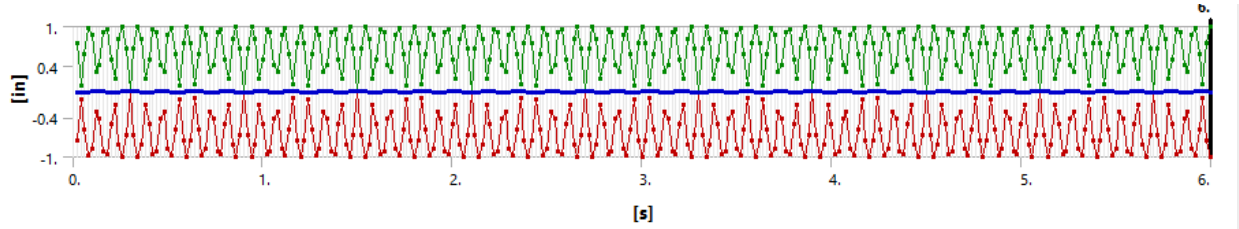

350_35

Total Deflection

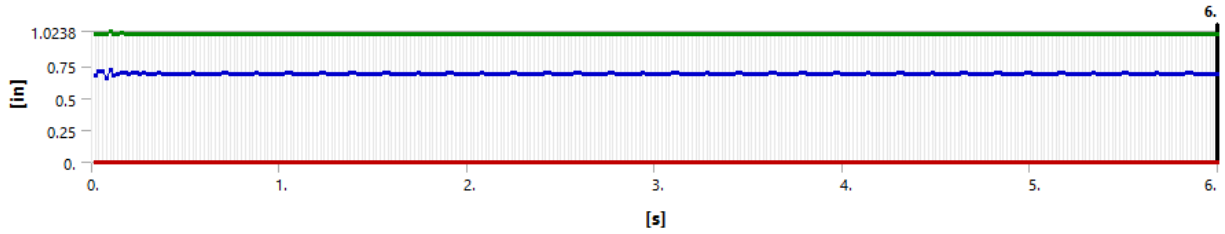

Axial Deflection

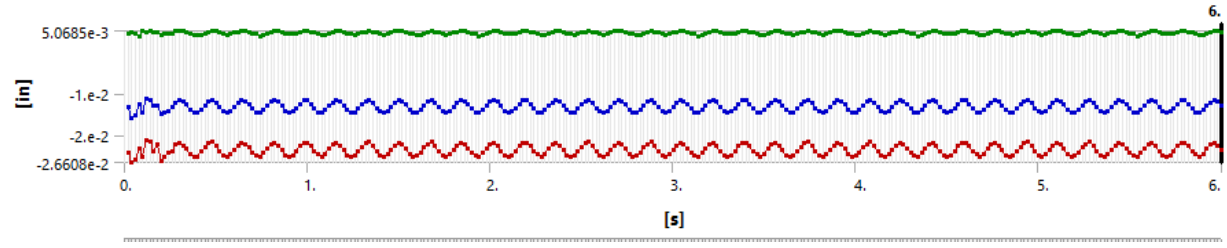

Lateral Deflection

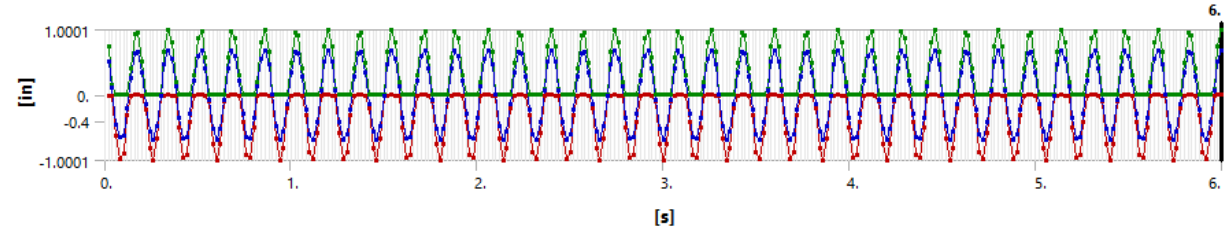

Torsional Deflection

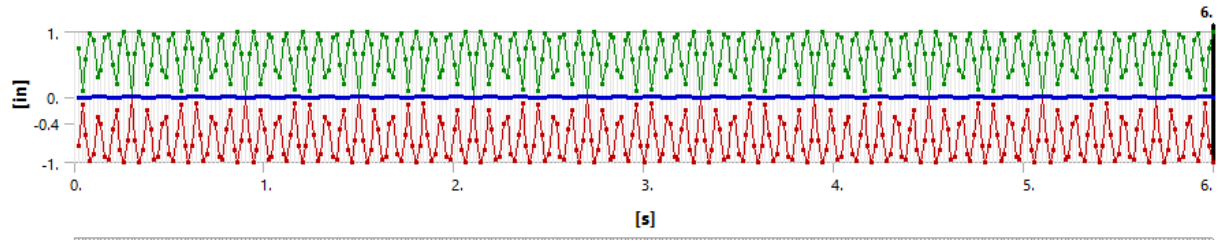

350_50

Total Deflection

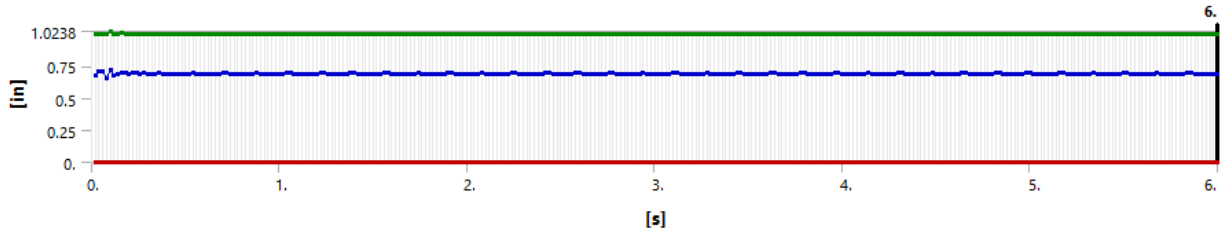

Axial Deflection

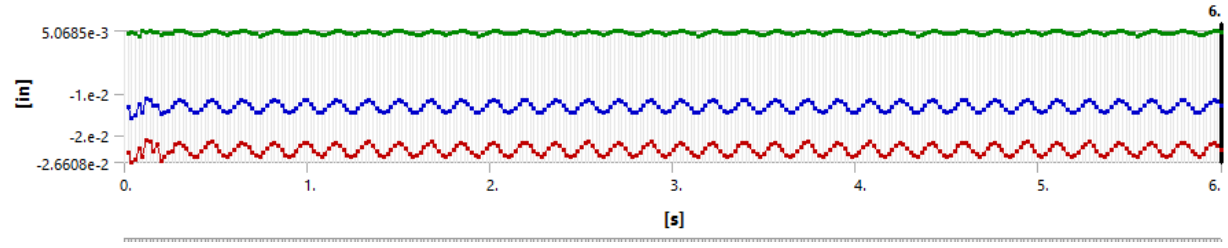

Lateral Deflection

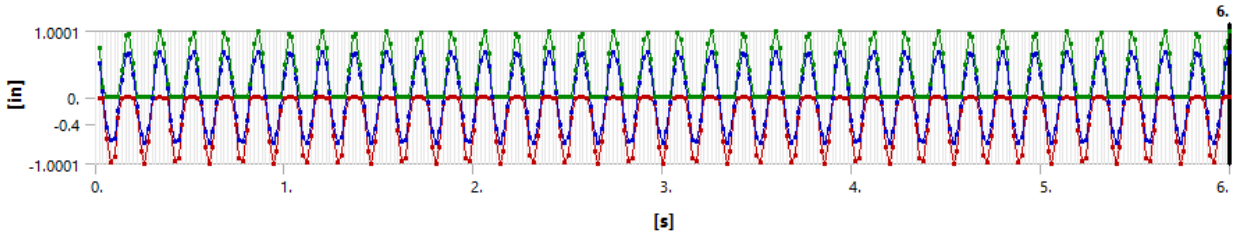

Torsional Deflection

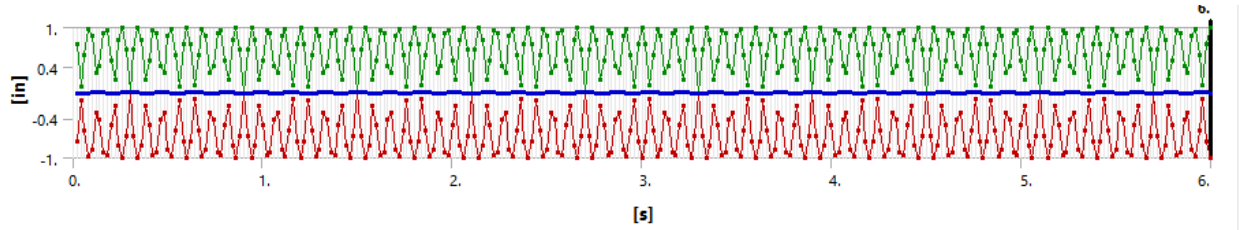

600_20

Total Deflection

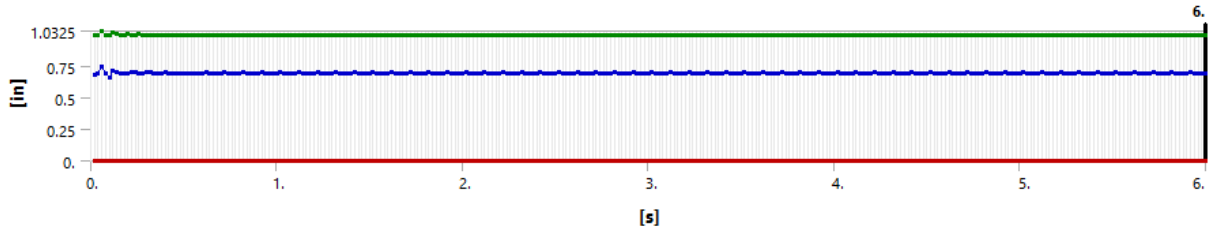

Axial Deflection

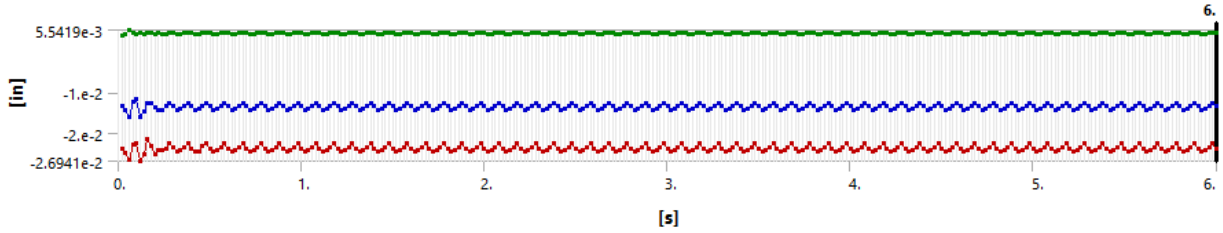

Lateral Deflection

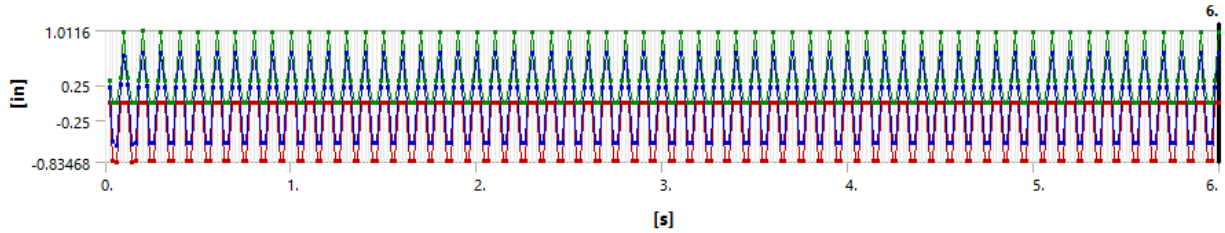

Torsional Deflection

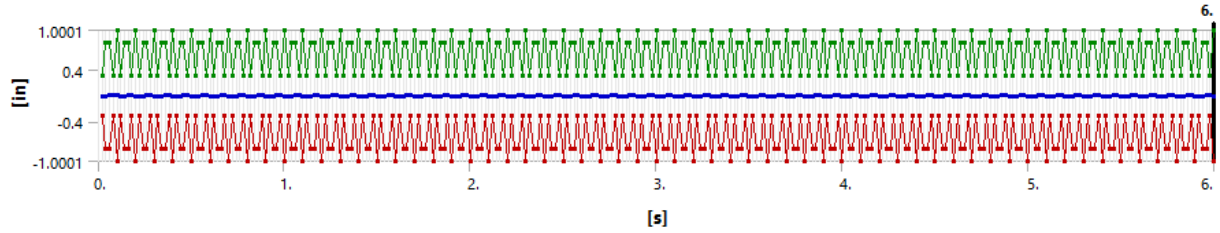

600_35

Tot Deflection

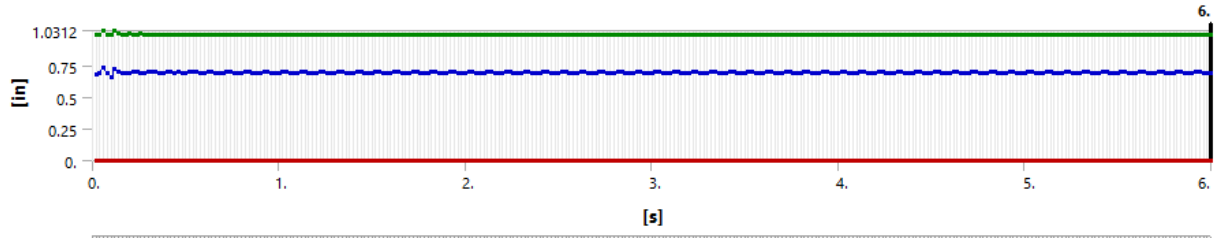

Axial Deflection

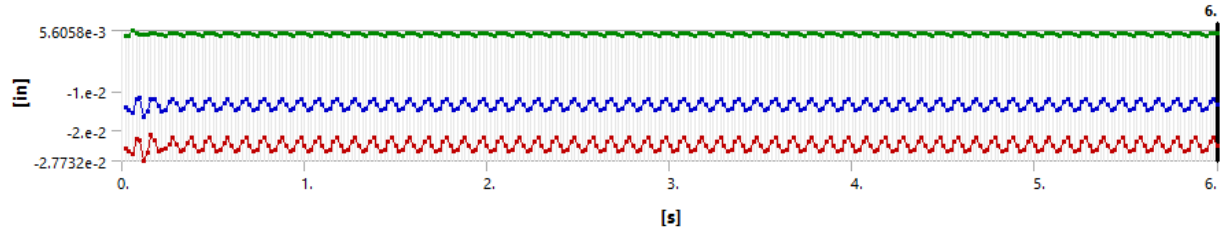

Lateral Deflection

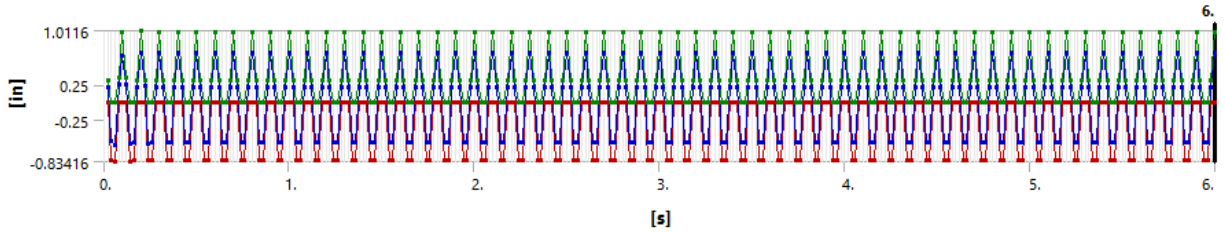

Torsional Deflection

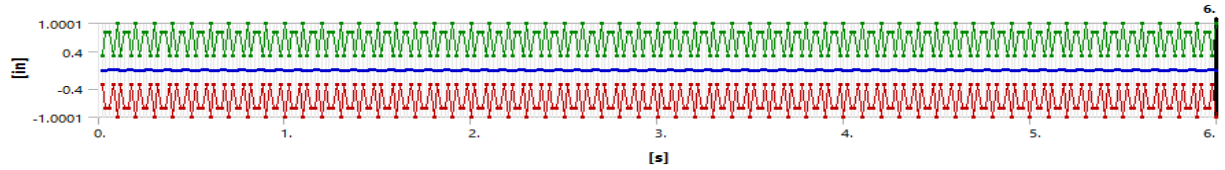

600_50

Total Deflection

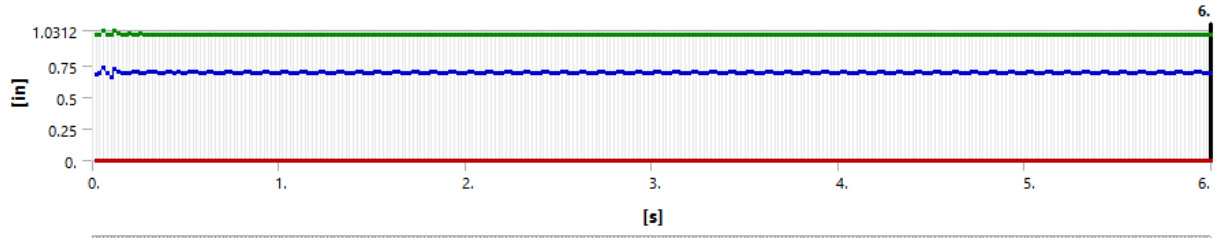

Axial Deflection

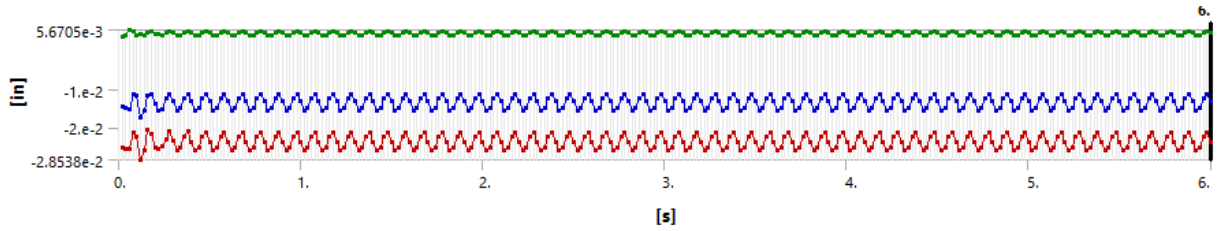

Lateral Deflection

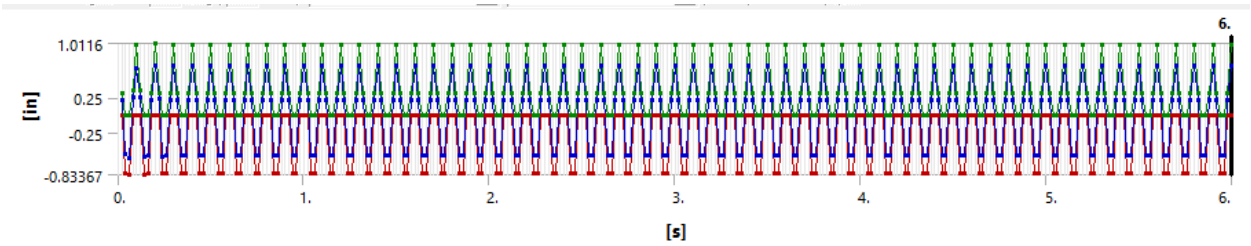

Torsional Deflection

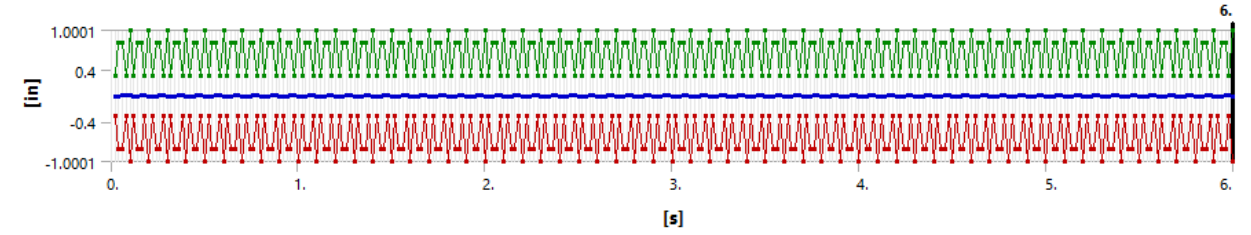

850_20

Total Deflection

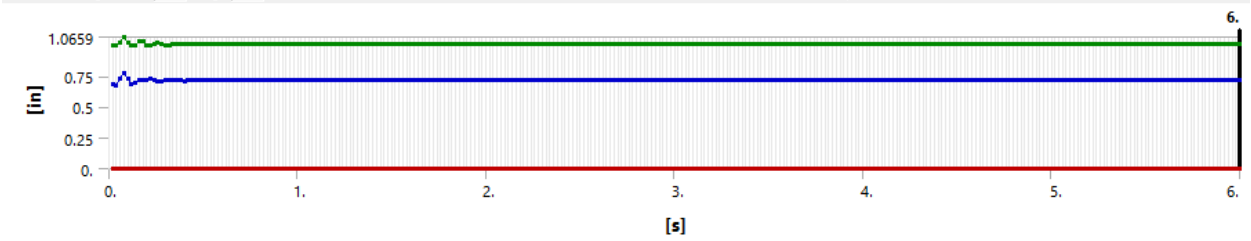

Axial Deflection

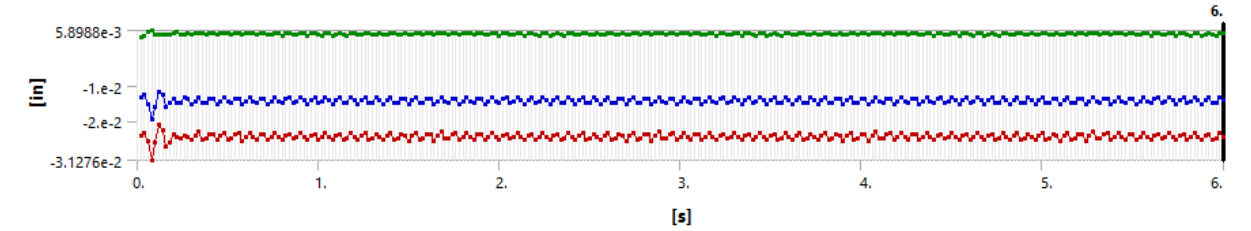

Lateral Deflection

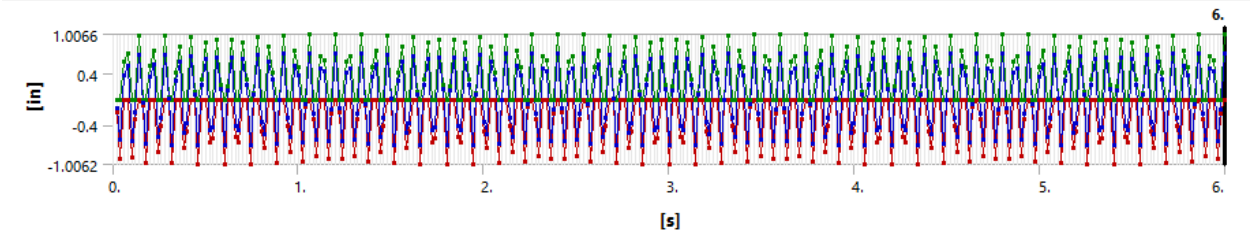

Torsional Deflection

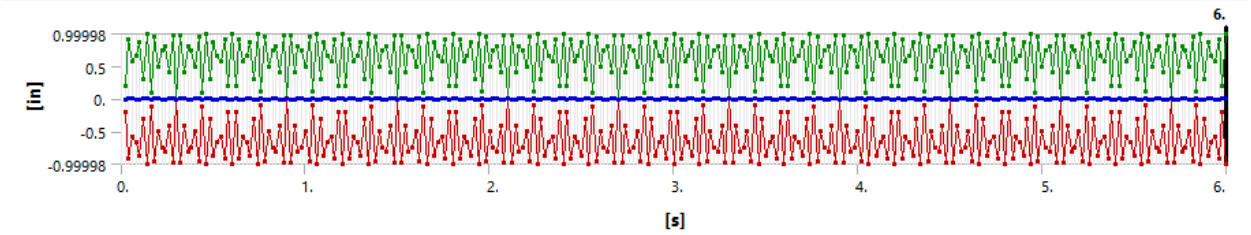

850_35

Total Deflection

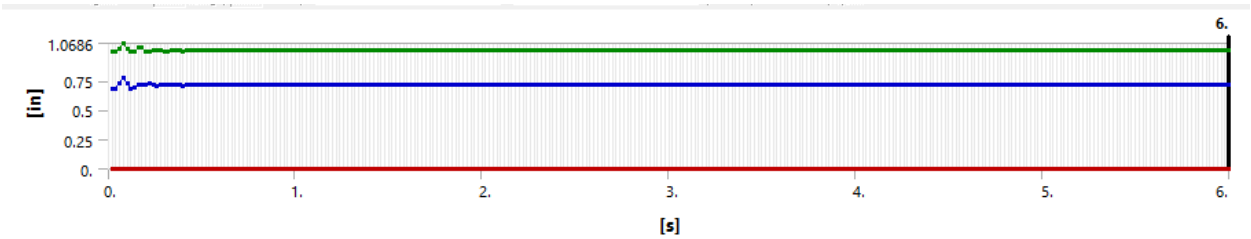

Axial Deflection

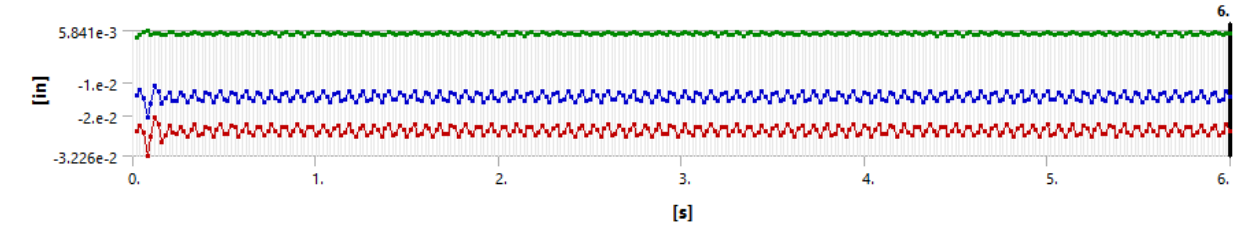

Lateral Deflection

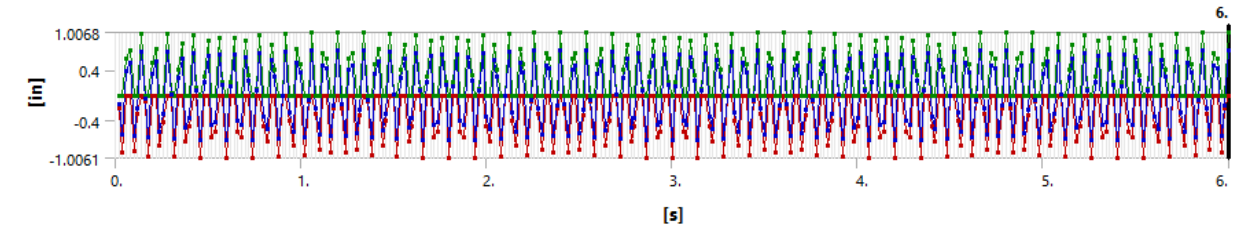

Torsional Deflection

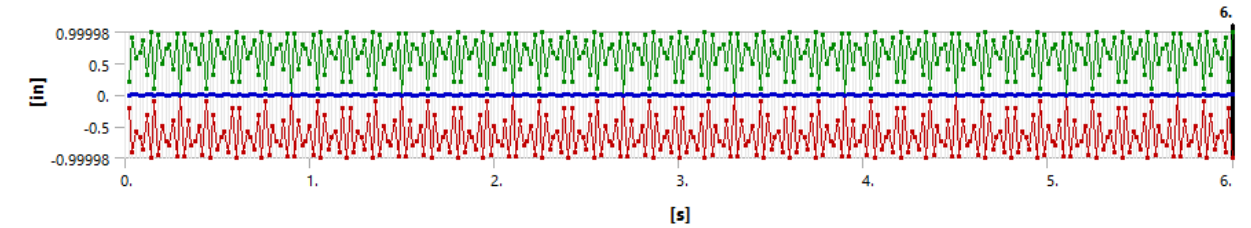

850_50

Total Deflection

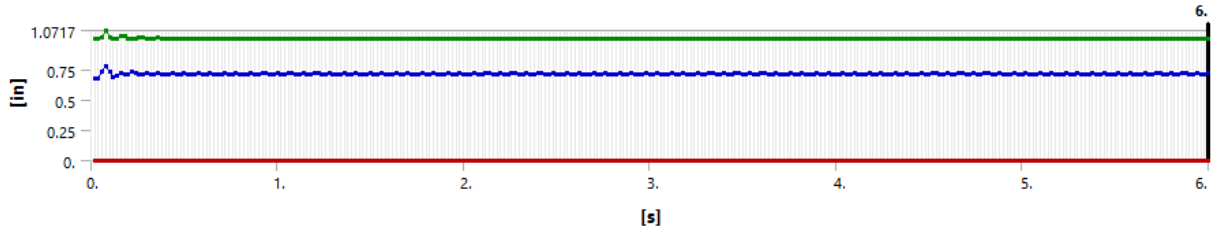

Axial Deflection

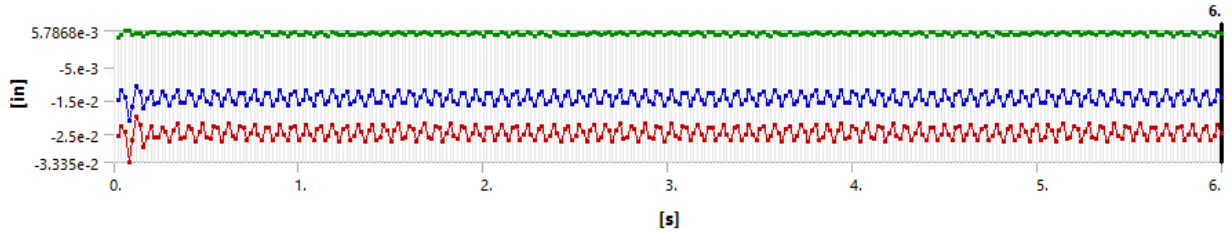

Lateral Deflection

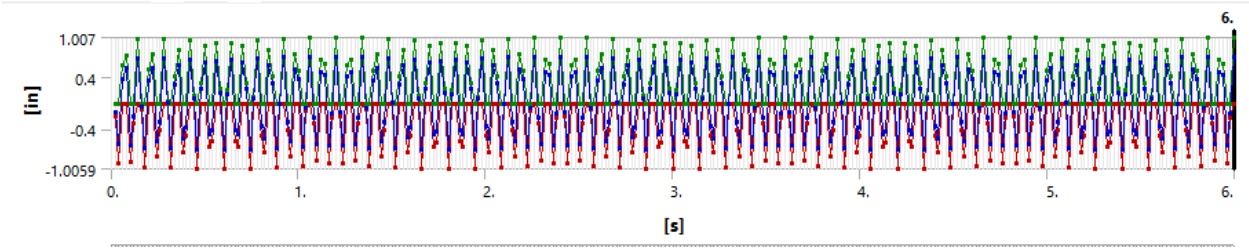

Torsional Deflection

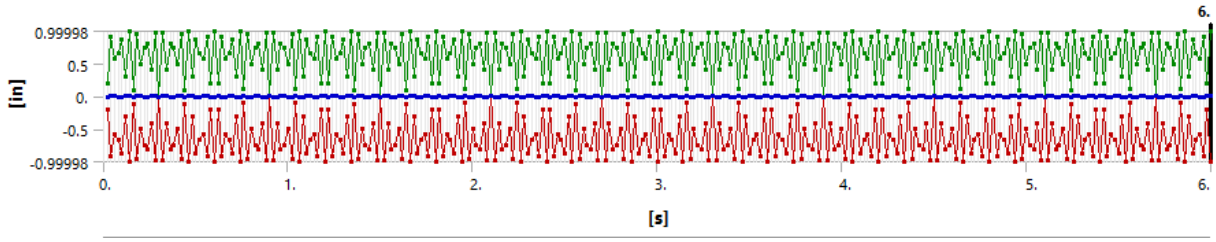

Appendix B

FEM Simulation Zoomed in Vibrational Response Graphs for the First 0.5 Seconds

Axial vibrational response for sinusoidal load application at WOB = 35 lbf

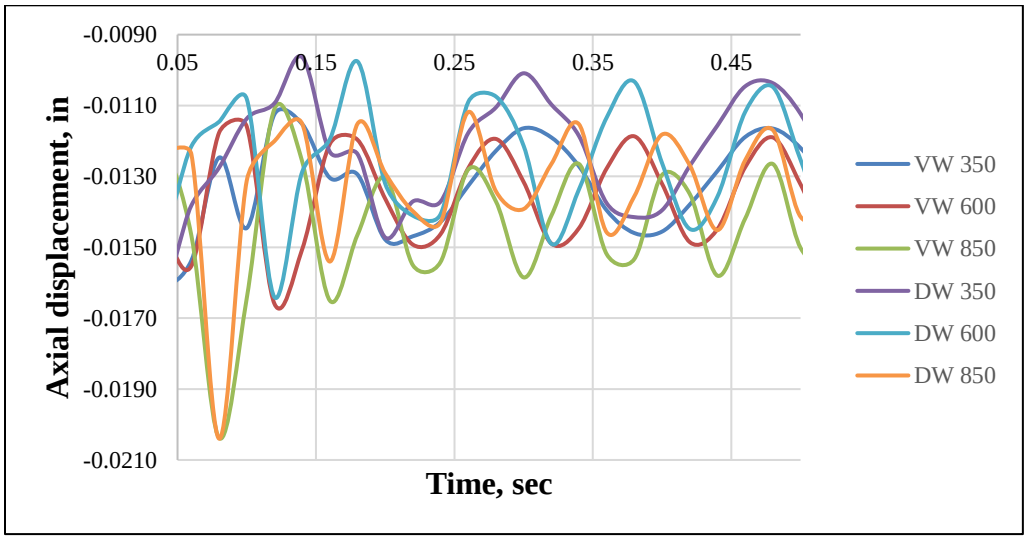

Lateral vibrational response for sinusoidal load application at WOB = 35 lbf

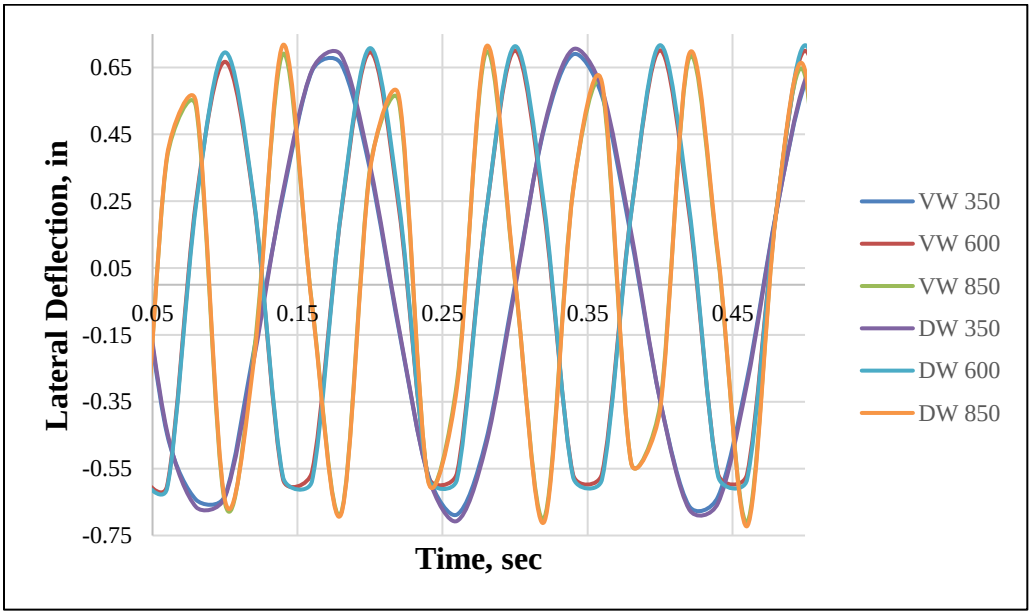

Torsional vibrational response for sinusoidal load application at WOB = 35 lbf

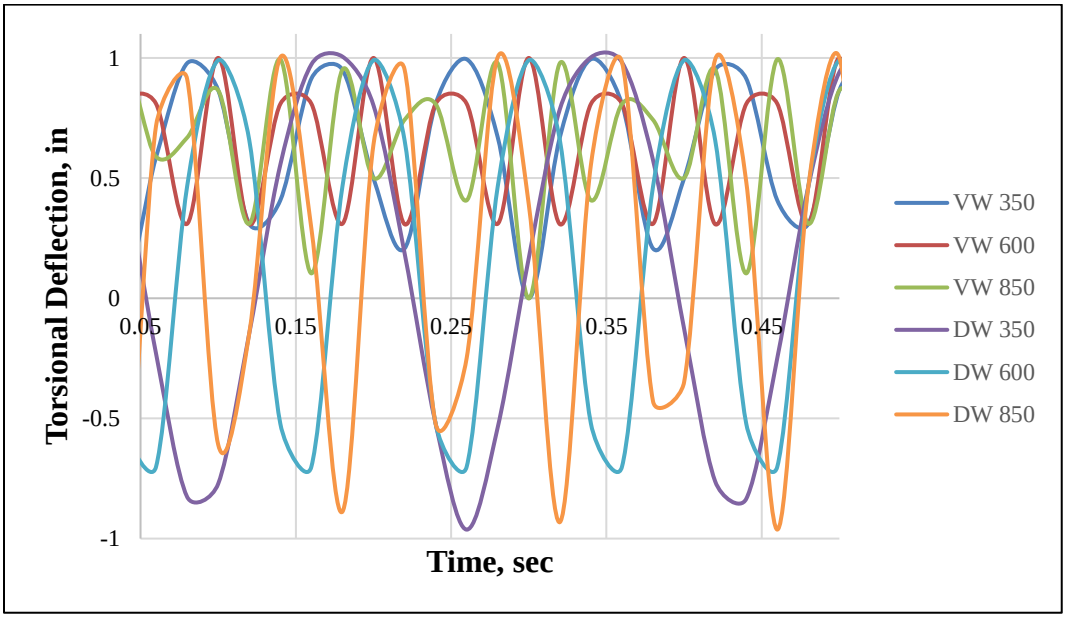

Total vibrational response for sinusoidal load application at WOB = 35 lbf